ADVANCES IN THE DESIGN OF SOLAR CONCENTRATORS FOR THERMAL APPLICATIONS

Diogo Canavarro

Tese apresentada à Universidade de Évora
para obtenção do Grau de Doutor em Física

ORIENTADORES: *Professor Doutor Manuel Collares-Pereira*
Doutor Júlio Chaves

ÉVORA, Janeiro 2014

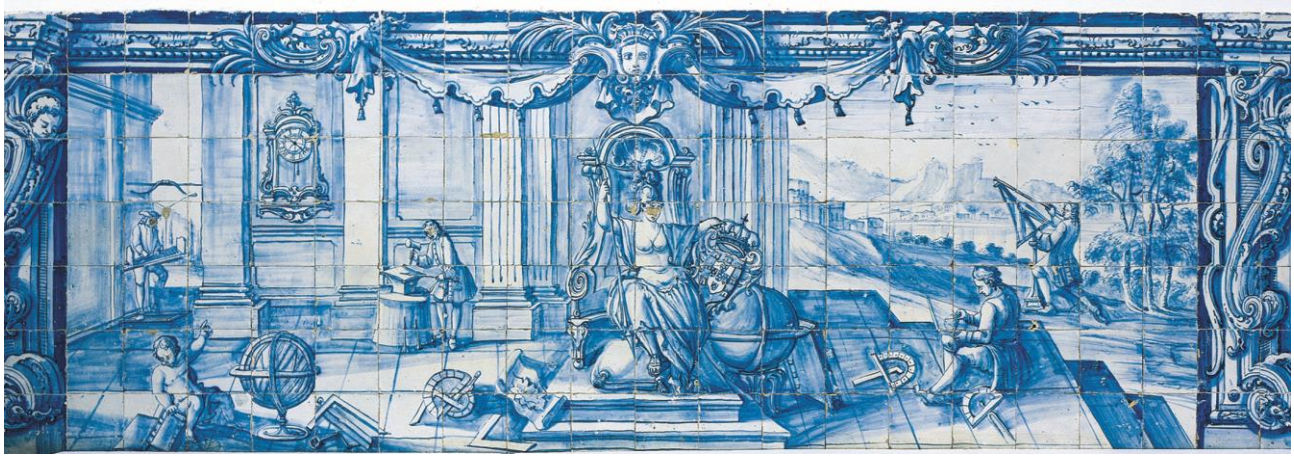

INSTITUTO DE INVESTIGAÇÃO E FORMAÇÃO AVANÇADA

"Still immersed in his dream, he drank down the tepid tea. It tasted bitter. Glory, as anyone knows, is bitter stuff."

- **Yukio Mishima**, *The Sailor Who Fell from Grace with the Sea*

Abstract

This thesis presents advances in the design of solar concentrators. Based on the study of the Compact Linear Fresnel Reflector Concentrator "Etendue-Matched" (CLFR-EM), this thesis developed optical solutions based on the Simultaneous Multiple Surface method (SMS) and new approaches of analysis of the characterizing parameters of a solar concentrator. This thesis is organized into five sections. In the first section (Chapters 1 and 2) an introduction to the topics addressed in this work is presented together with a revision of the underlying basic optics. In the second section (Chapters 3, 4, and 5) a study of the concentrator CLFR-EM is presented. In the third section (Chapters 6 and 7) a XX SMS concentrator for continuum primaries is developed and presented. In the fourth section (Chapter 8) the application of the concept XX SMS for Fresnel primaries is explained and shown. Finally, in the fifth section (Chapters 9 and 10) prospects for future developments and conclusions concerning this work are presented.

Keywords: Concentrated Solar Power, Simultaneous Multiple Surface Method; Anidolic Optics

Avanços no desenho de concentradores solares para aplicações térmicas

Resumo

Esta tese apresenta desenvolvimentos na análise de concentradores solares térmicos. Partindo do estudo realizado sobre o concentrador Compact Linear Fresnel Reflector "Etendue-Matched" (CLFR-EM), esta tese propõem soluções ópticas baseadas no método de Simultaneous Multiple Surface (SMS) e novas abordagens à análise dos parâmetros caracterizadores de um concentrador solar. A tese está organizada em cinco secções. Na primeira secção (Capítulos 1 e 2) é realizada uma introdução aos temas abordados neste trabalho e uma revisão dos conceitos básicos de óptica. Na segunda secção (Capítulos 3, 4 e 5) é apresentado um estudo do concentrador CLFR-EM. Na terceira secção (Capítulos 6 e 7) é apresentado um concentrador XX SMS para primários contínuos para concentração máxima e receptores fixos. Na quarta secção (Capítulo 8) mostra-se a aplicação do conceito XX SMS a primários Fresnel. Por último, na quinta secção (Capítulos 9 e 10) são apresentadas perspectivas para desenvolvimentos futuros e realizadas conclusões sobre este trabalho.

Palavras-chave: Energia Solar Térmica, Método de Simultaneous Multiple Surface, Óptica Anidólica

Acknowledgements

This thesis is the result of many years of study and dedication. However, this would not be possible without the support of many people and entities.

Firstly, I am deeply grateful to my supervisors Prof. Dr. Manuel Collares-Pereira and Dr. Julio Chaves for believing in my capabilities and for their support and encouragement throughout these years. It has been such a great pleasure to me to work and learn from them and grow, not only as a student but also as a person. As matter of fact, throughout these years we discussed many point of views about many different topics and not only about work. During these discussions it was quite clear to me that both have a great life experience and the knowledge that I received from them will certainly be very useful for me in the future.

I am also deeply grateful to University of Évora/BES Renewable Energies Chair for providing me the necessary conditions to perform my work. I thank all the technical support from the staff, especially to Maria Assunção Mexia, Eng. Cláudia Marques and Maria Augusta Carreira for helping me to deal with many bureaucratic issues. I also acknowledge the support of the Portuguese National Science and Technology Foundation - FCT (Fundação para a Ciência e Tecnologia) - through the PhD scholarship No. SFRH/BD/51613/2011.

I want to thank my co-workers from BES Renewable Energies chair: João Marchã, Tomás Fartaria, Tiago Osório, Pedro Horta, Luís Guerreiro, Luís Fialho, Afonso Cavaco and Nelson Luz for their fellowship, friendship and support during these years. Success is only possible when it is shared and they are the living proof of that. This work is also theirs.

I want to thank Prof. Dr. Paulo Canhoto, who provided me the template of this thesis.

I also want to thank my family which has been my safe haven throughout these years. To my grandmother (Ivone), parents (João and Maria), brothers (João, Susana and Zeza) and nephew (Bernardo) who gave me so much love and affection, a special kiss. I hope they can be proud of me as I am proud of them.

Last but not the least, I would like to thank Ana for all her love and affection. This work would not be possible without her.

Contents

List of Papers

This thesis includes the following papers:

I. Canavarro, D., Collares-Pereira, M., Lopes Guerreiro, L., *Increasing the efficiency of conventional LFR technologies: a new CLFR "Étendue Matched" CSP collector*, Proceedings 17th International SolarPACES Symposium, September, 20-23, Granada (Spain), 2011. [Chapter 3]

II. Horta, P., Collares-Pereira, M., Canavarro, D., Guerreiro, L., *Modeling thermal losses in a new CLFR "Etendue Matched" non-evacuated collector cavity*, Proceedings 17th International SolarPACES Symposium, September, 20-23, Granada (Spain), 2011. [Chapter 4]

III. Lopes Guerreiro, L., Canavarro, D., Collares-Pereira, M., *Increasing the cost effectiveness of CSP technologies trough the development of a new CLFR "Etendue Matched" collector*, ISES solar world congress, 28 August-2 September, Kassel (Germany), 2011. [Chapter 5]

IV. Canavarro, D., Chaves, J., Collares-Pereira, M., *New second-stage concentrators (XX SMS) for parabolic primaries; Comparison with conventional parabolic troughs concentrators*, Solar Energy, Volume 92, June 2013, Pages 98-105. [Chapter 6]

V. Canavarro, D., Chaves, J., Collares-Pereira, M., *Infinitesimal etendue and Simultaneous Multiple Surface (SMS) concentrators for fixed receiver troughs*, Solar Energy, Volume 97 November 2013, Pages 493-504 [Chapter 7]

VI. Canavarro, D., Chaves, J., Collares-Pereira, M., *Simultaneous Multiple Surface method for Linear Fresnel concentrators with tubular receiver*, Accepted for publication in Solar Energy [Chapter 8]

Other publications related with the subject of the present thesis, but not included, are:

i. Canavarro, D., Chaves, J., Collares-Pereira, M., *New optical design for large parabolic troughs*, Proceedings 19th International SolarPACES Symposium, September, 17-20, Las Vegas (EUA), 2013.

List of Figures

List of Tables

Chapter 1

Introduction

1.1 Background and general motivation

The energy question is today considered to be one of World's most difficult challenges. In fact, the depletion of the conventional energetic resources, polluting and non-renewable (oil, coal, natural gas, etc.) associated with a tremendous growth of energy consumption on a World scale, is leading, in many different ways, to an unsustainable situation, i.e., to a dangerous and uncontrollable growth of the imbalances of the ecosystems. These imbalances are reflected, in practice, in the irreversible pollution of the soil and of the atmosphere, continued increase of energy cost, military/diplomatic tensions associated with fossil energy resources, etc. On the other hand, the daily access to energy is still practically only granted in the so called developed countries. In fact, 4/5 of the World's population continue to have multiple difficulties in accessing it [1]. It is within this difficult scenario that Renewable Energies appear as a real alternative option, since they are inexhaustible in our timescale, non-pollutant and naturally distributed over of the World.

Among all renewable energies, Solar Energy appears as one of the most interesting possibilities due to its large potential and versatility, reflected in a large range of possible applications: domestic hot water, industrial process heat, desalination, solar cooling, thermal and photovoltaic electricity production, etc. In Portugal, Solar Energy is particularly relevant due to the high values of solar radiation, with a mean number of sunshine hours between 2200h and 3000h and mean values of annual global horizontal radiation from about 1500kWh/m^2 to >1900kWh/m^2, well above to European Union's average, as shown in Fig. 1.1.

As one among the large range of applications, thermal electricity production (CSP - Concentrated Solar Power) is one of the most interesting and promising applications. These systems use solar concentration collectors to increase the entrance aperture area and to facilitated operation at higher temperatures (typically greater than 250°C) allowing a saturated/overheated steam generation properly associated

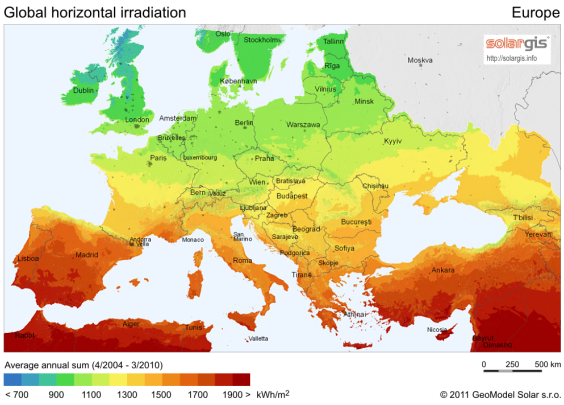

Fig. 1.1: Anual global horizontal solar radiation in Europe.

with a thermodynamic cycle (usually a Rankine cycle), as used in conventional thermoelectric power plants. These type of solutions are very interesting not only for the possibility of large-scale electricity production, but as well, for the possibility of heat energy storage increasing, in this way, the dispatchability of the electricity produced by the system. This dispatchability is important for a quick and efficient answer to the needs of the electric network but also to reduce the impact caused by the variability of the solar resource. These type of solutions are present in many parts of the World [2]. Usually four the technologies being proposed: Parabolic Through (PT), Stirling Dish (SD), Linear Fresnel (LFR) and Central Tower Receivers (CTR), as shown in Fig. 1.2.

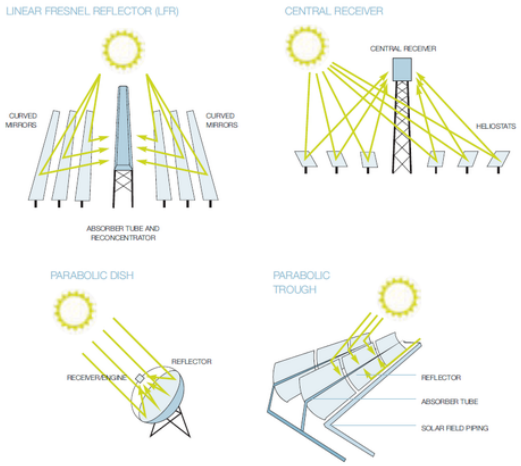

Fig. 1.2: The four main CSP technologies.

Among all CSP technologies, the most used so far is the PT concentrator. For instance, PT based plants represent 94% of all solar thermal electricity capacity

installed in Spain today [3]. However, LFR concentrators have seen an increase in development in recent years due to the potential they represent for low-cost electricity production when compared with the PT concentrator. In fact, LFR concentrators presents several advantages over the PT concentrators:

- A fixed receiver facilitating the energy extraction using, for instance, a direct steam generation.
- It uses plane or slightly curved low-cost mirrors.
- The mirrors are placed on the horizontal plane and at the same height which permits a simple geometric configuration as well as the use of higher values of aperture area.
- The use of a lower number of receivers per m^2 of aperture which implies lower thermal losses and other parasitic ones, associated with length of feed-in pipes, quantity and pumping of heat transfer fluid (HTF), etc.

However, LFR concentrators on the market are known to be less efficient than PT concentrators, with values of global solar-electricity yearly efficiency conversion of 8-9% while for PT concentrators present today reach values reach 14-15%. Nevertheless, the cost per aperture area for LFR concentrators is, today, around 151 EURO/m^2 while for PT concentrators this figure is around 275 EURO/m^2 [4, 5, 6, 7]. From these values the potential of LFR concentrators for a low-cost thermal electricity production becomes apparent, in particular if combined with the exploitation of the large room for improvement still existing for its global efficiency conversion.

This present difference in global solar-electricity yearly efficiency conversion has been a major obstacle for the market penetration of LFR technology, which, today, is still perceived as a developing technology. Nevertheless, there are already several companies and groups who decided to invest in it, such as Areva Solar, Novatec Solar or Solar Euromed [8, 9, 10], as shown in Fig. 1.3.

Fig. 1.3: LFR technologies. a) Areva Solar, b) Novatec Solar and c) Solar Euromed.

The results they have obtained have showed the potential of the LFR concept as well as its acceptance as a viable option for solar thermal electric production.

The need for an efficiency increase of the LFR technology has already led to several developments in its geometry, either through the use of second-stage Non-Imaging Optics concentrators of CPC-type (Compound Parabolic Concentrator) in order to increase the concentration factor, but also through the modification of the geometry of the primary mirror field with the use of multiple receivers in order to get a better optical performance [9, 10, 11, 12, 13, 14, 15].

For example: 1) the LFR concentrator of Novatec Solar uses a CPC secondary concentrator, as shown in Fig. 1.4;

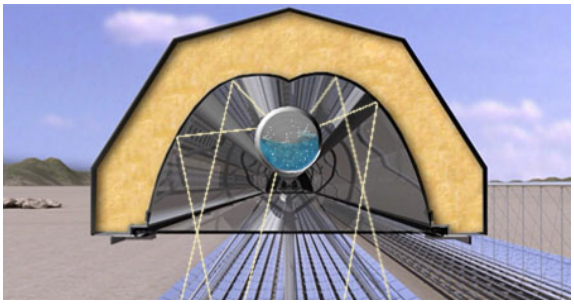

Fig. 1.4: The second-stage CPC concentrator of Novatec Solar.

2) recent developments showed the potential LFR concentrators using multiple receivers, originating a type of configuration known as Compact Linear Fresnel Reflector (CLFR) [13, 14, 15]. The use of multiple receivers (usually 2 per module) allows a better land-use (less space between the heliostat mirrors) without penalizing the optical performance of the system due to shading and blocking effects. Fig. 1.5 shows two examples of CLFR concentrators.

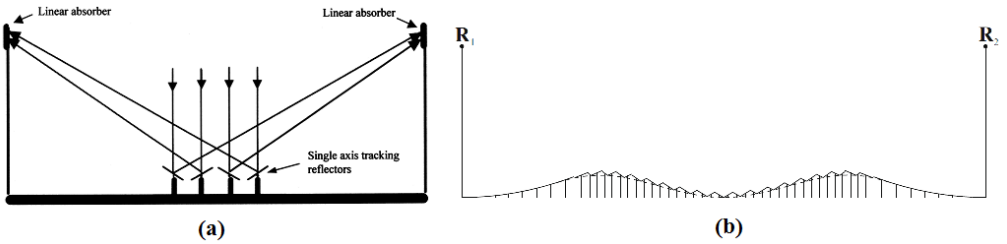

Fig. 1.5: CLFR concentrators. (a) Configuration proposed by D.Mills and G.Morrison; (b) Configuration proposed by J.Chaves and M.Collares-Pereira.

1.2 The path towards the PhD thesis

1.2.1 The MSc thesis

The configuration so called CLFR "Etendue-Matched" referred above assumes a particular importance in this context, because this represents a significant improvement in relation with other Fresnel configurations: the optimization of the primary in curve-shape in order to conserve the "etendue", that is, the design of a system which, in the ideal case, does not have shading or blocking losses [14]. This type of losses tend to increase as the incidence angle of the sun in relation to the vertical axis of the optics increases. In fact, this is one of the major drawbacks of convencional LFR concentrators and the reason for this is that the primary field is fixed in the horizontal direction and, thus, the system does not track the sun as a whole (unlike in the case of PT concentrators, for example). These losses corresponds to a loss of optical efficiency, concentration factor and energy collected, penalizing the overall global efficiency conversion, as mentioned before.

The work presented in this thesis started from this background, more specifically from a MSc. thesis with the title "Modeling linear solar collectors of the Fresnel-type; application to an innovative CLFR collector "Etendue-matched"" [16].

In fact, combining the innovative concept CLFR "Etendue-Matched" and the potential of this type of technology for low-cost electricity production, a software was initially developed to design the new solar CLFR concentrator being proposed [14] and calculate all the relevant parameters, such as the optical efficiency, incidence angle modifier (IAM) curves [17], anual energy collected, etc. The development of the work in this MSc. thesis [16] was based the need to overcoming an usual set of difficulties arising from the usual analysis of solar concentrators, which is based on analytical-type methodology, i.e., the analysis of the system as set of linear and/or non-linear equations which describes all the relevant parameters mentioned before. This analysis, although perfectly valid, contains several drawbacks:

- It is not a generic approach, i.e., it depends on the geometrical characteristics of the concentrator.
- In cases in which the geometry of the concentrator is complex, it might be practically impossible to describe it in a fully accurate way.
- Due to the nature of the set of equations used, the definition of the parameters of analysis of the concentrator (optical efficiency, IAM, etc.) might not be commons between different types of concentrators.

Thus, it became clear from the outset that it was necessary to have a calculation tool with a different nature from the usual analytical methodology, namely

through the use of existing raytracing type software appropriated for a such type of calculations, in which the results are obtained from a direct computational method, taking full advantage of all the potential resulting from the recent developments in this area. This was combined with an effort towards significant practical design and optimization processes. The calculation made used a new tool, a raytracing software to calculate all the relevant parameters and this method allowed for the analysis of different type of concentrators in a fully generic way. Fig. 1.6 shows an example of such raytracing over the particular concentrators proposed in this MSc. thesis.

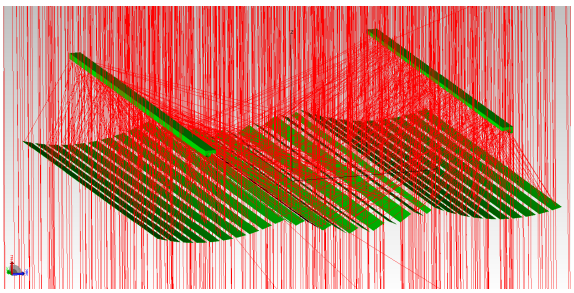

Fig. 1.6: An example of a raytracing using a CLFR "Etendue-Matched" concentrator.

The results obtained in [16] showed the reliability of the calculation tool but also the performance improvement potential of the CLFR "Etendue-Matched" concentrator with a prediction for the global efficiency conversion already around 11.8%, while its application to a conventional LFR led to only to 8.5% for the same location (Faro, Portugal).

1.2.2 The first steps of the PhD thesis

Due to the interesting results obtained in [16], a proposal for a demonstration-project of the CLFR "Etendue-Matched" concept was submitted, in collaboration with the Portuguese electric company EDP Inovação [18]. Thus, it was decided that the first part of the PhD thesis would be dedicated to a in-depth study of the CLFR "Etendue-Matched" concept. The main objective of this study was to obtain an optimized solution for an experimental demonstration, as mentioned before. This was to include an in-depth analysis with a careful study of the optical, thermal and cost parameters of a possible CLFR "Etendue-Matched" solution, with this analysis performed in collaboration with other BES Renewable Energies Chair co-workers. From that analysis the following scientific publications resulted. They are included in Chapters 3, 4 and 5 of this thesis:

- Chapter 3 - "Increasing the efficiency of conventional LFR technologies: A new CLFR "Etendue Matched" CSP collector", with emphasis on the optical issues [19].

- Chapter 4 - "Modeling thermal losses in a new CLFR "Etendue Matched" non-evacuated collector cavity", with emphasis on the thermal issues [20].
- Chapter 5 - "Increasing the cost effectiveness of CSP technologies through the development of a new CLFR "Etendue Matched" collector", with emphasis on cost-effectiveness and thermal storage issues [21].

1.2.3 The following work

As mentioned before, these three Chapters resulted in an in-depth analysis of the CLFR "Etendue-Matched" for practical purposes. It was soon concluded that there were two major difficulties concerning that CLFR "Etendue-Matched" concentrator: 1) It proposed the used of a non-evacuated tubular receiver for an operating temperatures of 400-450ºC and, still today, there are no tubular receivers on the market with a selective coating which can handle such range of temperatures, i.e., without a fast destruction of the selective properties. Some studies have already been made in order to overcome this difficulty but it has been impossible yet, i.e., at the present time, to reach a commercial solution [22]; 2) The design of the CLFR "Etendue-Matched" for tubular receivers implies the introduction of a gap between the receiver and the secondary mirror concentrator TERC (Tailored Edge Ray Concentrator) [23] in order to avoid thermal short-circuits. However, this results in the loss of optical efficiency and concentration since some light escapes through the gap, as shown in Fig. 1.7.

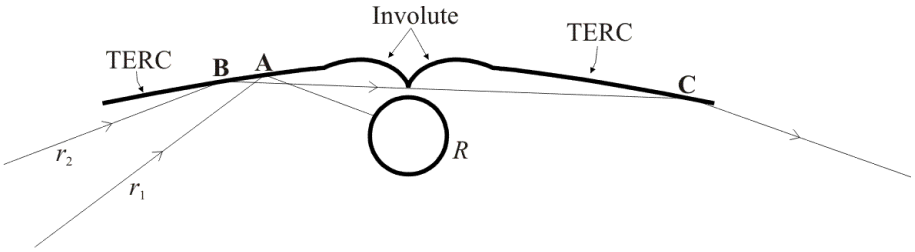

Fig. 1.7: A TERC secondary for a tubular receiver R. A ray r_1 hits the TERC mirror at a point **A** and it is reflected towards R. However, if there is a gap between R and TERC, a ray r_2 might be lost by following the path **B**-**C** hence reducing the overall optical efficiency.

Furthermore, it was not possible to fulfil the necessary conditions for the realization of the demonstration-project in collaboration with EDP Inovação. Thus, it was decided to steer the present PhD thesis in the direction of the development and simulation of solar concentrators capable to overcome the set of difficulties mentioned before, and others eventually resulting from other options. For instance, if vacuum receiver tubes are used (so to reduce the thermal losses and work at the mentioned

operating temperatures) implies, besides the gap losses, some optical losses due to the Fresnel losses which occurs in the glass cover around the receiver tube [24].

The gap problem is well known in literature and several solutions have already in order to overcome this difficulty [26, 27, 28, 29]. Nevertheless, these solutions require the introduction of new optical elements which increases the complexity of the system and decrease the concentration factor. But since the only receivers available on the market which can operate at temperatures above 400°C (up to $\approx$ 600°C) are the evacuated tubular ones, this gap problem had to be properly addressed.

Besides, the gap losses are a natural consequence from the flow-line or Winston-Welford design method [11, 12] of secondary concentrators. In this sense, it became clear that the right path to overcome this problem was to design new second-stage concentrators with a different design approach, for tubular technology with gaps.

A possible solution came from the use of the Simultaneous Multiple Surface (SMS) method [11, 12, 30, 31]. This design method is known for its potential for the design of efficient optics and it differs from the flow-lines method by the fact of using a simultaneous and cooperative design of all the elements which composes the optic. This allows a design of optics with high tolerances (high acceptance-angles) and, therefore, a significantly approach to the limits of concentration. In collaboration with the company Light Prescriptions Innovators (LPI) [32] - the owner of the SMS patent - an agreement between the later and BES Renewable Energies Chair was achieved in order for this method to be used in this PhD thesis program.

The use of the SMS method required, at first, an in-depth study and understanding of the method, its characteristics and possibilities of application. On the other hand, a natural step in designing a Fresnel concentrator is to start with the particular case in which the optic is composed by a single heliostat (which is the case of a PT concentrator) and only afterwards to design it for a set of heliostats. In this sense, two scientific publications were done (Chapters 6 and 7) about a possible doubly-reflective SMS XX solution ("X" stands for a reflection) for continuum primaries and with a shape approximately parabolic and with a significantly reduction of Fresnel losses around the glass cover of the vacuum receiver tube:

- Chapter 6 - "New second-stage concentrators (XX SMS) for parabolic primaries; Comparison with conventional parabolic trough concentrators", with emphasis on the approximation of the theoretical limits of concentration [24].
- Chapter 7 - "Infinitesimal etendue and Simultaneous Multiple Surface (SMS) concentrators for fixed receiver troughs", with emphasis in the design of a SMS XX concentrator with the center of mass localized in the center of the tubular receiver [25].

These publications established the potential of the new concept and its merits, through a comparison with a commercial PT concentrator and the Helmet SMS concentrator [27]. This analysis also proved that the SMS XX concentrator proposed is viable and it can be a good option for Fresnel concentrators.

The application of the SMS XX to convencional LFR concentrators could now be carried on since, as mentioned before, there was a large room for improvements in LFR optics. One possibility for substantial improvement is proposed and resulted in the scientific publication (Chapter 8), originated by this PhD. thesis:

- Chapter 8 - "Simultaneous Multiple Surface method for Linear Fresnel concentrators with tubular receiver" [33].

Due to the time schedule Chapter 8 is the last work of this PhD thesis and fulfils the major objective of this PhD. thesis: to design a new LFR concentrator which reaches higher concentration factors and better global conversion efficiencies - and therefore it can be said that this work was quite successfully completed. Nevertheless, it is clear that there are still in numerous paths to explore and improvements to be achieved in the near future, with the application of the SMS method to other configuration of the LFR-type (LFR SMS XX asymmetric, CLFR "Etendue-Matched", etc.), as shall be discussed in the Chapter 9 (Future perspectives and lines of investigation).

1.3 Structure of the PhD thesis

This PhD thesis is structured as follows:

- Chapter 1: Background and general motivation.
- Chapter 2: Theoretical introduction and basic definition for the contextualization of the type of optics and main used tools.
- Chapters 3/4/5: Study of the CLFR "Etendue-Matched" concentrator in optical, thermal and storage/costs aspects.
- Chapters 6/7: Study of a SMS XX concentrator for continuum primaries and tubular receivers and discontinuous primaries with fixed receiver.
- Chapter 8: Study of a SMS XX concentrator for a Fresnel concentrator with tubular receiver.
- Chapter 9: Future perspectives and lines of investigation.
- Chapter 10: Discussion and Conclusions.

References

[1] Collares-Pereira, M., 1998, *Energias Renováveis, a Opção Inadiável*, Edição SPES - Sociedade Portuguesa de Energia Solar.

[2] CSP today, *http://social.csptoday.com/tracker/projects*.

[3] Crespo, L., *The European solar thermal electric market*, Intersolar European Conference, Munich, June, 2011.

[4] Morin, G., et al., *Comparison of Linear Fresnel and Parabolic Trough Collector power plants*, Solar Energy 86 (2012) 1-12.

[5] Morin, G., et al., *Comparison of linear Fresnel and parabolic trough collector system – influence of linear Fresnel collector design variations on break even cost*, Proceedings 15^{th} International SolarPACES Symposium, September, 14-18 (2009), Berlin, Germany.

[6] Dersh, J., et al., *Comparison of linear Fresnel and parabolic trough collector system – system analysis to determine break even costs of linear Fresnel collectors*, Proceedings 15^{th} International SolarPACES Symposium, September, 14-18 (2009), Berlin, Germany.

[7] Hoyer, M., et al., *Performance and cost comparison of linear fresnel and parabolic trough collectors*, Proceedings 15^{th} International SolarPACES Symposium, September, 14-18 (2009), Berlin, Germany.

[8] Areva Solar, *http://www.areva.com/EN/solar-220/areva-solar.html*.

[9] Novatec Solar, *http://www.novatecsolar.com/*.

[10] Solar Euromed, *http://www.solareuromed.com/en*.

[11] Winston, R., Miñano, J.C., Benítez, P., (contributions by Shatz, N., Bortz, J.,C.), *Nonimaging Optics*, Elsevier Academic Press, Amsterdam, 2005.

[12] Chaves, J., 2008, *Introduction to Nonimaging Optics*, CRC Press, Taylor and Francis Group.

[13] Mills, D., Morrison, G., *Compact Linear Fresnel Reflector solar thermal powerplants*, Solar Energy, Volume 68, Issue 3, Pages 263-283.

[14] Chaves, J., Collares-Pereira, M., *Etendue-matched two stage concentrators with multiple receivers*, Solar Energy 84 (2009), pp. 196-207.

[15] Chaves, J., Collares-Pereira, M.,(2009), *Primary concentrator with adjusted etendue combined with secondaries associated to multiple receivers and with convention reduction*, International patent application PCT/PT2009/000026.

[16] Canavarro, D., *Modeling linear solar collectors of the Fresnel-type; application to an innovative CLFR collector "Etendue Matched"*, MSc thesis, Instituto Superior Técnico/Universidade Técnica de Lisboa, Lisbon, 2010.

[17] Rabl, A., (1985), *Active solar collectors and their applications*, Oxford University Press, New York, Oxford.

[18] EDP Inovação, *http://www.edp.pt/pt/Pages/homepage.aspx*.

[19] Canavarro, D., Collares-Pereira, M., Lopes Guerreiro, L., *Increasing the efficiency of conventional LFR technologies: a new CLFR "Étendue Matched" CSP collector*, Proceedings 17^{th} International SolarPACES Symposium, September, 20-23, Granada (Spain), 2011.

[20] Horta, P., Collares-Pereira, M., Canavarro, D., Guerreiro, L., *Modeling thermal losses in a new CLFR "Etendue Matched" non-evacuated collector cavity*, Proceedings 17^{th} International SolarPACES Symposium, September, 20-23, Granada (Spain), 2011.

[21] Guerreiro, L., Canavarro, D., Collares-Pereira, M., *Increasing the cost effectiveness of CSP technologies through the development of a new CLFR "Etendue Matched" collector*, ISES World Congress, 28 August - 02 September, Kassel (Germany), 2011.

[22] Zarza, E., et al., *Advances in Parabolic Trough Solar Power Technology*, Journal of Solar Energy Engineering, MAY 2002, Vol. 124.

[23] Gordon, J.M., Ries, H., (1993), *Tailored edge-ray concentrators as ideal second stages for Fresnel reflectors*, Appl. Opt., 32, 2243.

[24] Canavarro, D., Chaves, J., Collares-Pereira, M., *New second-stage concentrators (XX SMS) for parabolic primaries; Comparison with conventional parabolic troughs concentrators*, Solar Energy, 92 (2013) 98–105

[25] Canavarro, D., Chaves, J., Collares-Pereira, M., *Infinitesimal etendue and Simultaneous Multiple Surface(SMS) concentrators for fixed receiver troughs*, Solar Energy, 97 (2013) 493—504

[26] Collares-Pereira, M., Gordon, J.M., Rabl, A., Winston, R., *High concentration two-stage optics for parabolic trough solar collectors with tubular absorber and large rim angle*, Solar Energy 47 (6), pp. 457-466, 1991.

[27] Benítez, P., *Advanced concepts of non-imaging optics: design and manufacture*, PhD Thesis, Presented in Madrid, January 16, 1998

[28] Mclntire, W. R., *New Reflector Design Which Avoids Losses Through Gaps Between Tubular Absorbers and Reflectors*, Solar Energy Volume 25, Issue 3, 1980, Pages 215–220.

[29] Mclntire, W. R., *Elimination of the Optical Losses Due to Gaps Between Absorbers and Their Reflectors*, Proc. 1980 Ann. Meeting 3.1:600. AS Int. Solar Energy Society.

[30] Miñano, J.C., *High efficiency nonimaging optics*, United States Patent 6.6639.733 B2, 2003.

[31] Miñano, J.C. and González, J.C., *New method of design of nonimaging concentrators*, Appl. Opt., 31, 3051, 1992.

[32] Light Prescriptions Innovators *http://www.lpi-llc.com/index.php.*

[33] Canavarro, D., Chaves, J., Collares-Pereira, M., *Simultaneous Multiple Surface method for Linear Fresnel concentrators with tubular receiver*, Accepted for publication in Solar Energy.

Chapter 2

Basic concepts and definitions

2.1 Introduction to Geometrical Optics

Geometrical optics is a class of optics obtained from Maxwell's equations in which the spatial variations of the electromagnetic field are much bigger than the wavelength [1]. At this small-wavelength limit the ray can be defined as a normal to any surface of constant phase of light waves (in terms of the wave theory of light). This surface is called geometrical wavefront, or simply a wave front, as long as its scale is a large number of wavelengths. Then a ray trajectory is a characteristic curve of this field of normals, i.e. tangent to the field at all its points, which coincides with the trajectory of the photons from the quantum perspective.

In geometrical optics the rays are deflected in accordance with the laws of refraction and reflection. When the light is reflected from a smooth surface the reflected ray make the same angle with the normal (α_r) as the incident ray (α_i) and, therefore, $\alpha_i = \alpha_r$. In this case both rays and the surface normal are coplanar. When a ray passes from one refractive medium (n_1) to another (n_2) its direction changes according to Snell's law (Eq. 2.1).

$$n_1 sin\alpha_i = n_2 sin\alpha_r \tag{2.1}$$

2.1.1 Fermat's Principle and Hamiltonian Formulation

There are several equivalent formulations of geometrical optics. One of them is Fermat's principle, which states that light travels the path which takes the least time. In other words, a ray is an extremal curve of the following curvilinear integral:

$$S = \int_{\mathbf{P}_1}^{\mathbf{P}_2} n\, ds = \int_{\mathbf{P}_1}^{\mathbf{P}_2} n(x, y, z)\, ds \tag{2.2}$$

Where $n(x, y, z)$ it is the refractive index of the medium at point (x, y, z) and ds is the differential of length along the integration path between points $\mathbf{P}_1$ and $\mathbf{P}_2$.

The value S calculated on the extremal curve (i.e., on the ray trajectory) is called the optical path length (OPL) [2].

The laws of refraction and reflection, the reversibility of ray trajectories and the equality of optical path between the rays of a continuous bundle linking two given points are deduced directly from Fermat's principle.

The other equivalent formulation of geometrical optics is Hamiltonian [3]. Suppose a ray that passes through a point (x,y,z) with a direction given by the unitary vector $\mathbf{v}$, and thus is represented as the 6-vector (x, y, z, p, q, r), where (p, q, r) are the respective optical direction cosines of the ray, (i.e., cosines of the ray's angles with the three coordinate axes – their squares must sum to one). Note that (p, q, r) are conjugate variables of (x, y, z). The Hamiltonian formulation states that the trajectories of the rays are given as solution of the following system of first-order ordinary differential equations:

$$\begin{aligned} \frac{dx}{dt} &= H_p \\ \frac{dy}{dt} &= H_q \\ \frac{dz}{dt} &= H_r \\ \frac{dp}{dt} &= -H_x \\ \frac{dq}{dt} &= -H_y \\ \frac{dr}{dt} &= -H_z \end{aligned} \tag{2.3}$$

Where H is the Hamiltonian function given by $H = n^2(x, y, z) - p^2 - q^2 - r^2$ and t a parameter without physical significance. The solution should be consistent with $H = 0$, as is deduced from the definition of (p, q,r).

2.1.2 Phase Space

The choice of coordinate axes can be done in such a way in which at least one direction cosine is positive. The value of the refractive index n is included in the definition of a ray as a five-parameter entity defined by a point and two direction cosines, each multiplied by n. This five-dimension space is called Extended Phase Space [4]. In an extended phase space, two rays that belong to the same line but do not have different direction can not be distinguished.

A ray-bundle M_{4D} (or ray manifold) is a four-parameter entity, a closed set of points in the extended phase space (and of the space x-y-z-p-q-r). We shall say that M_{4D} is a ray bundle when there do not exist two points in M_{4D} that belong to the trajectory of a ray (which means they represent the same ray at different

"instants" of the parameter t). Often, a ray manifold M_{4D} is defined at its intersection with a reference surface Σ_R, which must observe the condition of intersecting only the trajectories of the rays belonging to M_{4D}. This reference surface defines a four-parameter manifold called Phase Space. For instance, if all rays intersect a given surface at $z = f(x,y)$, they can be fully described as a 4-dimensional bundle $M_{4D}(x,y,p,q)$ with the condition of $r = \sqrt{n^2 - p^2 - q^2}$.

In 2D geometry, all these concepts can be defined similarly. For example, the extended phase space is the three-dimensional sub-manifold, defined by $p^2 + q^2 = n^2(x, y)$, in the four-dimensional space of coordinates x-y-p-q. The reference surface becomes a curve in the xy plane, where a ray-bundle m_{2D} is a two parameter entity.

2.1.3 Poincaré Invariants. Concept of étendue. Hilbert's integral

Let M_{4D} be a tetraparametric ray bundle (dimension$(M_{4D}) = 4$). The étendue of the bundle M_{4D} is defined as the value of the integral [5]:

$$E(M_{4D}) = \int_{M_{4D}(\sum_R)} dxdydpdq + dxdzdpdr + dydzdqdr \tag{2.4}$$

The etendue is a measure of "how many" rays a bundle has. If the reference surface is a plane $z = c^{te}$, only the first addend of the integrand in Eq. 2.4 is non-null, and the étendue coincides with the volume defined by M_{4D} in the phase space x-y-p-q.

The conservation of the étendue states that this is an invariant of the ray bundle when it is propagated through an optical system, that is, it is independent of the reference surface on which it is calculated. The étendue it is one of the invariants of Poincaré, and this theorem is equivalent to the Liouville theorem in three dimensions [2, 5].

There is another Poincaré invariant named étendue for the bi-parametric rays (not necessarily coplanar). If m_{2D} is a bi-parametric ray bundle, the étendue for this bundle is [6]:

$$E(m_{2D}) = \int_{m_{2D}(\sum_R)} dxdp + dzdr + dydq \tag{2.5}$$

This second invariant is equivalent to Lagrange's invariant [3]. When the rays of the bundle are coplanar, this invariant is also equivalent to Lioville's theorem in 2D. Since the étendue must be conserved for any ray bundle, the differential étendue – the integrand of Eq. 2.4 and Eq. 2.5 – is also conserved.

A formulation equivalent to the invariant of Eq. 2.5 is obtained by applying Stoke's Theorem to the integral, which gives rise to the so-called Hilbert's integral [7]:

$$E(m_{2D}) = \oint_{2D(\sum_R)} (p, q, r)\vec{dl} \tag{2.6}$$

Which is the integral extending along the border of m_{2D} in the phase space of the reference surface. A particular case of the two-dimensional bundle are orthotomic (or normal) bundles, which are those for which a wave front can be defined, that is, for which there exists a surface to which they are orthogonal. It can be seen that a bundle m_{2D} is orthotomic if and only if $E(m_{2D}) = 0$ [3].

2.1.4 Geometrical Optics in 2D

The 2D Geometrical Optics develops in a similar way to the 3D case. In 2D geometry the concepts of ray bundle, phase space and extended phase space can equally be defined. Extended phase space will be the 3D manifold $p^2+q^2 = n^2(x,y)$ of the 4D space with coordinates x-y-p-q, and the reference surfaces will now be reference curves in the plane x-y. A bundle of rays M will have a dimension of at the most two (one less than the extended phase space), which is the dimension of the phase space of the reference surface. The étendue of M coincides with Poincaré's invariant for 2D bundles, given by Eq. 2.5, and is calculated as the area in the phase space x-p when the reference curve is a straight line $y = c^{te}$. As for terminology, we shall call the mirrors and dioptrics "optical surfaces" both in 3D and 2D geometry, although in 2D they are actually curves.

2.1.5 Concept of radiance. Sources and receivers

Physical significance of the étendue of a ray bundle is related to the luminous power it transports. The definition of luminous power in radiometry is based on the concept of radiance (luminance in photometry), as a property of light source, but it can also be defined as the infinitesimal power of a ray coming from that source. The concept of radiance has been well defined for incoherent light, very appropriate for a geometrical optics concept.

As well-known, radiance B in 3D is the power transferred per unit area normal to the ray trajectory and per unit of solid angle. Thus, the differential of power transferred by a ray having solid angle $d\Omega$ through the infinitesimal element of surface dS will be (see Fig. 2.1):

$$dP = Bd\Omega(\vec{v} \cdot dS) \tag{2.7}$$

Where $\vec{v} = (\frac{p}{n}, \frac{q}{n}, \frac{r}{n})$ and n is the refractive index. In spherical coordinates:

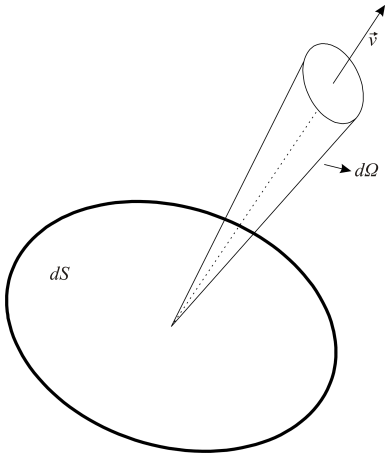

Fig. 2.1: Definition of radiance.

$$\begin{aligned} p &= n\cos\phi\sin\theta \\ q &= n\sin\phi\sin\theta \\ r &= n\cos\theta \end{aligned} \tag{2.8}$$

Therefore, one gets:

$$\begin{aligned} dpdq &= \left|\frac{\partial(p,q)}{\partial(\phi,\theta)}\right| d\phi d\theta = n^2\sin\theta\cos\theta d\phi d\theta \\ dpdr &= \left|\frac{\partial(p,r)}{\partial(\phi,\theta)}\right| d\phi d\theta = n^2\sin\phi\sin^2\theta d\phi d\theta \\ dqdr &= \left|\frac{\partial(q,r)}{\partial(\phi,\theta)}\right| d\phi d\theta = n^2\cos\phi\sin^2\theta d\phi d\theta \end{aligned} \tag{2.9}$$

From Eq. 2.8 and Eq. 2.9 we obtain:

$$\begin{aligned} d\Omega(\vec{v}\cdot d\vec{S}) &= (d\phi d\theta\sin\theta)\left[(\frac{p}{n},\frac{q}{n},\frac{r}{n})\cdot(dydz,dxdz,dxdy)\right] \\ &= \frac{1}{n^2}(dxdydpdq + dxdzdpdr + dydzdqdr) \\ &= \frac{dE}{n^2} \end{aligned} \tag{2.10}$$

Therefore the differential of power carried by the ray is proportional to the differential of étendue, with proportionality constant $B/n^2 dE$. As the étendue is conserved, and in a medium without losses the differential power also, the magnitude B/n^2 remains constant along any ray in that medium.

A surface that emits rays with any directional distribution of radiance over a hemisphere is called an extended source. When the radiance of all rays is constant,

the source is said to be Lambertian. If the radiance is constant in a subset of all possible directions and null in the rest, the source is said to be homogeneous. A receiver, understood as a surface sensitive to radiation, can be said to be Lambertian when its sensitivity is the same at all its points and for all directions of incidence [4].

The power of a ray bundle M crossing a reference surface Σ_R, with a known radiance distribution, is calculated by integrating in solid angle and area. From Eq. 2.10 it is deduced that if the bundle is homogeneous with radiance B, its power is proportional to its étendue:

$$P = \int_{M(\Sigma_R)} Bd\Omega(\vec{v}d\vec{S}) = \frac{B}{n^2}\int_{M(\Sigma_R)} dE = \frac{B}{n^2}E \tag{2.11}$$

The same definitions are valid in 2D, simply by changing the terms surface and solid angle for curve and angle. The proportionality constant between power and étendue in 2D case is B/n.

2.2 Introduction to Non-imaging Optics

Nonimaging optics (also called anidolic optics) is the branch of optics concerned with the optimal transfer of light radiation between a source and a target. Unlike traditional imaging optics, the techniques involved do not attempt to form an image of the source; instead an optimized optical system for optical radiative transfer from a source to a target is desired. A schematic representation of the difference between imaging optics and nonimaging optics can be seen in Fig. 2.2. Non-Imaging Optics is important to this thesis, seeking to find new ways of concentrating solar radiation to the highest values possible. Non-Imaging Optics (NIO) establishes the limits that are attainable for any given acceptance angle to be considered. Conventional focusing or imaging optics falls much short of those limits. It is precisely because the imaging capacity is no longer sought after in NIO, that the highest values can be reached for pure flux concentration.

2.2.1 Design problem in Nonimaging Optics

Nonimaging optics system essentially transfers the light power between two ray bundles. We may define the input bundle (M_i) as a bundle of rays impinging on the surface of the entry aperture of the nonimaging device, and the output (M_o) bundle a bundle of rays that connects the surface of the device's exit aperture with the receiver. Every optical design starts with a definition of input and output bundles. The set of rays common to M_i and M_o is called the collected bundle M_c. The input and output bundles are coupled by the action of the device. The output bundle M_o

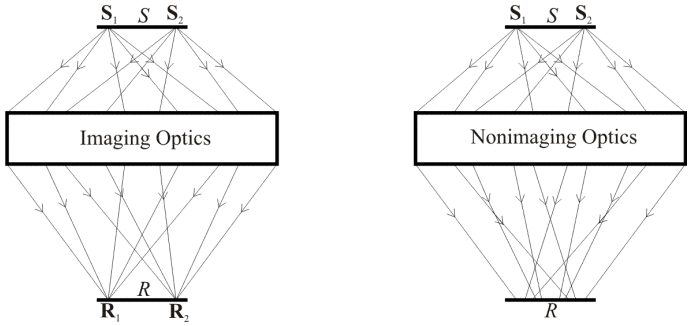

Fig. 2.2: In an imaging optics (left) the rays emitted from two points $\mathbf{S}_1$ and $\mathbf{S}_2$ inside of a source S are redirected by the imaging optical system to points $\mathbf{R}_1$ and $\mathbf{R}_2$ inside of a receiver R forming an image. In a Nonimaging optics (right) the same rays are redirected to the receiver but not necessarily forming an image (the rays are dispersed along the receiver R).

is a subset of the bundle formed by all the rays that can impinge on the receiver named M_R (e.g. in thermal concentrators M_R is the ray bundle that isotropically illuminates the receiver).

The design is loss-free when the bundle of collected rays M_c coincides with M_i. Ideal design is a design that perfectly couples the bundles M_i and M_o (i.e. $M_i = M_o = M_c$), and maximal one is a design that fulfils $M_c = M_o = M_R$. Optimal design is both ideal and maximal. In practice, it is not necessary for nonimaging designs to be maximal or ideal.

There are two main groups of design problems in nonimaging optics. The first group is called bundle-coupling and has the objective of maximizing the light power transferred from the source to the receiver. The design problem is to specify bundles M_i and M_o, and to design the nonimaging device to couple two bundles, i.e. $M_i = M_o = M_c$. This literally means that any ray entering the optical system as a ray of the input bundle M_i exits as a ray of the output bundle M_o, i.e. we have an ideal design. These types of problems are to be solved in collimators, condenser optics for a projector, light injection into an optical fiber, radiation sensors, thermal/photovoltaic concentrators, etc.

The second group of design problems is focused on obtaining a desired pattern at a certain target surface and it is called prescribed irradiance problem. In this type of design problem, it is only specified that one bundle must be included in the other, for example, M_i in M_o (so that M_i and M_c coincide), with the additional constraint that the bundle M_c produces a prescribed irradiance distribution on the target surface at the output side. As M_c is not fully specified, this problem is less restrictive than the bundle-coupling one. These designs are useful in automotive lighting, the light source being a light bulb or a LED and the target surface being the far field, where

the intensity distribution is prescribed. Street lights, RGB color blending, backlights, etc. are examples of possible applications where prescribed irradiance problem is to be solved.

Thermal or Concentrated Solar Power concentrators represents a good example of a design problem where both the bundle coupling problem (for obtaining maximum Concentration-Acceptance angle Product (CAP) [8, 9]) as well as the prescribed irradiance problem (uniform irradiance distribution on the receiver) may be needed in order to avoid the occurrence of hot-spots which may penalize the performance of the concentrator. This is a very difficult task and only partial solutions are available.

2.2.2 Geometric concentration and acceptance angle

Let M_i be the bundle with infinite source with acceptance angle θ defined by the entry aperture of the concentrator. Let us suppose that the refractive index of the medium surrounding the entrance is unit and that which surrounds the receiver is n. From conservation of the étendue it is deduced that if the concentrator collects the bundle M_i (i.e., M_i is part of M_R), the following inequality is verified [2, 4, 5]:

$$E(M_i) = A_E \pi \sin^2\theta \leqslant A_R \pi n^2 = E(M_R) \tag{2.12}$$

A_E and A_R being the areas of the entry aperture and of the receiver. From here it is deduced that, if we call the ratio between the area of the entry aperture and that of the receiver the geometric concentration:

$$C_g = \frac{A_E}{A_R} \leqslant \frac{n^2}{\sin^2\theta} = C_{Max} \tag{2.13}$$

Therefore a maximum limit of geometric concentration exists if the aim is to collect the entire bundle M_i, a limit associated with the use of the maximum étendue of the receiver. In two-dimensional geometry, this limit is:

$$C_g(2D) = \frac{L_E}{L_R} \leqslant \frac{n}{\sin\theta} = C_{Max}(2D) \tag{2.14}$$

L_E and L_R being the length of the entry aperture of the concentrator and that of the receiver, respectively.

2.2.3 Edge-ray Principle

The edge-ray principle is a fundamental tool in nonimaging optics design. This theorem states that for an optical system to couple two ray bundles M_i and M_o it suffices to couple bundles δM_i and δM_o, being the δM_i and δM_o the edge-ray subsets of bundles M_i and M_o (and as perimeters they have one dimension less). A perfect matching between bundles M_i and M_o implies the coupling of their edge-rays. This

theorem was proven by Miñano [10] in the mid-eighties, and Benítez [4] extended this demonstration in the late nineties. The edge-ray principle is the design key in most nonimaging devices, and shows the benefits that arise from the elimination of the imaging requirement.

2.2.4 Numerical calculation of performance parameters of a generic solar concentrator

Due to the complexity of the concentrators and the number of parameters which characterizes the latter, it is common nowadays to use a raytracing software in order to calculate the performance parameters, instead of using the standard analytical approach. In this sense, it is important to define which inputs should be considered in order to calculate efficiently the most common parameters, such as the optical efficiency, CAP, etc. Fig. 2.3 shown schematically what are the necessary parameters in order to perform a numerical calculation of the performance parameters.

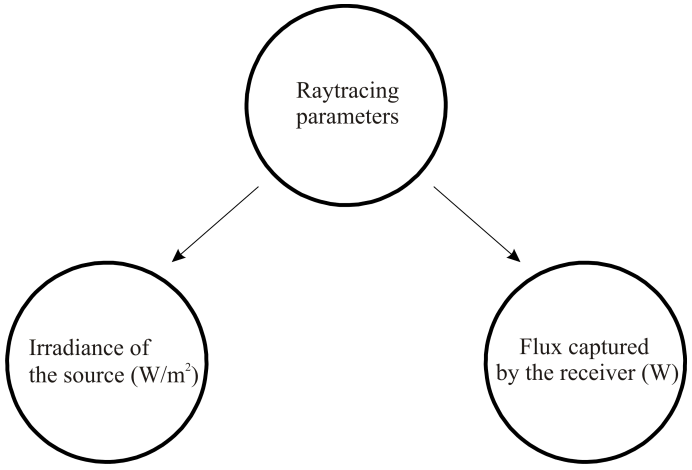

Fig. 2.3: The calculation of performance parameters of a generic solar concentrator can be done using a raytracing software. Only two parameters are necessary: the irradiance of the source and the flux captured by the receiver.

From these two parameters all the common parameters can be calculated.

- Optical Efficiency (η_{opt}): It is the ratio between the flux captured by the receiver and the flux intersected by the optic. This calculation can be done using a list of material proprieties for all the optical elements which composes the concentrator and also with a solar angular profile ($\simeq 0.27^{o}$) for a more practical calculation.
- Geometric Concentration (C_g): It is the ratio between the mean irradiance on the receiver (which can be calculated from the value of the flux captured by

it) and the irradiance of the source. This calculation should be done with an ideal material properties for all the optical elements as C_g only depends on the geometry of the concentrator.

- Incidence Angle Modifier (IAM): It is the variation of the flux captured the receiver for different incidence (zenith) angles θ_Z [11] (see Fig. 2.4) for the transversal and longitudinal planes (i.e., with the solar azimuth angle φ_S fixed at 0º and 90º, respectively). For this calculation the optic tracks the apparent motion of the sun in the sky.

- Acceptance angle (θ): It is defined as the incidence angle for which the flux captured by the receiver is 90% of the on-axis power. For this calculation the optic and all its components remains static as the sun moves in the sky.

- Concentration Acceptance Product (CAP): It is defined by the expression CAP $= C_g \sin\theta$.

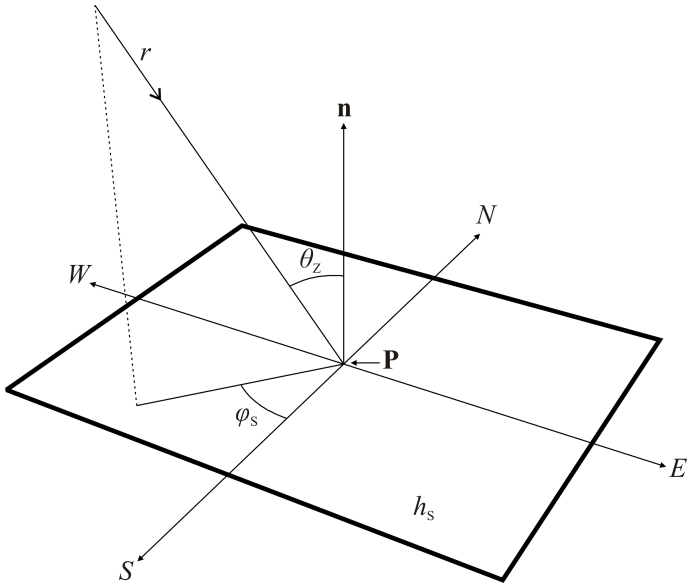

Fig. 2.4: Definition of θ_Z and φ_S. A ray r, representing the sunlight for a certain incidence direction, hits a horizontal surface h_S at a point **P** making an angle θ_Z with its normal **n**. On the other hand, the projection of r onto h_S makes an angle φ_S with the North-South axis.

As can be seen, this approach is absolutely generic for any concentrator and simple at the same time. This increases the reliability of the calculations and leads to a very comprehensive analysis.

References

[1] Born, M., Wolf, E., (1975), *Principle of Optics*, Pergamon, Oxford.

[2] Chaves, J., 2008, *Introduction to Nonimaging Optics*, CRC Press, Taylor and Francis Group

[3] Luneburg, R.K., (1964) *Mathematical theory of Optics*, U. California, Berkeley.

[4] Benítez, P., *Advanced concepts of non-imaging optics: design and manufacture*, PhD Thesis, Presented in Madrid, January 16, 1998.

[5] Winston, R., Miñano, J.C., Benítez, P., (contributions by Shatz, N., Bortz, J.,C.), *Nonimaging Optics*, Elsevier Academic Press, Amsterdam, 2005.

[6] J.C. Miñano, *Aspectos relativos a la síntesis de concentradores para fuentes solares extensas*, PhD. Thesis, E.T.S.I. Telecomunicación, Madrid (1985).

[7] Stavroudis, O.N., (1972), *The optics of rays, caustics, and wavefronts*, Academic, New York.

[8] Canavarro, D., Chaves, J., Collares-Pereira, M., *New second-stage concentrators (XX SMS) for parabolic primaries; Comparison with conventional parabolic troughs concentrators*, Solar Energy, 92 (2013) 98–105.

[9] Benítez, P., et al., *High performance Fresnel-based photovoltaic concentrator*, Optical Society of America, 26 April 2010, Vol. 18, No. S1, OPTICS EXPRESS.

[10] Miñano, J.C., *Two-dimensional nonimaging concentrators with inhomogeneous media: a new look*, J. Opt. Soc. Am. A 2(11), pp. 1826-1831, 1985.

[11] Rabl, A. (1985), *Active Solar Collectors and their applications*, Oxford University, Oxford.

Chapter 3

Increasing the efficiency of conventional LFR technologies: A new CLFR "Etendue Matched" CSP collector†

Abstract

Solar concentrating technologies are seen as an important part of the strategy to increase the production of both renewable electricity and heat. Several technologies have been proved to be technically feasible; commercial Parabolic Trough systems (PTR) have been in the lead in installed capacity in new power plants. One promising technology that has a lower investment cost per m^2 is the LFR, Linear Fresnel Reflector collector. First demonstration plants in Spain and in the USA, are proving the concept technically, but failing yet to be a generalised choice, since their global efficiency conversion is still low. CLFR technology said to be "Etendue Matched" and designed to take full advantage of ideal non-imaging optics is very promising alternative. In fact, through a joint optimization of primary and secondary stages of concentration, it is possible to find an answer to this problem, practically doubling the achieved concentration in conventional LFR configurations, substantially reducing optical losses due to shading and blocking and taking advantage of a multi-receiver design (that is what "C" stands for). The present paper explains the concept and describes the prototype being proposed for demonstration.

Keywords: CLFR "Etendue Matched", Concentrating Solar Power, Non-imaging Optics

---

†Diogo Canavarro[(1)], Luís Lopes Guerreiro[(1)], Manuel Collares-Pereira[(1)], Increasing the efficiency of conventional LFR technologies: A new CLFR "Etendue Matched" CSP collector, Proceedings 17th International SolarPACES Symposium, September, 20-23, Granada (Spain), 2011.

[(1)] BES Renewable Energies Chair, University of Évora.

3.1 Introduction

One of the problems with conventional LFR plants (Fig. 3.1) is the blocking and shading effect of the reflectors on each other, a consequence of the fact that etendue is not conserved which implies that undesirable losses are present plus maximum concentration is not achieved [1, 2]. Is important to correct the mismatch and approach and the concentration limits, which is, for a receiver immersed in air or vacuum (refractive index $n = 1$) and a 2D optics [3]:

$$C \sin(\theta) = 1 \tag{3.1}$$

Where C is the geometrical concentration and θ is the half-acceptance angle. This equation is also known as CAP - Concentration-Acceptance Product - which being applied to a concentrator it informs us how close is the latter to the theoretical limits. The CAP can be used, therefore, to perform a fair comparison between different concentrators, even if they are not from the same type/technology, since it is an equation absolutely generic.

Fig. 3.1: One LFR system (AUSRA) with mirrors facing the absorber constituted by a series of tubes, placed next to each other.

Concentration not being maximized makes it harder to operate at higher temperatures for higher efficiency in heat to electricity energy conversion. Present LFR demonstration or commercial plants operated with saturated steam at $270^{o}C$ rather than temperatures above $400^{o}C$ as can be obtained with PTRs and Tower concepts. There are other consequences from not having an optimized designed like not having as little land as possible for the collector, which also may influence costs. In previous work, comparisons between LFR and PTR technologies were made showing the difficulties of LFR systems, even when non-imaging second-stage concentrators of the type CEC (Compound Elliptical Concentrator) are used [4, 5, 6]. This happens, as was said before, due to the mismatch of the etendue between the incoming

and reflected light. It is important to notice that conserving the etendue, do not necessarily implies the achievement of the maximum CAP; for example, the (ideal) parabola - either for a flat or circular receiver - fall short of the theoretical limit, i.e., $\mathrm{CAP}_{Parabola} \ll 1$, but the correction of the mismatch can significantly improve the global behaviour of the optics [2].

Another important disadvantage of the conventional LFR is the rim angle. It was previously demonstrated that for conventional LFR the optimum rim angle is 40.4^{o} which corresponds to an (ideal) optical efficiency $\eta_{opt} = 0.91$ [1, 2]. But wider rim angles are desirable since they reduce the height of the receiver and, therefore, increase the compactness of the system.

The CLFR "Etendue Matched" concentrator appears as one strong possibility in order to solve these difficulties. Since the etendue of the reflected light is smaller that the etendue of the incoming light ($\cos(\phi)$ factor, where ϕ is defined as the angle to the vertical of the line connecting the receiver and the point of the heliostat field), one can reflect the "excess" towards another receiver, as shown in Fig. 3.2.

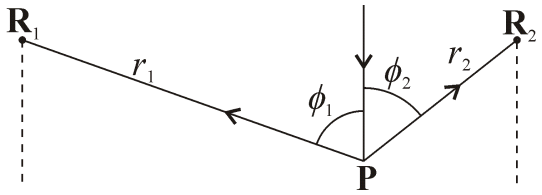

Fig. 3.2: Geometry of incoming and reflected light at a point **P** of a reflector for two receivers $\mathbf{R}_1$ and $\mathbf{R}_2$.

Now one can perform and etendue balance at point **P** (see Fig.3.3). The etendue of the incoming radiation in the vertical direction is given by $dU_0 = 2dl\cos\alpha\sin\theta$. The etendue of the light reflected to receiver $\mathbf{R}_1$ is $dU_1 = 2dl\cos(\theta_1 - \alpha)\sin\theta$ and that of the light reflected towards $\mathbf{R}_2$ is $dU_2 = 2dl\cos(\theta_2 + \alpha)\sin\alpha$. Conservation of etendue can then be written as [2]:

$$dU_0 = dU_1 + dU_2 \Rightarrow \cos(\phi_1 - \alpha) + \cos(\phi_2 + \alpha) = \cos\alpha \tag{3.2}$$

Given the position of receivers $\mathbf{R}_1$ and $\mathbf{R}_2$ and of point **P** angles ϕ_1 and ϕ_2 can be determined. Eq. 3.2 can then be used to calculate angle α. Performing this calculation for a certain starting point, we get the etendue-conserving curve as shown in Fig.3.4.

The symmetric etendue-conserving curve introduces a rim angle at the middle point **M** of 60^{o}, which dramatically decreases the height of the receivers and the second-stage concentrator TERC (Tailored Edge Ray Concentrator) allows a significantly approach to the ideal CAP [7].

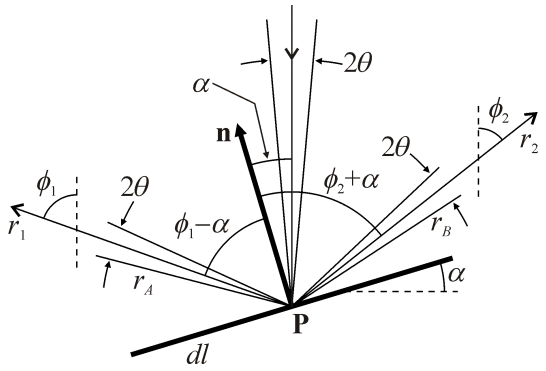

Fig. 3.3: Etendue balance at a point **P** of a Fresnel reflector for two receivers.

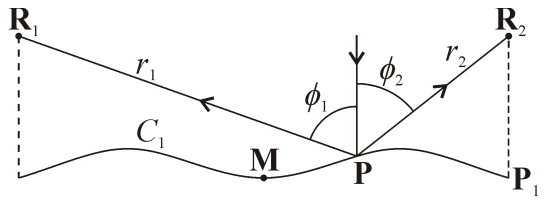

Fig. 3.4: Etendue-conserving curve.

In the present paper we present for the first time a practical solution for a CLFR "Etendue Matched" as shown in Fig.3.5, following the concepts covered by [8] and explained in [1, 2].

This new design has a set of advantages comparing to conventional LFR power plants, namely, increased energy collected per m^2 at higher temperature, the secondary receptor closer to the ground, lower land area usage. This is achieved through a joint optimization of primary ans secondary concentration to come as close as possible to the theoretical limit for a geometric concentration of 58× (which corresponds to an ideal acceptance-angle of $\approx 1^o$), with the reflectors being positioned along an etendue-conserving curve. This model was subject to optical and thermal (numerical) analysis with appropriated tool [9, 10]. In the next section we will see some of the results obtained.

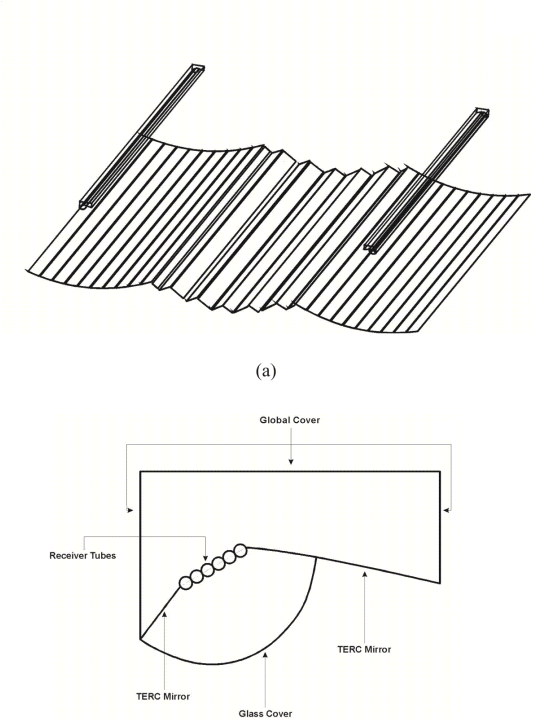

Fig. 3.5: a) Proposal for a new design for an improved CLFR plant with two collectors tubes; b) Cross-section of left side absorber cavity.

3.2 Results and Discussion

The analysis made was divided in two parts. In the first one, an optical model was developed and its optical efficiency, η_{opt}, was calculated with the raytracing method, for different θ_Z (zenite angle) and φ_S (solar azimuth angle) and 1000 rays for each iteration. The Fig.3.6 shows the raytracing for the perpendicular direction (using the solar angular profile) and Fig.3.7 shows η_{opt} as a function of θ_Z and φ_S.

The raytracing method allows us to calculate several parameters, such as IAM (Incidence Angle Modifier) or the acceptance angle [11] as shown in Fig.3.8.

The angle θ obtained was 0.514^o (considering the point at which losses relative to the maximum represent 90% of the value) which results, for an effective concentration of 58× (60× was the chosen concentration but must be taken into account the projected mirror area into the sun direction, in this case the perpendicular one (θ_Z=φ_S=0) for North-South direction) a CAP of 0.52.

In another paper, these optical results were combined with the thermal analysis developed and a final efficiency at perpendicular direction, η_0, for a receiver composed by a series of non-evacuated tubes, could be obtained, as shown in Table 1.1 [12].

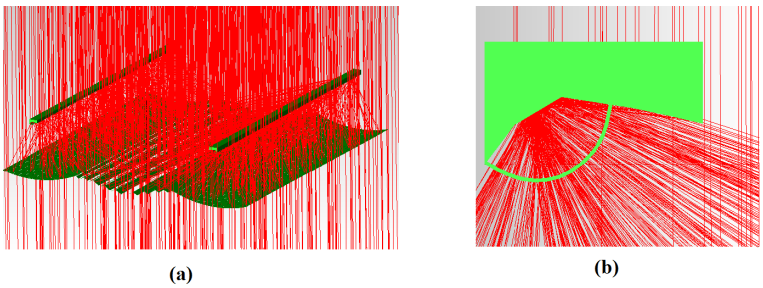

Fig. 3.6: a) 3D raytracing; b) Details on the cavity.

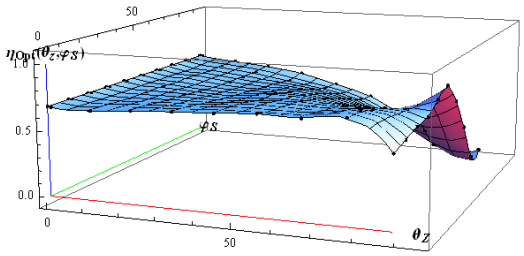

Fig. 3.7: η_{opt} as a function of θ_Z and φ_S. The black dots represent the results for each raytracing iteration.

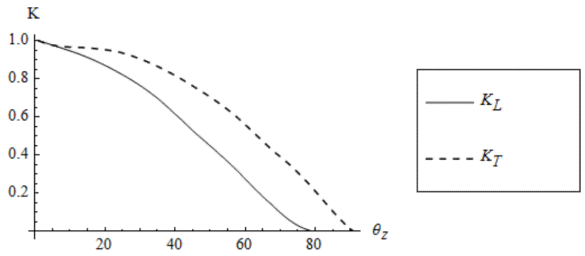

(a)

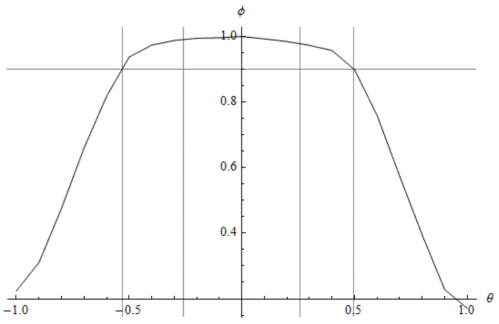

(b)

Fig. 3.8: a) IAM curves for longitudinal (K_L) and transversal (K_T) directions; b) Total acceptance-angle.

Table 3.1: Efficiencies by ground area and mirror area for perpendicular direction at different temperatures.

T_{abs}(°C)	$\eta_{0GroundArea}$ (%)	$\eta_{0MirrorArea}$ (%)
25	70	78
400	63	70

Where T_{abs} is the temperature of the absorber and the differentiation between ground area and mirror area is introduced due to the spacing between heliostats, i.e., mirror area < ground area.

These results are very promising. The CAP value obtained represents a new step towards the theoretical limits, much superior to the one obtained for current technologies. For PTRs, for example, which are composed by a parabola with a circular receiver, the maximum CAP is ≈ 0.32 $(1/\pi)$ [1] and, thefore, the CLFR "Etendue Matched" configuration developed represents an increase of 63.4% relative to the latter, with high possibilities of improvement in future as new studies and configurations are performed. The efficiencies obtained are also very interesting - especially when taking into account that solar angular profile, non-ideal surface errors and angular variation of optical properties were included [12]. This demonstrates the advantage of using the etendue balance into the design of CSP systems to achieve better performances and, in this sense, what CLFR with "Etendue Matched" primary and secondary optics allow is for more energy delivered at higher temperatures thus enhancing the overall solar energy conversion into electricity, since conversion efficiency is combined with a high CAP [9].

3.3 The demonstration plant

In collaboration with EDP-Inovação a demonstration plant is planned to be built in a near future in Évora, Portugal (Lat.: 38.4ºN; Long.: 7.9ºW). The reflector configuration (nr. mirrors, size, etc.) is currently being optimized taking into consideration practical issues. For instance, there are no (today) commercially available non-evacuated tubes to operate above temperatures of 400ºC. In order to circumvent this difficulty, a new type of configuration is being developed for vacuum tubes, practically with no gap losses between the glass cover and receiver, and therefore, with high efficiency and getting as close as possible to the theoretical limits. Another important technical issue is the number of heliostats. It would be desirable to have a large number of small heliostats with different lengths and curvatures, so they could be more adjustable to the etendue-conserving curve (which is in the ideal

case composed by an infinite number of heliostats), but this would also increase the costs (number of trackers, manufacture of the heliostats, etc.). By other hand, if the etendue-conserving curve isn't minimally adjusted the optical behaviour of the system will be penalized, i.e., CAP value will decrease. In this sense, the optimization being performed takes into account these topics, developing a commitment between performance and economical components [13]. At the present moment this model (which can be modified depending o the outcome of the analysis performed) has an area of 530 m^2 ($\approx 22\ m \times 24\ m$), two receivers at $6m$ above the ground, 24 heliostats with $0.55m$, $0.9m$ and $1.20m$ of length and a mean curvature of $19m$. The heliostats will be mounted on a steel structure of rectangular type which ensures their ability to act on a shaft (tracking) the relative height needed to put each one on the curve that keeps the etendue-balance.

In short, this project will enable the measurement of the effective efficiency of this new design and get a closer look to the advantages of the concept "Etendue Matched" applied to Fresnel concentrators.

References

[1] Collares-Pereira, M., *Etendue matched reflective Fresnel concentrators*, Proceedings 15th International SolarPACES Symposium, September, 14-18, Berlin (Germany), 2009.

[2] Chaves, J., Collares-Pereira, M., *Etendue-matched two stage concentrators with multiple receivers*, Solar Energy 84 (2009), pp. 196-207.

[3] Chaves, J., (2008), *Introduction to nonimaging optics*, CRC Press, Boca Raton FL.

[4] Morin, G., et al., *Comparison of linear Fresnel and Parabolic Trough collector system - influence of linear Fresnel collector design variations on break even cost*, Proceedings 15th International SolarPACES Symposium, September, 14-18, Berlin (Germany), 2009.

[5] Dersh, J., et al., *Comparison of linear Fresnel and Parabolic Trough collector system - system analysis to determine break even costs of linear Fresnel collectors*, Proceedings 15th International SolarPACES Symposium, September, 14-18, Berlin (Germany), 2009.

[6] Hoyer, M,, et al., *Performance and cost comparison of linear Fresnel and Parabolic Trough collectors* Proceedings 15th International SolarPACES Symposium, September, 14-18, Berlin (Germany), 2009.

[7] Gordon, J.M., Ries, H., (1993), Tailored edge-ray concentrators as ideal second stages for Fresnel reflectors, Appl. Opt., 32, 2243.

[8] Chaves, J., Collares-Pereira, M.,(2009), *Primary concentrator with adjusted etendue combined with secondaries associated to multiple receivers and with convention reduction*, International patent application PCT/PT2009/000026.

[9] Canavarro, D., (2010), *Modelling linear solar collectors of the Fresnel-type; application to an innovative CLFR collector "Etendue Matched"*, MSc thesis, Instituto Superior Tecnico/Universidade Tecnica de Lisboa, Lisbon.

[10] Horta, P., (2011), *Study and mitigation of internal convection processes inside a Compound Parabolic Concentrator solar collector*, PhD thesis, Instituto Superior Tecnico/Universidade Tecnica de Lisboa, Lisbon.

[11] Rabl, A., (1985), *Active solar collectors and their applications*, Oxford University Press, New York, Oxford.

[12] Horta, P., Collares-Pereira, M., Canavarro, D., Guerreiro, L., *Modeling thermal losses in a new CLFR "Etendue Matched" non-evacuated collector cavity*, Proceedings 17th International SolarPACES Symposium, September, 20-23, Granada (Spain), 2011.

[13] Lopes Guerreiro, L., Canavarro, D., Collares-Pereira, M., *Increasing the cost effectiveness of CSP technologies trough the development of a new CLFR "Etendue Matched" collector*, ISES solar world congress, 28 August-2 September, Kassel (Germany), 2011.

Nomenclature

C	geometrical concentration ($\times$)
dU	infinitesimal etendue
CAP	concentration-acceptance product
CEC	Compound Elliptical Concentrator
CLFR	Compact Linear Fresnel Reflector
IAM	Incidence Angle Modifier
LFR	Linear Fresnel Reflector
n	refractive index
PTR	Parabolic Trough Reflector
TERC	Tailored Edge Ray Concentrator
U	etendue

Greek symbols

α	tilt angle, (grad)
η_{opt}	optical efficiency
θ	acceptance angle, (grad)
θ_Z	solar zenith angle, (grad)
ϕ	rim angle, (grad)
φ_S	solar azimuth angle, (grad)

Chapter 4

Modeling thermal losses in a new CLFR "Etendue Matched" non-evacuated collector cavity[†]

Abstract

A new CLFR concentrating optics has been proposed [1, 2] and patented [3] and a project is being initiated at the University of Évora, to test the concept on a scale of a collector field with a mirror area of about 530 m^2. The goal will be to demonstrate the possibility of a collector instantaneous efficiency above 60% at 450°C, extrapolating from tests carried out to at least 400°C. The present paper addresses the optical and thermal characterization of the second stage non-evacuated concentrator, an asymmetric TERC [4] type cavity optimized simultaneously with the étendue matched primary, after simulation results obtained with an integrated numerical tool designed for such purposes [5]. The presented optical and thermal losses results are a crucial guide for the final design of the proposed CLFR concept, prior to actual prototype production and installation for real performance tests.

Keywords: CLFR "Etendue Matched", Concentrating Solar Power, Non-imaging Optics; Modeling thermal losses

---

[†]Pedro Horta[(1)], Manuel Collares-Pereira[(1)] Diogo Canavarro[(1)], Luís Guerreiro[(1)], Modeling thermal losses in a new CLFR "Etendue Matched" non-evacuated collector cavity, Proceedings 17th International SolarPACES Symposium, September, 20-23, Granada (Spain),2011.

[(1)] BES Renewable Energies Chair, University of Évora.

4.1 Introduction

The performance of an optical system converting a (solar) radiative flux into heat is a matter of combined optical and thermal effects. In the present paper, a preliminary performance assessment to the asymmetric non-evacuated TERC [4] absorber cavity designed as secondary concentrator for a new CLFR "Étendue Matched" system [2], is presented. This study follows a preliminary design of the entire primary and secondary CLFR system, composed by a field of heliostats illuminating a secondary concentrator cavity accommodating the absorber, as illustrated in Fig. 4.1 [6].

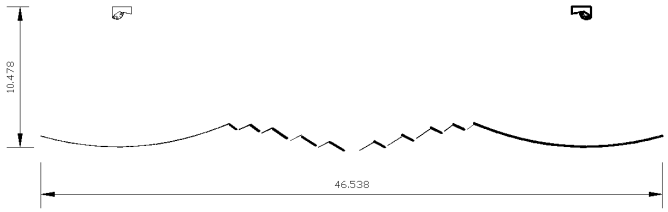

Fig. 4.1: Front view of the full CLFR system with double asymmetrical TERC cavity design.

The system optical assessment results from a ray-trace analysis to a transversal section, considering real optical properties (and corresponding angular variation) of the different materials assumed for reflectors, glazing or absorber surfaces, including image spread effects due to solar disk shape and reflector surface errors. A thermal assessment results from a finite element approach to the fluid flow occurring inside the secondary TERC concentrator cavity. The definition of heat flux boundary conditions enables a complete analysis to the different heat loss terms affecting the system performance at a given operation temperature. Considering the previewed operation conditions, a 400°C absorber temperature was considered in this analysis.

4.2 Optical assessment

The optical assessment of the system is traduced in an optical efficiency, η_{0b}, a ratio of the radiative fluxes reaching the absorber and available at full system aperture, Q_{aper}. Such parameter allows comparison of different radiative flux concentrating systems, accounting also for land occupation. An alternative optical efficiency might be referred to the radiative flux available in the projected area of the primary system, Q_{proj} , here represented by η^*_{0b}. The cavity is composed by two lateral TERC shaped reflectors, a glass cover and an absorber surface, formed by seven steel tubes externally coated with a spectrally selective coating. The rear side of the reflector and absorber surfaces is thermally insulated with EPS (Expanded Polystyrene)

externally protected with an aluminium casing. The properties of the materials considered for reflectors, glazing or absorber tubes follow common characteristics of solar energy industry components and are presented in Table 4.1.

Table 4.1: Materials dimensional, thermal and (average) optical properties. (1) from [7] at 300K, (2) from [7] at 400K, (3) experimentally measured in material samples.

Element	Thick (mm)	k (W/mK)	α (W/mK)	ρ (W/mK)	ϵ (W/mK)
Glass (cover)	3.0	$1.40^{(1)}$	-	-	$0.925^{(1)}$
Primary Reflectors	1.0	$240.00^{(1)}$	$0.08^{(3)}$	$0.92^{(3)}$	$0.060^{(3)}$
Secondary Reflectors	1.0	$240.00^{(2)}$	$0.05^{(3)}$	$0.95^{(3)}$	$0.060^{(3)}$
Selec. Surf. (absorber)	1.0	$393.00^{(2)}$	$0.91^{(3)}$	-	$0.090^{(3)}$
EPS (insulation)	200.0	$0.04^{(1)}$	-	-	-
Aluminium (casing)	2.0	$240.00^{(1)}$	-	-	-

As for the angular variation of optical properties for glazing and mirror materials the following assumptions were considered:

- Mirror reflectivity traduced by a normal reflectivity value without angular variation;
- Selective surface follows a polynomial black surface approach for the angular variation of absorptivity [8];
- Glazing transmissivity accounts for unpolarized radiation reflection, according to Fresnel equations, as well as absorption effects according to Bouguer equation [8].

The impact of image spreading due to both the solar disk shape and to reflector surface imperfections is also considered. Gaussian distributions are considered in the description of both effects. Solar disk shape is described after a very clear sky condition, corresponding to a $\sigma_{sun,line} = 2.6$ mrad [9]. Different levels of reflector imperfections are described after increasing standard deviation values for specular reflection angles, namely $\sigma_{spec.,refl.} \in [1.0, 2.0, 3.0, 4.0]$ mrad. Optical efficiency calculations follow a ray trace analysis with a normal incidence beam initially divided into 5000 equally spaced rays on the wavefront associated with the absorber cavity. Individual rays are subdivided upon reflection on primary or secondary reflectors into 9 new rays, each of which accounting for different specular reflection error angles and having an energy content in accordance to the Gaussian distribution considered for the surface imperfections. Results for a beam irradiation flux of I = 900W/m^2 are presented in Table 4.2.

Table 4.2: Optical efficiency for the full asymmetric CLFR system (I = 900 W/m^2).

$\sigma_{sun,line}$ $(mrad)$	$\sigma_{spec.,refl.}$ $(mrad)$	Q_{aper} (kW/m)	Q_{proj} (kW/m)	Q_{abs} (kW/m)	η_{0b} (%)	η^*_{0b} (%)
0.0	0.0	41.88	37.54	29.35	70.1	78.2
2.6	0.0	41.88	37.54	28.98	769.2	77.2
2.6	1.0	41.88	37.54	28.80	68.8	76.7
2.6	2.0	41.88	37.54	28.51	68.1	75.9
2.6	3.0	41.88	37.54	27.33	65.3	72.8
2.6	4.0	41.88	37.54	25.91	61.9	69.0

The influence of solar disk shape and reflector surface imperfections is reflected on the results presented in Table 4.2 and illustrated in Fig. 4.2.

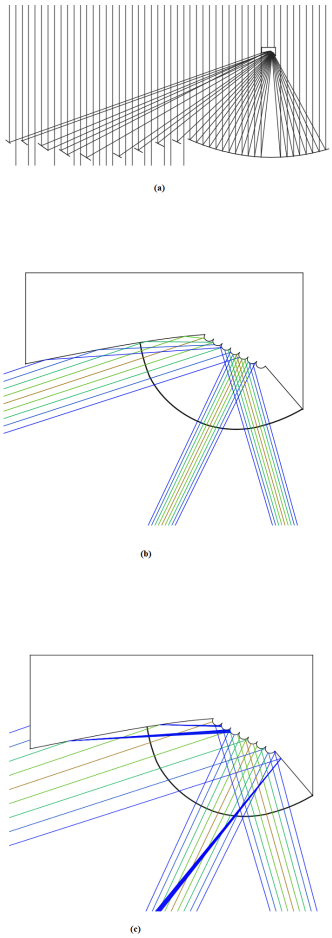

Fig. 4.2: Ray-trace diagram for a normal incidence beam: a) half system (no optical errors); detail of secondary cavity effect of b) solar disk; and c) specular reflection errors ($\sigma_{sun,line}$ = 2.6 $mrad$; $\sigma_{spec.,refl.}$ = 2.0 $mrad$).

Incidence angle modifier (IAM) calculations were performed after an optical model developed in a parent work [6]. A 3D ray tracing approach with 1000 rays on the system aperture was used to study the impact of zenith angle, θ_Z, and solar azimuth angle, φ_S, variations on the system optical efficiency, traduced in the longitudinal and transversal IAM variations presented in Fig. 4.3.

4.3 Thermal assessment

Heat transport inside the secondary TERC cavity is modelled has a natural convection problem inside a non-uniformally heated cavity. There are several physical phenomena contributing to the overall heat balance: heat conduction along the cavity walls (Q_{cond}), external convection ($Q_{conv,ext}$), internal convection ($Q_{conv,int}$), cavity long-wave radiative exchanges (Q_{rad}), absorption of solar beam irradiation (Q_{solar})

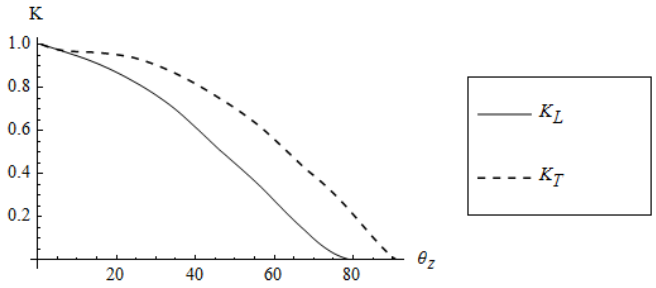

Fig. 4.3: IAM curves for longitudinal, K_L, and transversal, K_T, directions.

and collector heat removal after an usefull heat flux (Q_{util}). The thermal analysis to the cavity is based on the numerical modeling of the internal flow, with boundary conditions defined after calculation of the different heat fluxes involved in the fluid flow problem [5, 10]. The Navier-Stokes equations describing the problem are discretized using a standard Galerkin Finite Element Method. To this end a triangular elements discretization was used, as illustrated in Fig. 4.4.

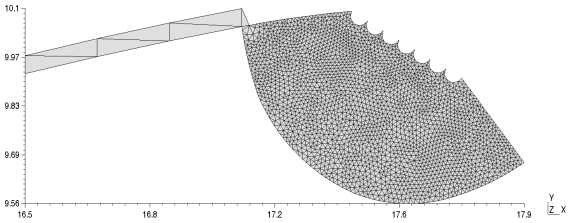

Fig. 4.4: Adimensionalized mesh used in the domain discretization.

In the calculation of internal heat fluxes, the following assumptions were considered:

- Long-wave radiative exchanges within the cavity result from the calculation of adequate nodal shape factors and from the (emissivity) properties of the different materials (see Table 4.1);
- Heat conduction along the cavity walls results from averaged surface conditions, assuming a thermal blocking between cover, reflector and absorber surfaces (no heat losses or gains between surfaces);
- Absorption of solar beam irradiation ($\sigma_{sun,line} = 2.6\ mrad$; $\sigma_{spec.,refl.} = 1.0\ mrad$) results from the ray-trace analysis to the cavity and from the properties (absorptivity) of the different materials (see Table 4.1).

External conditions are expressed in terms of empirical expressions for an external convection coefficient, accounting for airflow effects over the external cavity

surfaces [11]. Considering that the transparent cavity cover faces the ground, no radiative losses to the sky where included in this coefficient. For calculation purposes an ambient temperature of $T_{amb} = 25°C$ and an external airflow velocity of $U_{amb} = 3.0\ m/s$ were considered. External convection losses are calculated from the internal to the external cavity wall, therefore including normal wall conduction losses. Internal convection heat losses result from the velocity and temperature fields obtained from the flow simulation and, therefore, are the unknown of the energy balance and do not involve the prescription of boundary conditions. In the preliminary thermal assessment of the cavity, and given the expected operation conditions of the CLFR system, an imposed temperature condition was set at the absorber: $T_{abs} = 400°C$. Velocity and temperature fields obtained for these boundary conditions are presented in Fig. 4.5.

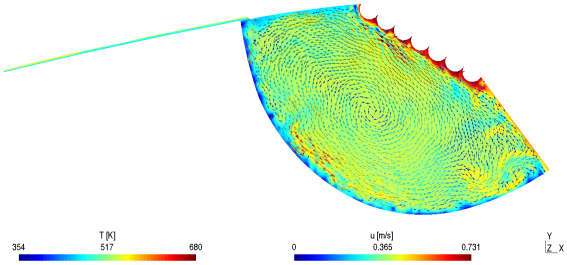

Fig. 4.5: Temperature and velocity fields obtained for $T_{abs} = 400°C$, I = 900 W/m^2, T_{amb} = 25°C and $U_{amb} = 3.0\ m/s$ conditions (cavity and left TERC mirror view).

The heat balance to the absorber surface is presented in Table 4.3. Results regarding the thermal efficiency of the system under the prescribed operation conditions are presented in Table 4.4.

Table 4.3: Absorber heat balance under $T_{abs} = 400°C$, I = 900 W/m^2, T^{abs} = 25°C and $U_{amb} = 3.0\ m/s$ conditions.

Parameter	(kW/m)	Percentage of total heat losses (%)
Q_{solar}	14.40	-
$Q_{conv,ext}$	-0.04	2.1
Q_{rad}	-0.31	15.2
Q_{cond}	0.00	0.0
$Q_{conv,int}$	-1.66	82.7
Q_{util}	12.39	-

Table 4.4: System thermal efficiency under T_{abs} = 400°C, I = 900 W/m^2, T_{amb} = 25°C and U_{amb} = 3.0 m/s conditions.

Parameter	(kW/m)	%
Q_{aper}	41.88	-
Q_{proj}	37.54	-
Q_{util}	24.78	-
η	-	59.2
η^*	-	66.0

4.4 Conclusions

The preliminary optical and thermal analysis presented in this report characterizes the CLFR and are the essential ingredients for the calculation of system performance. The results obtained for both optical and thermal efficiencies correspond to a $\approx 10\%$ (see Table 4.5) efficiency decay from ambient to $T_{amb} = 400$°C operating conditions, a result which includes the impact of image spread effects due to both solar disk shape and reflector surface imperfections ($\sigma_{sun,line} = 2.6\ mrad$; $\sigma_{spec.,refl.} = 1.0\ mrad$); these results constitute a good preliminary indicator of the system behaviour.

Table 4.5: System optical ($\sigma_{sun,line} = 2.6\ mrad$; $\sigma_{spec.,refl.} = 1.0\ mrad$) and thermal efficiency under $T_{abs} = 400$°C, I = 900 W/m^2, $T_{amb} = 25$ C and $U_{amb} = 3.0\ m/s$ conditions.

$T_{abs}(K)$	$\eta_{0b}(\%)$	$\eta^*_{0b}(\%)$	$\eta(\%)$	$\eta^*(\%)$
400.0	68.8	76.7	59.2	66.0

Thermal losses affecting the absorber cavity result mainly from internal convection; in future work the study of the impact of internal convection reduction strategies, such as the adoption of optical flow-line [4] aligned baffle will be carried out. The reduced weight of external convection (including normal wall conduction) and long-wave radiation losses, results from the adoption of a well-insulated casing for the cavity and a spectrally selective coating on the absorber, respectively. Considering the importance of internal convection heat losses, the steps to be further followed in this study are aim the study of the impact of adopting internal convection baffles.

References

[1] Collares-Pereira, M., *Etendue matched reflective Fresnel concentrators*, Proceedings 15th International SolarPACES Symposium, September, 14-18, Berlin (Germany), 2009.

[2] Chaves, J., Collares-Pereira, M., *Etendue-matched two stage concentrators with multiple receivers*, Solar Energy 84 (2009), pp. 196-207.

[3] Chaves, J., Collares-Pereira, M.,(2009), *Primary concentrator with adjusted etendue combined with secondaries associated to multiple receivers and with convention reduction*, International patent application PCT/PT2009/000026.

[4] Winston, R., Miñano, J.C., Benítez, P., (contributions by Shatz, N., Bortz, J.,C.), *Nonimaging Optics*, Elsevier Academic Press, Amsterdam, 2005.

[5] Horta, P., (2011), *Study and mitigation of internal convection processes inside a Compound Parabolic Concentrator solar collector*, PhD thesis, Instituto Superior Tecnico/Universidade Tecnica de Lisboa, Lisbon.

[6] Canavarro, D., Collares-Pereira, M., Lopes Guerreiro, L., *Increasing the efficiency of conventional LFR technologies: a new CLFR "Étendue Matched" CSP collector*, Proceedings 17th International SolarPACES Symposium, September, 20-23, Granada (Spain), 2011.

[7] Incropera, F.P., and De Witt, D.P., (1990), *Fundamentals of Heat and Mass Transfer*, John Wiley & Sons, Inc., 3^{rd} Edition.

[8] Duffie, J.A., and Beckman, W.A., (2006), *Solar Engineering of Thermal Process*, John Wiley & Sons, Inc., Hoboken, New Jersey, 3^{rd} Edition.

[9] Rabl, A., *Active Solar Collectors and their applications*, Oxford University, Oxford, 1985

[10] Horta, P., Henriques, J.C.C. and Collares-Pereira, M., *Impact of different internal convection control strategies in a non-evacuated CPC collector performance*, Solar Energy 86 (2012) 1232-1244.

[11] Watmuff, J. H., Charters, W.W.S. and Proctor, D., *Solar and wind induced external coefficients for solar collectors*, Comples, 2, 1977.

Nomenclature

CLFR Compact Linear Fresnel Reflector

EPS Expanded Polystyrene

IAM Incidence Angle Modifier

k heat transfer coefficient (W/mK)

K_L longitudinal direction

K_T transversal direction

Q_{abs} radiative flux at the absorber receiver (kW/m)

Q_{aper} radiative flux at the system aperture (kW/m)

Q_{cond} heat conduction along the cavity walls (kW/m)

$Q_{conv,ext}$ external convection (kW/m)

$Q_{conv,int}$ internal convection (kW/m)

Q_{proj} radiative flux at the projected area of the primary system (kW/m)

Q_{rad} cavity long-wave radiative exchanges (kW/m)

Q_{solar} absorption of solar beam irradiation (kW/m)

Q_{util} collector heat removal after an useful heat flux (kW/m)

T_{abs} temperature at the absorber receiver (°C)

T_{amb} ambient temperature (°C)

TERC Tailored Edge Ray Concentrator

U_{amb} external airflow velocity (m/s)

Greek symbols

α absorptivity (W/mK)

ε emissivity (W/mK)

η thermal efficiency

η^* thermal efficiency (projected mirror area)

η_{0b} optical efficiency

η^*_{0b} optical efficiency (projected mirror area)

θ_Z solar zenith angle (grad)

ρ reflectivity (W/mK)

$\sigma_{spec.refl.}$ specular reflection angles (mrad)

$\sigma_{sun,line}$ solar disk shape (mrad)

φ_S solar azimuth angle (grad)

Chapter 5

Increasing the cost effectiveness of CSP technologies through the development of a new CLFR "Etendue Matched" collector[†]

Abstract

A new CLFR "Etendue Matched" is a promising CSP technology to achieve a better cost effectiveness with a lower levelized cost per m^2. This new technology can significantly reduce shading and blocking existing in a conventional LFR [1, 2], while at the same time optimizing primary and secondary concentration to the limits allowed by first principles in optics. A preliminary evaluation of the optical and thermal performance has been performed [3, 4], and a configuration for a full scale CSP power plant proposed, with two secondary receivers (Fig. 5.1), i.e a multiple receiver solution.

Keywords: CLFR "Etendue Matched", Concentrating Solar Power, Non-imaging Optics; Cost-effectiveness

5.1 Simulation Model

In the last 10 years several CSP plants have been built, more than 90% of them are PTR plants. In Spain, due to the tariff scheme, most plants are 50 MW plants, some

[†]Luís Guerreiro[(1)], Diogo Canavarro[(1)], Manuel Collares-Pereira[(1)], Increasing the cost effectiveness of CSP technologies through the development of a new CLFR "Etendue Matched" collector, ISES World Congress, 28 August - 02 September, Kassel (Germany), 2011.

[(1)] BES Renewable Energies Chair, University of Évora.

of them have now several years of operation with well monitorized data.

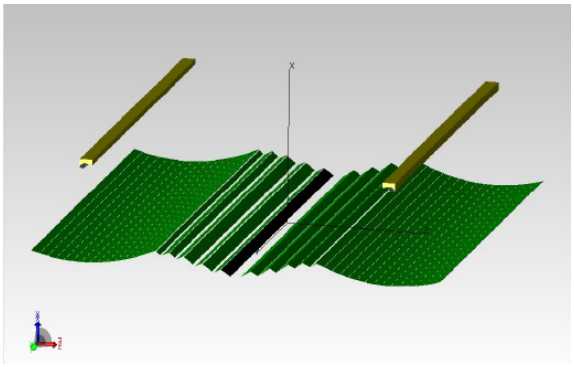

Fig. 5.1: New CLFR "Etendue Matched" proposed.

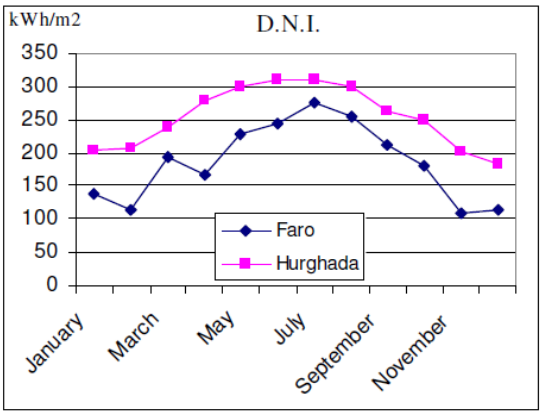

Fig. 5.2: Yearly DNI for the locations considered.

Performance data for LFR and PTR systems come from simulations and from real data available; one example is the paper by Hoyer et al. [5] reporting the overall system efficiency as well as overall losses (shading, blocking, reflection, thermal, optical receiver) Hurghada, Egypt (27°N), Guadix, Spain (37°N) and Faro, Portugal (37°N) for both Linear Fresnel (overall efficiency of 9%) and Parabolic Through (overall efficiency of 15%) collector types.

In order to evaluate the new CLFR-EM concept, first a simulation model has been developed for the optical optimization of the primary and secondary mirrors using a commercial software [3] and afterwards for the thermal optimization using an FEM model simulating the energy balance in the receiver using the Navier Stokes equations [4] with a finite element approach to the convection occurring inside the secondary TERC, together with the definition of heat flow boundary conditions enabling a complete analysis of the different heat loss terms affecting system performance at any given operating temperature.

The model developed was first applied to PTR and LFR collectors for Hurghada and Faro. Losses calculated were within +/-2% of the ones reported by [5], which can be considered a validation of the calculations involved. With the model calibrated both in the optical and thermal aspects, these tools were applied to the evaluation of the performance to be expected from the optically optimized CLFR "EM" configuration which is the object of this paper. A ray trace study was performed defining the heliostat positioning in order to take advantage of the new Etendue Matched concept patented [1] and described in detail in [2]. This way, shading and blocking effects were minimized, and the irradiance level was studied in order to evaluate how the configuration for the receiver, TERC type, should be, having the aim of increasing the concentration factor up to 60× (Fig. 5.3 and Fig. 5.4). Apart from the reduction of losses and higher concentration factor, this configuration has the extra advantage of enabling a lower height for the optimal position of the receiver to about $6m$ height against the usual 14-16m of a conventional LFR type collector, with the same width. This feature reduces the investment costs, but also the operational risk failure.

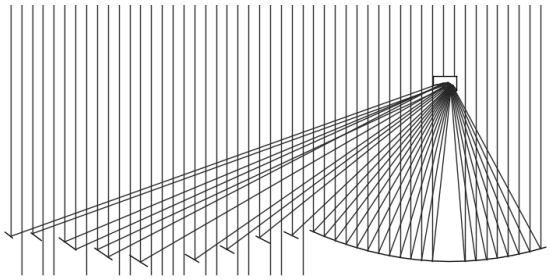

Fig. 5.3: New CLFR "Etendue Matched", ray-trace, one half only.

The thermal efficiency calculation, it was made for a non-vacuum cavity with selective coated tubes with a diameter of $50mm$, placed side by side. The energy input considered was the equivalent of an direct normal irradiance (DNI) of 900W/m^2, ambient temperature of 25°C and wind velocity of 1m/sec. In Fig. 5.5 the velocity and temperature fields are showed for a temperature of 400°C in the fluid. The results obtained report a 70% optical efficiency per mirror surface area (considers losses of 4% due to non-specular effect) equivalent to 66% per soil surface area, resulting in a value of 0.16 W/m^2/°C for the heat loss coefficient $F^{'}U_l$ at 400°C (see Table 5.1) [4, 6].

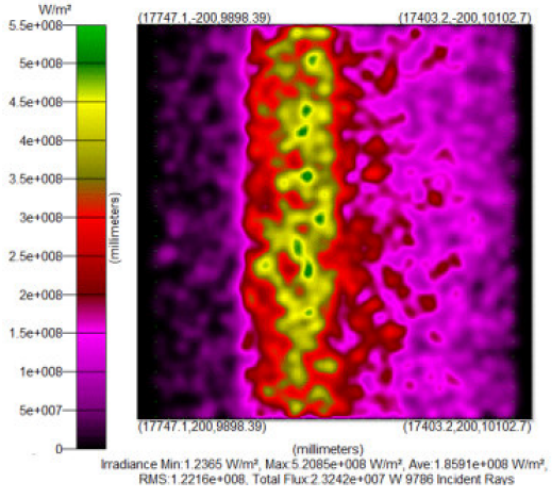

Fig. 5.4: CLFR "Etendue-Matched", radiation concentration.

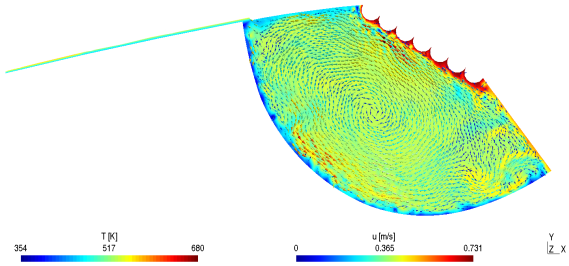

Fig. 5.5: CLFR-EM, receiver thermal and velocity field.

The data obtained suggests that due to the increase in the concentration factor, operating temperatures above 400°C, up to 500°C in the thermal fluid can be achieved with good efficiencies.

Table 5.1: System thermal efficiency under T_{abs} = 400°C, I = 900 W/m^2, T_{amb} = 25°C and U_{amb} = 3.0 m/s conditions.

Parameter	(kW/m)	%
Q_{aper}	41.88	-
Q_{proj}	37.54	-
Q_{util}	24.78	-
η	-	59.2
η^*	-	66.0

5.2 Model Application

With the model described in the previous section, and using Meteonorm weather data, energy production for the two locations previously mentioned was computed for three different technologies: conventional PTR and LFR as well as for the new CLFR-EM concept.

In the calculation, a slight energy dumping effect (of 1%) was considered, that is, in all cases the plant was dimensioned to produce only slightly more energy than the rated peak output power of 50MW. The data considered in the energy output calculation is presented in Table. 5.2

Table 5.2: Data considered in the energy output calculation.

Technology	Optical eff. (%)	Losses Coef. $(W/m^2/K)$	Operating Temp. (°C)	Pipping Losses (%)	Turbine eff. (%)
CLFR-EM	74	0.16	450	8	37.5
PTR	78	0.16	400	16	36.5
LFR	66	0.30	270	5	25.0

In Table. 5.3 it is shown the thermal energy output for the CLFR-EM, LFR and PTR concentrators and in Table. 5.4 a summary for the three technologies.

Table 5.3: Thermal energy output for Faro for the 3 different technologies.

Month	CLFR-EM (kWH/m^2) Soil area	CLFR-EM (kWh/m^2) Mirror area	LFR (kWh/m^2) Soil area	LFR (kWh/m^2) Mirror area	PTR (kWH/m^2) Soil area	PTR (kWh/m^2) Mirror area
Jan	33,48	37,21	30,18	41,16	26,48	52,96
Feb	32,55	36,17	27,55	37,56	26,21	52,43
Mar	63,97	71,07	51,80	70,63	52,19	104,37
Apr	60,76	67,52	48,24	65,78	49,57	99,13
May	88,78	98,95	68,99	94,07	74,21	148,43
Jun	98,26	109,18	75,89	103,49	83,55	167,09
Jul	110,35	122,62	85,36	116,40	93,25	186,51
Aug	93,11	103,46	73,27	99,91	77,27	154,55
Sep	73,06	81,18	58,70	80,04	59,54	119,08
Oct	54,75	60,83	45,56	62,13	44,58	89,15
Nov	28,09	31,21	25,03	34,13	22,09	44,18
Dec	25,12	27,91	23,14	31,55	19,70	39,40
Total	762,29	846,99	613,70	836,86	628,63	1257,27

Table 5.4: Mirror area, soil occupation and energy production in each case, Faro, with 1% of dumping.

Technology	Mirror area (m^2) (%)	Soil area (ha)	Anual energy production (GWh)
CLFR-EM	300 000	36	79
PTR	220 000	66	72.5
LFR	450 000	68	85

The same thermal energy output for the three technologies was calculated for Hurghada (Egypt). The results are presented in Table. 5.5.

Table 5.5: Thermal energy output for Hurghada for the 3 different technologies.

Month	CLFR-EM (kWH/m^2) Soil area	CLFR-EM (kWh/m^2) Mirror area	LFR (kWh/m^2) Soil area	LFR (kWh/m^2) Mirror area	PTR (kWH/m^2) Soil area	PTR (kWh/m^2) Mirror area
Jan	55.80	65.33	49.45	67.43	48.29	96.57
Feb	70.91	78.79	57.18	77.97	57.17	114.34
Mar	90.24	100.27	71.33	97.27	72.24	144.49
Apr	111.53	123.93	86.18	117.52	92.35	184.71
May	124.01	137.78	94.97	129.51	107.15	214.31
Jun	127.48	141.65	97.75	133.29	111.69	223.38
Jul	130.67	145.19	99.85	136.16	113.60	227.20
Aug	121.31	134.79	93.22	127.12	102.41	204.83
Sep	101.64	112.93	79.64	108.60	82.07	164.14
Oct	84.66	94.07	68.31	93.15	68.53	137.07
Nov	66.19	73.55	54.26	73.99	53.42	106.84
Dec	55.44	61.60	46.82	63.85	44.76	89.53
Total	1142.88	1269.87	898.97	1225.87	953.70	1907.40

Final figures for overall system energy efficiency, both in Faro and Hurghada is summarized in Table. 5.6.

Table 5.6: Optical efficiency and overall system efficiency.

Technology	Optical efficiency (per mirror area) (%)	Overall system efficiency (per mirror area) Faro(%)	Overall system efficiency (per mirror area) Hurghada(%)
CLFR-EM	74	11.8	13
PTR	78	14.8	16.4
LFR	66	8.5	9.1

Considering the data presented in Table. 5.3 and Table. 5.5 and the efficiencies described in Table. 5.6, the electricity output for Faro and Hurghada was calculated (see Fig. 5.6 and Fig. 5.7) in kWh/m^2 of mirror surface area, being respectively 263 and 394 kWh/m^2 per year for the CLFR-EM system.

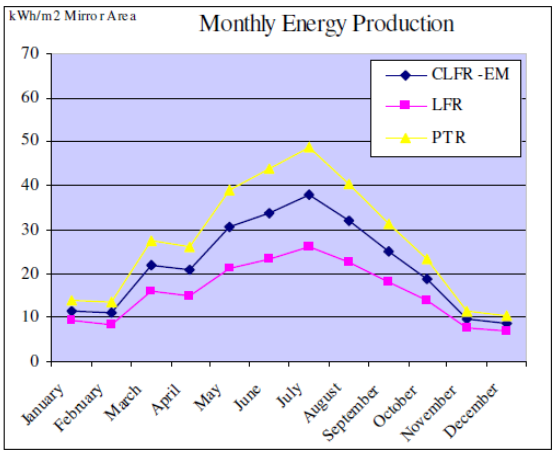

Fig. 5.6: Electricity produced per mirror area, Faro.

In the Iberian peninsula, in practice it is economical to size collector fields for a number of operating hours equivalent at full power between 2000 and 2300 hours considering no thermal storage.

If a choice is made for 2220 hours, there will be an oversizing of the collector field with respect to that in Table 3, of about a factor of 1.4× (420 000 m^2) resulting in a production of 111 GWh for the CLFR-EM in Faro, and resulting in an energy dumping of about 12%.

For PTR the equivalent choice would yield an oversizing of about 1.53× (336 000 m^2) for the same production and comparable energy dumping.

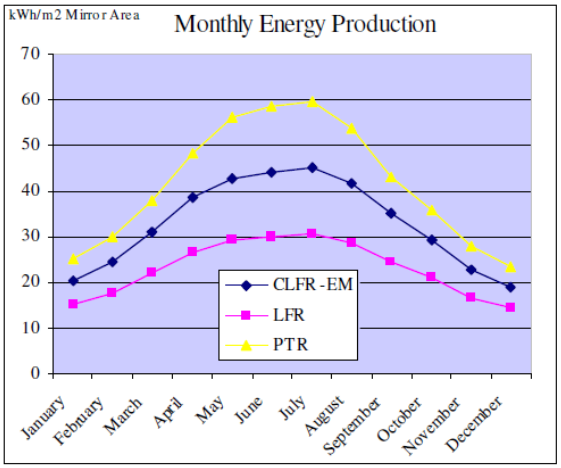

Fig. 5.7: Electricity produced per mirror area, Hurghada.

This dumping effect might be eliminated either by delivering to the grid more than the rated 50MW whenever necessary, or by taking advantage of a possible thermal storage facility, a concept that is more and more critical for solar thermal plants.

These results show that CLFR-EM overall efficiency can be up to 13% for Hurghada where LFR would only achieve 9,1%. This is due to the optimized optical efficiency through the reduction of shading, blocking and TERC design upgrade which enables a higher concentration factor with the corresponding increase in the operating temperature. Comparing with PTR collectors the efficiency is still lower, however, when the comparison is made in terms of costs (per installed power or mirror surface), then CLFR-EM is more advantageous than PTR.

5.3 Cost Evaluation

In order to confirm the simulated data, and due to the interest in this concept manifested by several companies, a demonstration plant at the University of Évora will be installed and monitored, (see Fig. 5.1). It will have a total heliostat surface of $530m^2$, and will demonstrate only optical and thermal performance. The high operating temperatures demand tubular receivers with selective coatings that were not yet possible to find in the market. The decision was reached to use, instead, evacuate tubular receivers and limit the demonstration to temperatures around 400^oC. Standard receiver tubes available in the market specific for CSP plants (PTR70) was used for the calculations, with a thermal losses factor (with a factor $60\times$ concentration) of 0.12 $W/m^2/^oC$ [7], lower than the initially considered due to vacuum. The configuration of the cavity was also re-evaluated reporting a slight decrease

in the optical efficiency due to the 1-tube configuration, however this reduction is counter balanced with the lower thermal losses of the receiver, thus the overall system efficiency is considered to be the same (at $400^{o}C$) as the one calculated in detail with results presented in the previous section. Additionally, the planning of a 50MW CLFR-EM plant (420.000 m^2) was evaluated with a procurement phase for a cost estimation considering relevant players in the market (Table. 5.7 and Table. 5.8).

Table 5.7: Plant configuration considered in the cost analysis.

Element	CLFR-EM demonstration plant	CLFR-EM 50MW plant
Number of heliostats, rows	24	24 × 12
Total receiver length (m)	24 × 2	1455 × 2 × 12
Collectors in a row	8	485
Row width (m)	0.55; 0.9; 1,2	0.55; 0.9; 1.2
Average distance between rows (m)	0.3	0.3
η_{opt0} (%)	74	74
Receiver type	PTR 70	PTR 70
HTF-medium	Therminol VP1	Therminol VP1
Solar field location	Évora, PT (40°N); North-South	Évora, PT (40°N); North-South
Other settings	Thermal loop w/ heat dissipation	Power block w/ turbine $\eta = 37.5\%$

Table 5.8: Cost estimation for CLFR-EM and PTR systems for a 50MW plant with similar electricity production for Faro, Portugal.

Element	CLFR-EM (mirror area of 420.000 m2)		PTR (Morin, adapted for 336.000 m2)	
	Total Cost (MEuro)	Cost (Euro/m2)	Total Cost (MEuro)	Cost (Euro/m2)
Receiver	7.2	17	93	275
Reflector	5.2	12	93	275
Base structure	40	95	93	275
Control system	3.3	8	93	275
Thermal Block	40	95	40	119
Comissioning and others	3.8	9	30	90
Overall Cost (50MW)	99.5	237	163	484
Cost per Wp installed	2.0		3.3	

To evaluate the opportunity of an investment in a CLFR-EM plant in a Southern European location, an economic evaluation was performed computing the project NPV and its IRR considering following assumptions: Investment costs= 99.5MEuro, maintenance costs= 2MEuro/year, system availability=100%, electricity selling price=0.27Euro/kW for 25 years, WACC=10%. Results are presented in Table. 5.9.

Table 5.9: Economic project valuation.

NPV	62 M.Euro
IRR	19.9 (%)
Pay back time	7.5 years

In order to evaluate the impact of possible changes in the expected scenario, a sensitivity analysis was performed considering different scenarios (best, better, expected, worst, worse) for 3 different cases:

- **Case 1**: Initial investment costs (receiver, base structure, etc.). Variation of +20%; +10%; 0%, -10%; -20%.
- **Case 2**: Overall system efficiency. Variation of +10%; +5%; 0%, -5%; -10%.
- **Case 3**: Feed-in electricity tariff. Variation of 0%, -5%; -10%; -15%; -20%.

The economic project valuation for the three different cases is presented is Table. 5.10

Table 5.10: Economic project valuation for 3 different cases.

Case	NPV "Best" (M.Euro)	NPV "Worst" (M.Euro)	IRR range
1	88	37	17.8% - 21.8%
2	101	32	17.3% - 22.1%
3	62	15	14.4% - 19.9%

The results show that in the scenarios analysed the IRR varies in a range between 14,4% and 22,1%. The three cases have different impact on the project evaluation. Case 1 is dependent on the market size and number of players which enhances competition, it is foreseen that with the rising number of CSP facilities, this cost will tend to decrease (experience and scale economies). The results are shown in Fig. 5.8.

Case 2 is dependent on technological improvements and its implementation pace. If initiatives like Desertec will move forward, the market size will increase signifi-

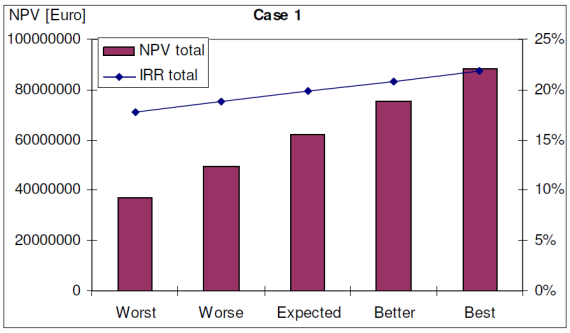

Fig. 5.8: Case 1, NPV and IRR.

cantly and therefore increasing RD spending and learning curve will drive efficiency values higher. The results are shown in Fig. 5.9.

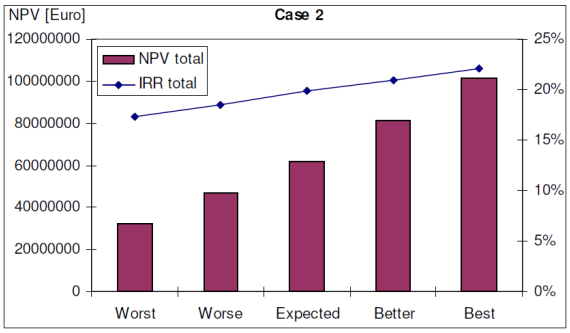

Fig. 5.9: Case 2, NPV and IRR.

Case 3 is dependent on the economic framework and to the existence of a guaranteed feed-in tariff. Theses values are always dependent on the solar radiation available, and are foreseen to be reduced in the future, due both to CSP technology economies of experience and to the pressure of cutting this kind of benefits. For this reason, only scenarios with same or reduced feed-in tariff were analysed. The outcome shows that with a reduction in the tariff down to 0,21 Euro/kWh, the IRR is reduced to 14%. This is close to the lowest acceptable value for the cost of capital considered, and is therefore considered to be the lowest point for a still attractive investment under the current difficult scenario of the international capital markets. The results are shown in Fig. 5.10.

The analysis performed considered that the investment was done by a company already with CSP technology and experience, with a WACC of 10%. For a new player, WACC would be increased due to its higher business risk, making the investment a more riskier one.

Concluding the sensitivity analysis, the two more relevant variables were considered (investment costs and feed-in tariff) and assuming different probabilities of

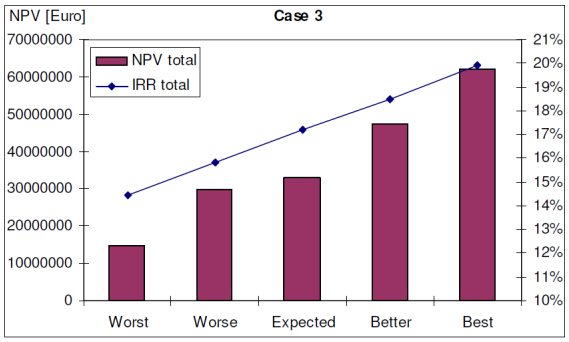

Fig. 5.10: Case 3, NPV and IRR.

occurrence for the various scenarios a global value for the NPV and IRR was calculated (Fig. 5.11). The probability of occurrence was 20% for the expected scenario, 15% for each combined scenario "better" vs. "worse" and 5% for the more extreme combined scenarios.

		Initial investment costs			
		Worse	Expected	Better	
Feed-in Tarif	Worse				
	NPV total	10 279 798	29 779 681	49 279 565	7 444 920
	IRR total	14.0%	15.8%	17.9%	
	Pay back	8	8	8	
	Probability	5%	15%	5%	
	Expected				
	NPV total	25 940 288	33 013 394	40 086 500	16 506 697
	IRR total	15.3%	17.2%	19.3%	
	Pay back	8	8	8	
	Probability	15%	20%	15%	
	Better				
	NPV total	39 733 783	65 643 691	91 553 600	16 410 923
	IRR total	16.6%	18.5%	20.7%	
	Pay back	8	8	7	
	Probability	5%	15%	5%	
	NPV total	6 391 722	20 916 185	13 054 633	**40 362 540** Euro

Fig. 5.11: Sensitivity analysis with probabilities for different scenarios.

To finalize the evaluation, a comparison between CLFR-EM and PTR technologies was made, considering the investment costs mentioned in Table 7, analysing the sensitivity to the value of the feed-in tariff for an IRR=14% in both situations (Table. 5.11). Although it can be argued that the costs considered in [5] are somewhat high for the current state of the art of the PTR systems, it is evident the difference in profitability of both concepts, meaning that with the pressure for a reduction in the feed-in tariff, the CLFR-EM concept has a good perspective for becoming an important technology in a near future.

An identical calculation for Hurghada (EGY) yields a tariff at least 30% lower in both cases, all else being equal, not just because solar radiation (and the number of equivalent operating hours) is 30% higher, but, in the case of CLFR-EM, the

Table 5.11: Feed-in tariff for 25 years for systems with 2200h if yearly production.

	CLFR-EM (Euro/kWh)	PTR (Euro/kWh)
IRR = 14%	0.21	0.305

overall conversion efficiency is higher, in particular because of the lower latitude. This analysis will be the topic of a future paper.

As a final calculation, and in spite of the fact that a sensitivity analysis was carried out with respect to several variables, in particular to cost, it is interesting to use the tools developed to perform a final estimate, a one shot estimate of what tariff one would obtain if a more substantial cost reduction can be achieved in the future, due to the usual learning curve, scale effects, optimum control, optimization of collected versus dumped energy, etc., items not included in the analysis done above. For this, supposing a Capex cost reduction of 35% can be achieved, i.e. if a value of 1.3 Euro/Wp is considered for the CLFR-EM technology, the equivalent tariff to the one found in Table 10 (same IRR of 14%, same investment conditions, same location, etc) would lead to a tariff lower than 0.15Euro/kWh.

5.4 Conclusions

Efficiency and economic results of a new CLFR-EM system have been presented. Overall efficiency shows a potential increase from 8.5% (9.1%) for LFR conventional systems to 11.8% (13%)for the new CLFR-EM system for sunny locations like Faro, PT (Hurghada,EGY). This higher efficiency associated with investment costs similar to the conventional LFR makes the new CLFR-EM attractive. Comparing with the standard PTR technology, the CLFR-EM has a lower output in kWh/m^2 of mirror area, however is much more compact in the soil usage, and globally the cost of the kWh produced is lower than the PTR cost. The calculations for the tariff supporting an IRR of 14% indicate a value around 0,21Euro/kWh for a sunny location in Southern Europe (Faro, PT). The same calculation yields a higher value of 0,305 Euro/kWh for PTR technology. This result depends on real performance data and should be confirmed; thus a demonstration plant is currently being planned for Evora, PT where real performance data will be obtained, with the support of the utility company group EDP. It is clear that identical calculation for a sunnier location, like Hurghada (EGY) will yield a lower tariff value (at least 30% lower), all else being equal.

References

[1] Chaves, J., Collares-Pereira, M.,(2009), *Primary concentrator with adjusted etendue combined with secondaries associated to multiple receivers and with convention reduction*, International patent application PCT/PT2009/000026.

[2] Chaves, J., Collares-Pereira, M., *Etendue-matched two stage concentrators with multiple receivers*, Solar Energy 84 (2009), pp. 196-207.

[3] Canavarro, D., Modeling linear solar collectors of the Fresnel-type; application to an innovative CLFR collector "Etendue Matched", MSc thesis, Instituto Superior Técnico/UniversidadeTécnica de Lisboa, Lisbon, 2010.

[4] Horta, P., (2011), *Study and mitigation of internal convection processes inside a Compound Parabolic Concentrator solar collector*, PhD thesis, Instituto Superior Tecnico/Universidade Tecnica de Lisboa, Lisbon.

[5] Hoyer, M,, et al., *Performance and cost comparison of linear Fresnel and Parabolic Trough collectors* Proceedings 15th International SolarPACES Symposium, September, 14-18, Berlin (Germany), 2009.

[6] Horta, P., Collares-Pereira, M., Canavarro, D., Lopes Guerreiro, L., *Modeling thermal losses in a new CLFR "Etendue Matched" non-evacuated collector cavity*, Proceedings 17th International SolarPACES Symposium, September, 20-23, Granada (Spain), 2011.

[7] NREL, Burkholder and Kutscher, *Heat Loss Testing of Schott's PTR 70 Parabolic Trough Receiver*, 2009.

Nomenclature

CLFR − EM Compact Linear Fresnel Reflector "Etendue-Matched"

CSP Concentrated Solar Power

DNI Direct Normal Irradiance (kWh/m^2)

F$'\eta_0$ Optical Efficiency Loss Coefficient

$F'U_l$	Heat Loss Coefficient
HTF	Heat Transfer Fluid
IRR	Internal Rate of Return
LFR	Linear Fresnel Reflector
NPV	Net Present Value
PTR	Parabolic Trough Reflector
Q_{aper}	radiative flux at the system aperture (kW/m)
Q_{proj}	radiative flux at the projected area of the primary system (kW/m)
Q_{util}	collector heat removal after an useful heat flux (kW/m)
T	temperature at the absorber receiver (°C)
T_{amb}	ambient temperature (°C)
TERC	Tailored Edge Ray Concentrator
WACC	Weighted Average Cost of Capital

Greek symbols

η	thermal efficiency
η^*	thermal efficiency (projected mirror area)

Chapter 6

New second-stage concentrators (XX SMS) for parabolic primaries; Comparison with conventional parabolic trough concentrators[†]

Abstract

Parabolic Trough concentrators are the predominant Concentrated Solar Power (CSP) technology today. However this technology is facing substantial challenge from the need to reduce costs and/or increase performance. This paper address this challenge by exploring the room left from the fact thus type of optic falls short from the theoretical limits of concentration, proposing a new solution enabling the design of larger troughs with higher concentration or larger acceptance angles, through the use of second stage concentration of a novel type. This new optic is designed with the Simultaneous Multiple Surface (SMS) method for two reflective (X) surfaces (XX SMS) - of which the primary is approximately parabolic - using a different assignation of the edge rays in order to significantly reduce the Fresnel losses around the glass cover of the evacuated tubes commonly used in CSP applications. To analyse the merits of this new optic, two different comparisons are made. The first one with the SMS Helmet concentrator through the calculation of *CAP* (Concentration-Acceptance Product) and the second one with a commercial Parabolic Trough concentrator, using an estimate of the total amount of collected energy (kWh)for one particular location, Faro (Portugal). The paper ends with a discussion of the results obtained, their impact and possible applications in the future.

Keywords: Parabolic Trough; SMS method; Non-imaging optics; Concentrated Solar Power

[†]Diogo Canavarro[(1)], Julio Chaves[(2)], Manuel Collares-Pereira[(1)], New second-stage concentrators (XX SMS) for parabolic primaries; Comparison with conventional parabolic trough concentrators, *Solar Energy* 92 (2013) 98–105.

6.1 Introduction

Parabolic Trough (PT) technology is the most commonly used today for STE (Solar Thermal Electricity) production. 94% of all solar thermal power plants already installed in Spain ($\approx$ 1800 MW) and also those under installation use this technology. [1].

The technology has thus achieved an impressive degree of maturity, but must now go down a cost reduction curve, in order to be competitive in the future against other solar and non-solar alternatives. One possible way to contribute towards this goal is to address some of the present fundamental limitations of the technology and propose alternative optical configurations. A conventional PT[1] is a well-known and simple optical solution, concentrating - focusing - incident solar beam radiation on a receiver (typically a tube, where a heat transfer fluid [HTF] is directly circulated). It is usually designed to be compact (low f-number) and to achieve a high level of concentration. These devices are meant to deliver energy at high temperatures (resulting into higher [thermodynamic] conversion efficiency into electricity) which, in turn, means higher heat losses. Heat losses are proportional to receiver area, thus the smaller the receiver with respect to the aperture area, the highest the concentration and the better performance will result.

Optical efficiency is defined as the fraction of the (direct) sunlight intercepted by the concentrator that is absorbed by the receiver [2, 3]. In the particular case of perfect optics there are no losses in the concentrator due to the optical characteristics of the materials (no absorption losses, no reflection losses, etc.) and one gets the geometrical efficiency [4], because it depends only on the geometry of the system and not on the optical characteristics of its components. The geometrical efficiency may also be called intercept factor [5].

The PT has a half-acceptance angle θ [6] designed to accommodate the angular spread of the sun's disc and several possible optical errors [2]. If the design was meant to achieve the highest concentration these optics can achieve and since the half angular width of the sun is 0.26deg, the resulting maximum concentration would be $\approx 70\times$ (see Eq. 6.1, below). In practice PT's are designed to have a concentration value from $25\times$ to $30\times$, i.e., they are designed for an angle corresponding to a value between two and three times the apparent angular width of the sun's disk. This larger angle helps relaxing tracking accuracy, wind induced deviations, manufac-

[1] In the paper 2D geometries will be considered, i.e., all optical devices are treated on a plane, exhibiting translational symmetry on the perpendicular direction to it; for instance a tubular receiver is completely characterized by the circumference of its perimeter.

[2] In fact an "intercept factor" is defined as one if no radiation is lost; losses come from the angular width of the incoming radiation, alignment effects, manufacturing imperfection, wind effects, etc.

turing tolerances, sagging effects, etc., and still yield an "intercept factor" close to one.

Concentration (C) is defined as the ratio of aperture width to receiver perimeter.

Eq. 6.1 shows [3, 7] the relationship between concentration and angular acceptance, for a PT with a receiver immersed in air ($n = 1$).

$$C_{PT} = \frac{\sin\varphi}{\pi \sin\theta} \tag{6.1}$$

The angle φ is called rim angle and the highest concentration is achieved when φ is 90º. In practice φ is chosen to be very close to this value and will be considered as such for the comments below.

During the last few years, PT technology has been mainly installed in Spain, mostly with trough fields corresponding each to an installed capacity of 50MWe of peak electrical power (a limitation imposed by the present Spanish legislation). The typical size of the PTs used corresponds to an aperture width of $\approx$ 6m and a tubular receiver of 70 mm diameter.

A PT collector fields typically covers a ground area of about 2ha per MWe (troughs, typically aligned North-South, must be distant enough from each other to reduce mutual shadow losses to acceptable values). Troughs are modular in nature, but are assembled to form very long lines with many hundreds of meters in length.

PT manufacturing companies are considering several ways of achieving kWh cost reduction, mainly by:

- Increasing solar field peak power (to values at least 3 to 5 times larger) since this significantly reduces the weight on final production cost of all other plant costs (like turbine, steam cycle components, controls, transformers, etc.)
- Increasing the aperture area of the PTs, since this can directly reduce manufacturing costs (per mirror area), installation costs, auxiliary components cost, connecting pipe length and all related pipe costs and even help solve some other practical operation problems.

These problems have an impact on kWhe cost and include, for instance, pipe heat losses, heat transfer fluid (HTF) quantity (and cost), parasitic power consumption as well as the number of moving joints, connecting the moving troughs and their receivers to the fixed piping and their tendency to give problems. Larger aperture areas would certainly reduce all these items for a given fixed energy production of the complete multiple row collector field, and the industry [8] is already considering them.

But Eq. 6.1 implies that, in order to preserve concentration value, the tube should then have a larger diameter. In fact, in line with this, diameters of up to 90mm are

already being considered by the main manufacturers [9, 10]. However the present standard on the market is the 70mm tube and it is not expected to change soon.

A tubular receiver is typically enclosed in a larger glass tube, concentric with it, with a diameter of 12.5 cm [9, 10] and a partial vacuum ($\leqslant 10^{-3}$ mbar) is made in the volume between the two, to eliminate conduction/convection losses which would be present if the inner tube was immersed in air. This procedure helps significantly in establishing a very low heat loss coefficient (250 W/m at 400 °C/750 °F) [9] for the receiver; the other feature they have is the use of a selective coating for the reduction of radiative heat losses.

This paper proposes a solution to achieve substantially higher concentration, thus substantially larger aperture areas, for the same acceptance angle, a possibility which arises from the fact that the concentration (Eq. 6.1) achieved by conventional focusing PT optics, is very far from the limits established by first principles in Physics. In fact the same acceptance angle can be combined with a higher concentration solution, once a new nonimaging optics alternative (a second stage concentrator combined with a new primary concentrator) is considered as a substitute for the conventional focusing optics PT currently used.

For any given half acceptance angle θ, the highest concentration that can be achieved, for a receiver immersed in air (n=1), is given by [2, 6, 7]:

$$C_{max} = \frac{1}{\sin\theta} \tag{6.2}$$

Comparing Eq. 6.2 with Eq. 6.1 there is at least a factor of π between the values achievable (note that, as stated above, PTs are designed with $\varphi \approx 90^{o}$). For the same half angle of 0.26 deg, the limit for maximal concentration is about 213×.

This large difference shows that there is ample room for improvement and that is the key to the development proposed in this paper.

One class of solutions is as proposed in [8], just by considering a larger through, a feasible option, but implying a corresponding reduction in acceptance angle, which places a higher demand in tracking accuracy and reduces tolerances with respect to wind loads, geometrical imperfections, quality of mirror specular reflection, etc. These limitations and their relative weight and effect are very well explained in [6, 3]. This class of focusing optics solutions will not be further considered in this paper.

Further literature search shows that several attempts have been made in order to improve concentration in PT optics [2, 11, 12, 13]. These different solutions all have in common the fact that a second concentrator is used to bring the concentration value as close to the limit as possible.

Flow-line optics [7] or Compound Parabolic Concentrator (CPC) type optics, when developed for very small acceptance angles (like those considered here) tend to produce very tall collectors [2, 7], thus being very difficult, or even impossible, to

manufacture and operate in large sizes. Therefore the usual approach is to take advantage of the low aspect ratio (low f-number) values of focusing primary optics and use second stage concentration at the receiver, to increase the overall concentration value.

However, these second stage solutions introduce some limitations of their own. Some will produce reflectors that touch the absorber which will result in thermal losses (thermal short circuits) and others, designed to accommodate a gap between the second stage reflectors and the absorber, will have the so called optical gap losses ("etendue" is lost) [7].

Another inconvenience results from transmission losses (Fresnel losses) from the glass envelope of the evacuated tubular receiver and still another from shading losses produced by the secondary on the primary mirror.

One particular limitation comes from the fact that primary and secondary concentrators tend to have smaller rim angles (φ) resulting in a total system with a larger aspect ratio.

In this paper we propose a solution with second-stage concentration overcoming all of these different drawbacks. The solution is based on a method called Simultaneous Multiple Surface (SMS) method, using reflective surfaces (hence the initials XX). The paper explains why, and presents the basic characteristics of the new optic, formed by a primary and a secondary concentrator. Next it evaluates its merits through two comparisons with conventional PT optics. The first is made with direct raytracing results and the second with a calculation of energy delivered by the new concept and the conventional one.

6.2 A new XX SMS concentrator

6.2.1 The XX SMS concentrator solution

Many possible solutions exist with second stage concentration. For instance in [11, 12] proposals were made for second stage optics with multiple second stage reflectors which in theory might be fitted inside a glass envelope. However these were not practical solutions for evacuated tubes and suffer from the fact that, particularly under vacuum, the energy absorbed (not reflected) might induce a self-destroying temperature increase effect, at least if conventional materials were used for their manufacture.

Besides, the idea is to seek a solution able to accommodate a large gap, like the one between the glass envelope and the receiver tube. Recently [13] proposals were made that could accommodate a large gap, without losses, and be compatible with the placement of the second stage mirrors outside a glass envelope, making use of the SMS method.

This method allows for the primary and the secondary concentrator to be simultaneously designed to guarantee etendue matching, either having recourse to refractive (R) or to reflective surfaces (X). In the case of 2D optics it is necessary to use reflective surfaces (X), because refraction would affect the handling of the incoming radiation in the longitudinal direction in unwanted ways.

The new approach yielded the so called Snail and Helmet concentrators (mirror-based, i.e XX, where these letters stand for the fact that two reflective surfaces are used for primary and secondary) which managed to achieve: (i) a concentration very close to the maximum limit; (ii) a gap between the secondary and the receiver, practically with no light losses (iii) be applied either to an asymmetrical optic (Snail) or to a symmetric optic (Helmet). Nevertheless, these solutions were designed for a large gap but for non-evacuated tubular receivers, i.e., a glass envelope was not included. When a glass envelope is considered, even though most of the light goes directly to the absorber, there are possible high multiple transmission losses; and not all light goes through the glass envelope in a perpendicular direction, i.e, concentrated light hitting the glass envelope perpendicularly is an exception and not the rule, thus resulting in even higher losses than what might be expected at first sight. In Fig. 6.1 a schematic explanation of this is presented, using a schematic secondary concentrator and an evacuated tubular receiver.

As can be seen from Fig. 6.1(a), some rays may have significant losses on their way to the receiver R. Fig. 6.1(a) shows a ray r entering the vacuum tube g at a point **A**, leaving it at another point **B**, bouncing off the secondary mirror m_S and crossing the vacuum tube again at a point **C** before reaching R. A simpler light path would be as shown in Fig. 6.1(b) in which another ray r bounces off the secondary mirror m_S, crosses the vacuum tube at a point **D** and reaches R.

In the next section a solution is presented for a new XX-SMS secondary concentrator that:

- Is optimized to approach the theoretical limit, that is, the CAP ($CAP{=}C\sin\theta$) is as close as possible to 1 (absorber in air or vacuum).
- Includes a gap without significant light losses.
- Minimizes the transmission losses through the glass envelope.

6.2.2 The XX SMS concentrator design method

The SMS method can be well described by direct application to the case at hand. It takes advantage of the degrees of freedom provided by the shape of both primary and secondary mirrors, using one or the other in alternation from set of points to the next, conserving the etendue [7] in the process.

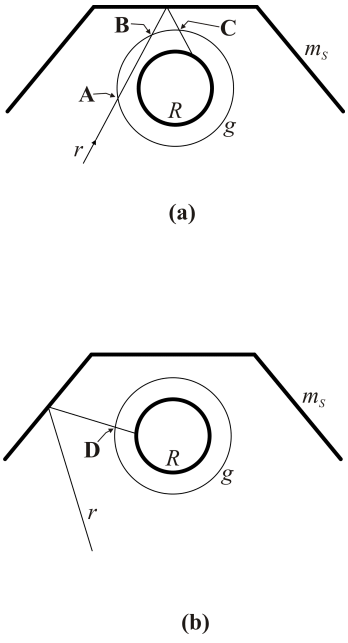

Fig. 6.1: Fresnel losses in a glass enclosed receiver combined with a second-stage concentrator optic. (a) A ray r enters the vacuum tube g at point **A** (two Fresnel losses), exits at point **B** (two Fresnel losses), bounces off the secondary mirror m_S (reflection loss), enters the vacuum tube at point **C** (two Fresnel losses) and finally reaches the receiver R. (b) Another ray hits the mirror, crosses the glass tube at point **D** and reaches the receiver R.

The circular receiver is chosen and the initial points $\mathbf{P}_0$ for the primary mirror and $\mathbf{S}_0$ for the secondary mirror are as shown in Fig. 6.2(a). The way to choose these initial points, just like in other SMS optics [13], is done by coupling the étendue captured by the primary and the étendue captured by the receiver [7]. As shown in Fig. 6.2(b), the point $\mathbf{S}_0$ is chosen along the flow-line f_{S0} (perpendicular to the receiver) and the point $\mathbf{S}_1$ and the flow-line f_{S1} are symmetric with respect to the symmetry axis of the concentrator.

The angle α between these two flow-lines can be defined as an angular gap, which, in the ideal case, should be zero in order to maximize the étendue captured by the receiver (the receiver "sees" the light in an angle of 2π). Nevertheless, this cannot be done since the secondary mirror will surround completely the receiver and, therefore, the light reflected by the primary cannot reach it. Thus, the maximum étendue that the receiver (immersed in air or vacuum, $n = 1$) can capture, E_R, is given by:

$$E_R = 2L_R(\alpha) \tag{6.3}$$

Where $L_R(\alpha)$ is the length of the arc between f_{S0} and f_{S1} as a function of α, given by:

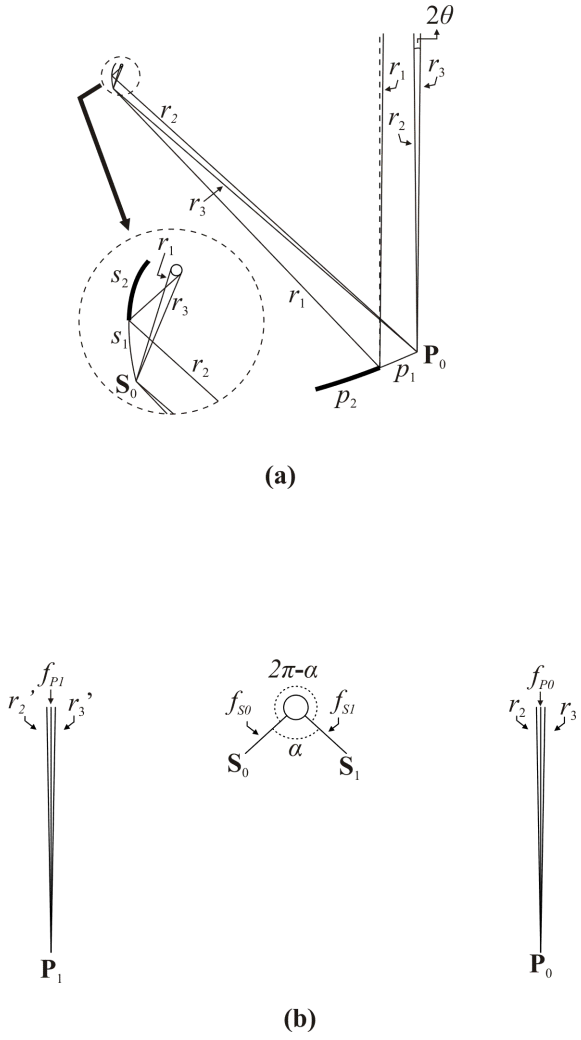

Fig. 6.2: The XX SMS design method; and (b) The initial points $\mathbf{S}_0$ and $\mathbf{P}_0$ are chosen through an étendue conservation balance between the primary mirror and the receiver.

$$L_R(\alpha) = (2\pi - \alpha)r \tag{6.4}$$

With r being the radius of the receiver.

The point $\mathbf{P}_0$ can be chosen in a very similar way. In this case the flow-line f_{P0} comes from a source at an infinite distance, that is, the flow-line is a vertical line bisecting the edge-rays r_2 and r_3. Again, $\mathbf{P}_1$, f_{P1}, $r_2^{'}$ and $r_3^{'}$ are symmetric with respect to the symmetry axis of the concentrator. Now, the étendue captured by the primary, E_P, is given by:

$$E_P = 2[\mathbf{P}_0, \mathbf{P}_1] \sin\theta \tag{6.5}$$

Where [$\mathbf{P}_0$,$\mathbf{P}_1$] is the distance between $\mathbf{P}_0$ and $\mathbf{P}_1$. Naturally, these points must be chosen in a way that E_R=E_P.

The incoming rays reflected at edge $\mathbf{P}_0$ of the primary are reflected by portion s_1 of the secondary in directions tangent to the "bottom" of the circular receiver (rays r_2 and r_3).

Reflecting a set of rays coming from the top of the circular receiver (r_1 is an example of one of these rays) on s_1 a new portion p_2 of the primary is calculated; next, reflecting a set of rays parallel to r_2 (coming from the sun) on p_1 a new portion s_2 of the secondary is calculated.

Repeating the process [7], a primary mirror approximately parabolic is obtained step by step, as shown in Fig. 6.3. The process stops at point **A** just below the rightmost point of the secondary in order to ensure that the secondary concentrator does not produce any shading over the primary. The other half of the optic is symmetric with respect to the origin (center of the receiver).

It should be noticed that no edge rays are directly reflected by the primary towards the receiver. According to the edge ray principle, incoming edge rays are instead first reflected by the primary mirror and then by the secondary mirror which redirects them towards the edges of the receiver (see Fig. 6.3) [2]. This method is the key to ensure that all rays cross the glass tube close to the perpendicular direction, minimizing Fresnel losses. In practice this is not always possible, especially when a highly compact and optimized optic is desired, since some of the light reflected on the primary mirror hits the receiver rather than the ideal primary-secondary-receiver optical path. Nevertheless, this effect can be controlled and managed, that is, the great majority of the light follows the optical path mentioned before.

When compared to the Helmet, this design increases reflection losses but reduces Fresnel losses at the vacuum tube glass envelope.

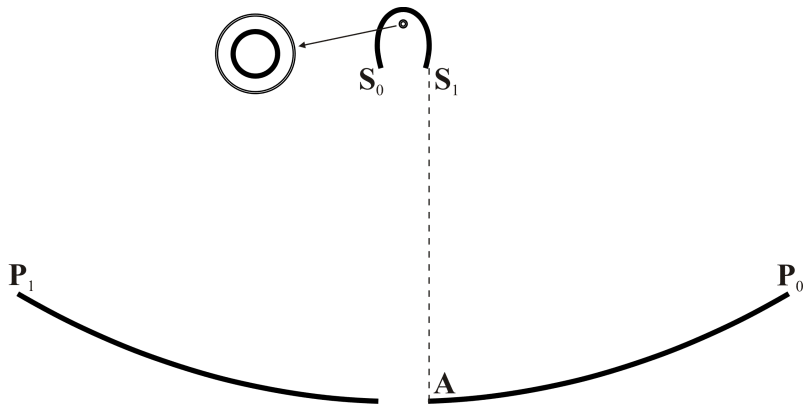

Fig. 6.3: The complete XX SMS optic.

6.3 Results and comparison

6.3.1 Results and comparison

The XX SMS optic in Fig. 6.3 was compared with the parabolic through (PT) solar concentrator with the same vacuum receiver tube, with the following assumptions:

- The half-acceptance angle, θ, is the same (same overall tolerances for both optics). In this analysis the effective acceptance angle of the optic is defined as the incidence angle at which the concentrator collects 90% of the on axis-power [14].
- The size (diameter) of the receiver is the same.

A comparison of optics with the same acceptance angle is one between optics that have the same overall tolerances to errors, such as optics quality, assembly of components, tracking of the sun, wind, dust and others. Optics with the same tolerances can be made and assembled using similar methods. Since the diameters of the vacuum tubes are standard the entrance aperture of the concentrators must vary to accommodate different concentrations (different CAP values) of the different optical architectures, i.e., concentrators to be compared have the same acceptance angle and same exit aperture, but varying entrance apertures. Note that a fixed entrance or exit aperture is only a scale factor of the concentrators. This is similar to what is done in Concentrated PhotoVoltaics (CPV) field in which concentrators to be compared have the same acceptance angle and the same entrance aperture, but varying exit apertures, since solar cells can then be cut in different sizes to accommodate the different CAP values [14].

Both optics were compared for η_{opt0} (optical efficiency at normal incidence), C_g (geometric concentration) and CAP. The details of the PT considered are shown in Table 6.1 [15].

Table 6.1: Details of the conventional PT concentrator.

Optic	Aperture size (m)	Receiver radius (m)	Focal length (m)	φ (deg)	C_g	θ
PT	5.77	0.035	1.71	80.3	26.26	0.694

Materials properties considered for both optics are as follows (Table 6.2):

Table 6.2: Materials properties.

Optical element	Reflectivity	Absorptivity	Transmissivity
Primary mirror	92% [16]	-	-
Secondary mirror	92% [16]	-	-
Receiver tube	-	95% [9]	-
Glass cover	-	-	96% AR-coated glass tube [9]

The optimization of the XX SMS optic leads to the results presented in Table 6.3.

Table 6.3: Comparison results.

Optic	η_{opt0}	η^*_{opt0}	C_g	CAP	φ (deg)	Aspect ratio (Height/Width)	Aperture width (m)	Mirror length (m)
PT	0.80	0.81	26.24	0.32	80.3	0.30	5.77	6.40
XX SMS	0.68	0.72	50.38	0.61	55	0.51	11.08	11.71

The values of η_{opt0} and CAP were calculated by raytracing. η^*_{opt0} is the optical efficiency without the shading losses, i.e., it is the optical efficiency defined as the fraction of the (direct) sunlight captured by the mirror aperture that is absorbed by the receiver. This value is important to calculate the total amount of collected energy because, for such calculation, it makes more sense to use the mirror aperture area and not the total aperture area (which includes the gap between the two heliostats, as shown in Fig. 6.3). Besides materials properties, the raytracing includes the solar angular profile (non-parallel rays). The rim angle obtained for the XX SMS optic is lower than in the PT optic. Now the aperture area is on the order of twice as large ($\approx 11\ m$) as that of the chosen PT trough, i.e. for the same collector field the number of troughs (rows) would be reduced by half. This lower rim angle is responsible for a lower mirror length per aperture area which may represent a reduction of the cost manufacturing.

The results in Table 6.3 show that the new XX SMS optic has almost double concentration – for the same half-acceptance angle, which shows the potential advantage of using a second-stage concentrator based on the SMS method. The optical efficiency at normal incidence η_{opt0} for the XX SMS optic is lower and this happens since in this optic (almost) all the light reflected by the primary mirror is reflected by the secondary mirror and, therefore, there is, at least, one more reflection than in the PT optic. The XX SMS optic, however, delivers 1.71 times more light onto the

same vacuum tube than the parabolic trough (0.72/0.81×50.38/26.24=1.71) when the direction of sunlight is parallel to the optical axis of the concentrator.

However, in order to determine the amount of energy delivered to the receiver in real world operating conditions, a more detailed calculation is needed. Such an analysis was done using commercial raytracing software, as well a numerical method developed in previous work [17]. This method evaluates the optical efficiency for different θ_Z (zenith angle) and φ_S (solar azimuth angle) [6] (ray tracing for all relevant pairs of θ_Z and φ_S), calculating function $\eta_{opt}(\theta_Z,\varphi_S)$.

This function is then multiplied by the corresponding DNI (Direct Normal Irradiance) and a factor (<1) which contains the relevant "cosine of incidence angle effect" correction to finally obtain the amount of energy collected by the receiver.

Often this calculation is alternatively performed with the help of incidence angle modifier (IAM) functions [6]. These curves are obtained from the function $\eta_{opt}(\theta_Z,\varphi_S$ for the longitudinal plane ($\varphi_S = 0^o$) and transversal plane ($\varphi_S = 90^o$). For the sake of completeness, in Appendix A of this Chapter the IAMs for the XX SMS optic presented in this paper are shown.

For this simulation and performance comparison, Faro, Portugal (37°02'N, 07°55'W), was selected, with an annual average DNI of 2234kWh/m^2 [18]. As mentioned before in this simulation thermal losses were not included, that is, only optical losses were considered. The results are shown in Table 6.4.

Table 6.4: Comparison of collected energy in Faro, Portugal. The calculations were done for a receiver of 70 mm of diameter and 1 m of length.

Optic	DNI (kWh/m^2)	Collected energy same vacuum tube (kWh)
PT	2234	7526.56
XX SMS	2234	12739.23

The XX SMS optic has almost double the aperture area than PT optic, for the same receiver and acceptance angle and, in spite of its lower optical efficiency, collects 1.69 times more energy (12739.23/7526.56 = 1.69). In practice other considerations can have some impact on the difference in collected energy.

However the real advantage of the XX-SMS will be manifest when the total field for a given power delivery (or for a given energy production) is considered, since then total heat losses would have to be taken into account and the XX SMS parabolic solution presented may have significantly lower thermal and parasitic losses due to the corresponding reduction of the number of troughs. The operating costs may also be lower (less parasitic pumping losses, less heat transfer fluid, etc.) and installation

costs (less pipes, less insulation and less components) thus seemingly favoring a solution with larger aperture widths. An optimization of this sort is well past the scope of this paper, since the authors currently do not have the necessary information to do it.

6.3.2 XX SMS and Helmet comparison

The XX is an SMS optic and it can be compared to the Helmet concentrator [13], another SMS optic designed in the past for a similar purpose as the XX. For this comparison, the data that has been published on the Helmet was used. Again, the XX SMS was optimized and tested for the same conditions and compared both concentrators.

This comparison was made based on two different models (#2 and #5) [13], which were designed and published for given concentrations. Therefore, for the sake of this comparison we use XX SMS optic design with the same geometrical concentrations, C_g. Also, the results published for the Helmet were obtained for a tubular receiver in air (no glass envelope around it). Therefore, in this comparison, the XX SMS concentrator was developed for the same type of receiver. The characteristics of the two Helmet models are shown in Table 6.5.

Table 6.5: Characteristics of the Helmet concentrators [13]. The unit of length is the receiver radius and the unit of angle is degree.

Optic	C_g (×)	θ	Focal length	Space receiver-secondary	Upper rim angle φ	Lower rim angle φ'
Helmet #2	65.6	0.51	117.1	14.7	86.9	7.7
Helmet #5	54.6	0.75	98.6	11.1	85.9	7.0

The optimization of the equivalent XX SMS optics was done and Fig. 6.4(a) and Fig. 6.4(b) shows the angular transmission for both cases. The Fig. 6.5 shows the cross-section of the Helmet concentrator.

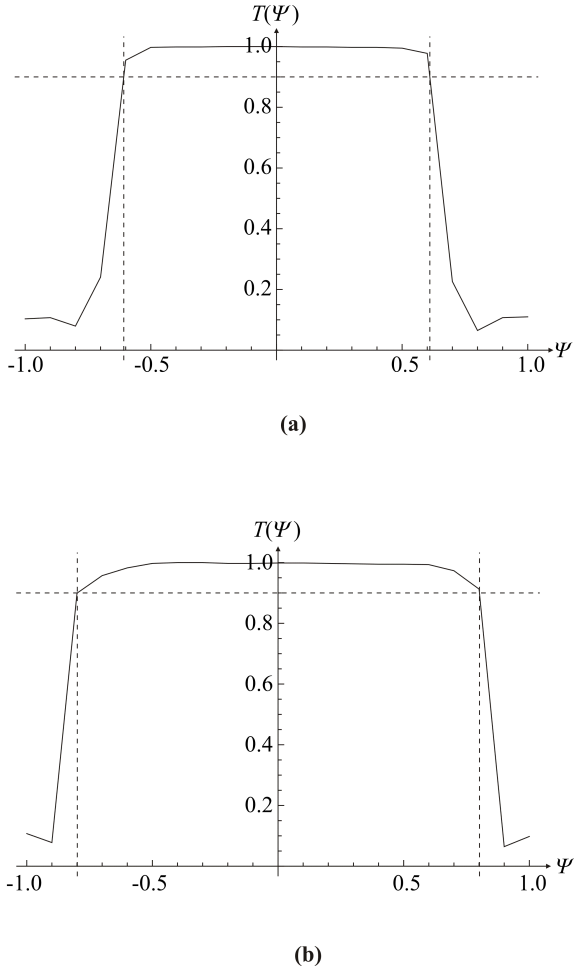

Fig. 6.4: Angular transmission of the XX SMS. (a) XX SMS equivalent to Helmet #2; (b) XX SMS equivalent to Helmet #5.

With these results, the optical efficiency can be calculated and compared for the perpendicular direction, η_{opt0}, as well as the CAP for both optics. The η_{opt0} for the Helmet concentrators was also provided by [13] and the calculations were done in the same conditions, in this case with a reflectivity of 100% and no scatter for the mirrors and a solar angular profile for the source.

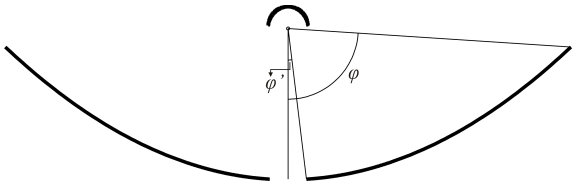

Fig. 6.5: Cross-section of the Helmet concentrator [13].

Table 6.6: Comparison of η_{opt0} and CAP between Helmet and XX SMS.

Optic	η_{opt0} (%)	CAP	θ (°)	C_g (×)
Helmet #2	93.6	0.58	0.51	65.6
XX SMS #2	98.1	0.70	0.61	65.6
Helmet #5	98.5	0.71	0.75	54.6
XX SMS #5	97.4	0.76	0.80	54.6

The results presented in Table 6.6 show that the XX SMS optic provides higher (#2) or similar (#5) efficiency with a higher CAP than that of the Helmet optic. It should be noted that the CAP is a fundamental characteristic when evaluating the potential of a solar concentrator to operate efficiently in real world conditions. The CAP for both concentrators is shown in Fig. 6.6. It can be seen that, for the same acceptance angle, the XX SMS has a higher CAP than the Helmet.

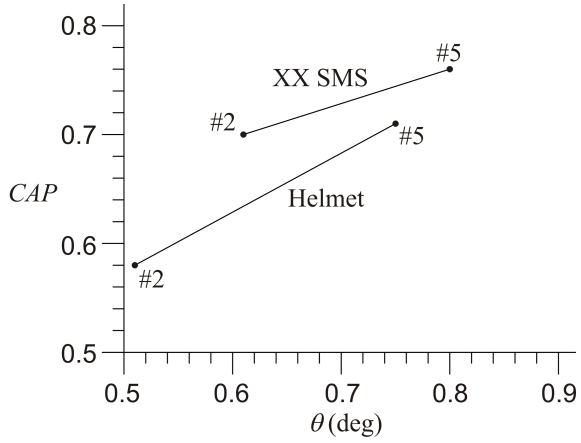

Fig. 6.6: CAP comparison between the Helmet and XX SMS concentrators. It can be seen that, for the same acceptance angles, the XX SMS has a higher CAP and, therefore, reaches higher concentrations.

6.4 Conclusions

In this paper a new XX SMS solar concentrator is presented and discussed, through comparisons with a conventional PT and other previously developed solutions.

A strong motivation for this exercise is a direct result of the need to find ways to reduce costs in PT solar collector CSP systems. An outstanding possibility is the reduction of the number of rows in a collector field, for the same energy delivered, with the associated reduction of receivers, pipe length, pipe losses, heat transfer fluid quantities, number of components, operational costs, etc. However, since the standard (i.e. on the market) evacuated receiver has a fixed diameter, it is very hard to do anything about parabolic size, without completely revising the associated optics. This is what the present paper attempted at doing, by proposing a new concept for PT–like concentration technology for evacuated tubes, pushing to the limits the concentration achieved and also comparing it with previously proposed similar higher concentration optics (Helmet) albeit designed for non-evacuated tubular receivers.

The new optical solution - XX SMS - was shown to provide a slight improvement over other XX SMS solutions like the Helmet, both for CAP and for optical efficiency.

With respect to conventional PT the new solution was shown to deliver considerable more energy onto the same vacuum tube receiver, in line with what would be expected.

Thermal and other losses (calculations not included in this paper) and cost of a full collector field using these technologies will be quite different from those in a conventional PT field. This is a study to be made by collector manufacturers and system installers, optimizing energy yields at a given operating temperature and overall costs. This paper is useful for that optimization since it provides a specific design for the optics and a value for the comparison in the energy delivered. The authors do not possess the specific information, field by field, manufacturer by manufacturer, to carry this exercise further in this paper.

It is also clear that intermediate strategies are possible, with the design along these principles, for a trough which would not have as high a concentration (but would still be significantly larger: for instance 1.5 or 1.6× larger) and would have a larger acceptance angle, and perhaps lower manufacture and installation costs.

This design approach should also be of interest for troughs designed for lower temperatures, with non-evacuated receivers, where a lower heat loss (thus higher efficiency) can be obtained through higher concentration, all else being equal. In short, the new XX SMS optic represents a theoretical/practical novelty, significantly approaching the limits of concentration, circumventing the difficulty of Gap/Fresnel losses when evacuated tubular receivers are used in CSP parabolic trough fields, but also outside the CSP area, for other Solar Energy applications, like process heat,

desalination or cooling.

Appendix A

The Fig. 6.7 shows the IAM curves of the PT Concentrator.

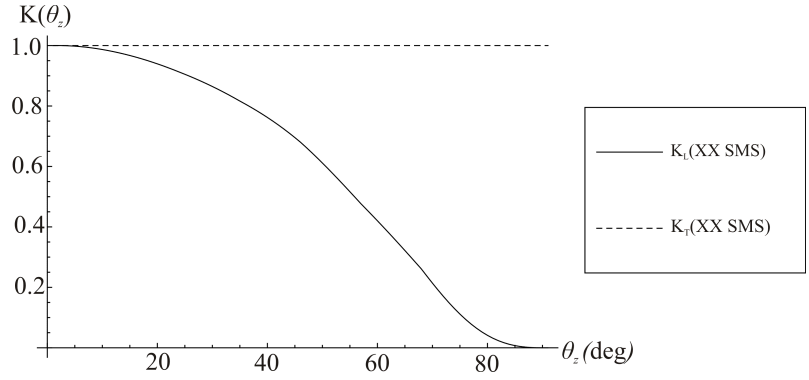

Fig. 6.7: IAM curves for the XX SMS optic (longitudinal (K_L) and transversal (K_T) planes).

References

[1] Crespo, L., *The European solat thermal electric market*, Intersolar European Conference, Munich, June, 2011.

[2] Winston, R., Miñano, J.C., Benítez, P., (contributions by Shatz, N., Bortz, J.,C.), *Nonimaging Optics*, Elsevier Academic Press, Amsterdam, 2005.

[3] Bendt, P., *Optical analysis and optimization of line focus solar collectors*, Colorado, September, 1979.

[4] R. John Koshel, Illumination Engineering: Design with Nonimaging Optics, Wiley, 2013.

[5] Reeken, F., et al., *Extended Rabl-method to assess the optical quality of parabolic trough collectors*, Proceedings 18th International SolarPACES Symposium, September 11-14, Marrakech, Morocco, 2012.

[6] Rabl, A., *Active Solar Collectors and their applications*, Oxford University, Oxford, 1985.

[7] Chaves, J., 2008, *Introduction to Nonimaging Optics*, CRC Press, Taylor and Francis Group.

[8] Riffelmann, K.J., Lüpfert, E., Richert, T. and Nava, P., *Performance of the Ultimate Trough Collector with Molten Salts as Heat Transfer Fluid*, Proceeding 18th International SolarPACES Symposium, September 11-14, Marrakech, Morocco (2012).

[9] SCHOTT PTR 70 Receiver brochure.

[10] SIEMENS Solar, *http://www.energy.siemens.com/hq/en/power-generation/renewables/solar-power/*

[11] Collares-Pereira, M., Gordon, J.M., Rabl, A., Winston, R., *High concentration two-stage optics for parabolic trough solar collectors with tubular absorber and large rim angle*, Solar Energy 47 (6), pp. 457-466, 1991.

[12] Mills, D.R., *Two-stage tilting solar concentrators*, Solar Energy 25, pp. 505-509, 1980.

[13] Benítez, P., *Advanced concepts of non-imaging optics: design and manufacture*, PhD Thesis, Presented in Madrid, January 16, 1998.

[14] Benítez, P., et al., High performance Fresnel-based photovoltaic concentrator, Optical Society of America, 26 April 2010, Vol. 18, No. S1, OPTICS EXPRESS.

[15] Kearney, D.W., *Parabolic Trough Collector Overview*, Parabolic Trough Workshop, 2007.

[16] *http://www.saint-gobain-solar-power.com/mirrors-solar-glass-7* (SGG MIRALITE SOLAR 4 mm).

[17] Canavarro, D., *Modeling linear solar collectors of the Fresnel-type; application to an innovative CLFR collector "Etendue Matched"*, MSc thesis, Instituto Superior Técnico/UniversidadeTécnica de Lisboa, Lisbon, 2010.

[18] Meteonorm hourly DNI data.

Nomenclature

A	a point **A**
C_g	geometric concentration (×)
C_{Max}	maximum theoretical concentration (×)
C_{PT}	geometric concentration of a PT (×)
CAP	Concentration Acceptance Product
CPC	Compound Parabolic Concentrator
CPV	Concentrated PhotoVoltaics
CSP	Concentrated Solar Power
DNI	Direct Normal Irradiance
E_P	etendue captured by the primary
E_R	maximum etendue captured by the receiver
f	a flow-line
HTF	Heat Transfer Fluid
IAM	Incidence Angle Modifier
L_R	length of the arc between two flow-lines of the receiver (m)
n	refractive index
PT	Parabolic Trough

R	refractive surface
R	A circular receiver
r	A ray r
SMS	Simultaneous Multiple Surface
STE	Solar Thermal Electricity
X	reflective surface

Greek symbols

α	angle between two flow-lines (grad)
η_{opt0}	optical efficiency at normal incidence
η^*_{opt0}	optical efficiency at normal incidence without shading losses
θ	half-acceptance angle (grad)
θ_Z	solar zenith angle (grad)
φ	rim angle (grad)
φ_S	solar azimuth angle (grad)

Chapter 7

Infinitesimal etendue and Simultaneous Multiple Surface (SMS) concentrators for fixed receiver troughs†

Abstract

In order to increase the cost-effectiveness of conventional Parabolic Trough (PT) fields it is essential to reduce Capital Expenditure (Capex) as well as Operations and Maintenance (OM) costs, in particular the need for flexible hosing or rotating joints, which are used because the tubular receiver also tracks in a solidary way with the trough. One possible alternative is to design a different type of optic with the center of mass on the center of the tubular receiver, generating the possibility of it being fixed, thereby dispensing with flexible hosing or rotating joints, without penalizing its overall efficiency or even concentration. In this work, two possible optical solutions, combining parabolic-type primaries with second-stage non-imaging optics concentrators for fixed receivers, are presented. These concentrators are designed using the Simultaneous Multiple Surface (SMS) design method and the infinitesimal etendue limit. A performance comparison with a conventional PT in terms of optical efficiency, CAP (Concentration-Acceptance Product) and other performance data are also presented, including an estimate of the total amount of yearly collected energy (kWh/m^2 of entrance aperture) for one particular location – Faro (Portugal).

Keywords: Parabolic Trough; Fixed receiver; SMS method; Infinitesimal etendue

---

†Diogo Canavarro[(1)], Julio Chaves[(2)], Manuel Collares-Pereira[(1)], Infinitesimal etendue and Simultaneous Multiple Surface (SMS) concentrators for fixed receiver troughs, *Solar Energy* 97 (2013) 493–504.

[(1)] BES Renewable Energies Chair, University of Évora (Portugal).

[(2)] Light Prescriptions Innovators, UPM, Madrid (Spain).

7.1 Introduction

Presently, parabolic trough (PT) concentrators are the leading technology for CSP (Concentrated Solar Power). For instance, they represent 94% of all solar thermal electricity capacity installed in Spain today [1, 2]. However, PT and the other CSP technologies are facing a steep challenge for cost reduction, which is likely to come from reduction of manufacturing costs, new optical and thermal solutions, new materials, larger scale and /or migration towards regions of the World with higher DNI (Direct Normal Irradiance).

One of the problems facing parabolic troughs of today is the fact that each trough and its associated receiver track together the apparent motion of the sun, creating the need for flexible hosing or rotating joints to connect them to the fixed piping transporting the Heat Transfer Fluid (HTF). This results in mechanical and thermal stresses, increased Operations and Maintenance (O&M) costs and vulnerability of the full collector field.

A possible solution to this problem has been well known for many years: it would be sufficient to track the sun with only the parabolic mirror and leave the receiver fixed, if only the tracking axis coincided with the receiver center and focal point. Conventional PTs are designed to take advantage of the highest concentration (C) possible (see Eq. 7.1 and Fig. 7.1 where θ is the half-acceptance angle for the radiation incident on the aperture and φ is the rim angle of the parabola), which is achieved for every half-acceptance θ, when φ is close to 90^{o} [3, 4].

$$C = \frac{\sin\varphi}{\pi \sin\theta} \tag{7.1}$$

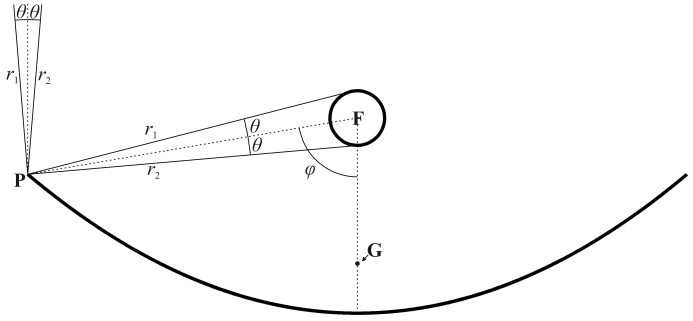

Fig. 7.1: The parabolic trough concentrator (PT). It has a circular receiver centered in **F**, a center of mass located in **G**, a rim angle φ; it is designed to accomodate the edge rays r_1 and r_2 and the receiver at the edge of the primary **P**. The size of the circular receiver is exagerated for clearer viewing.

For obvious mechanical reasons and substantial reduction of parasitic power losses with tracking, these troughs are designed to rotate about an axis which goes

through their center of mass, which in a conventional PT is substantially below the focal point (center of the receiver).

If a parabolic trough is to track about an axis going through its focal point the design would be much more like that of Fig. 7.2. Eq. 7.1 still holds, but now the value of $\sin\varphi$ penalizes the overall resulting concentration and for the same θ, the receiver diameter would have to be larger. Most present day CSP parabolic troughs are designed for evacuated receiver tubes and there is today a sort of standard on the market, with a receiver diameter of 70 mm [5, 6], which means that to keep on using it, the trough would have to be smaller (a smaller entrance aperture).

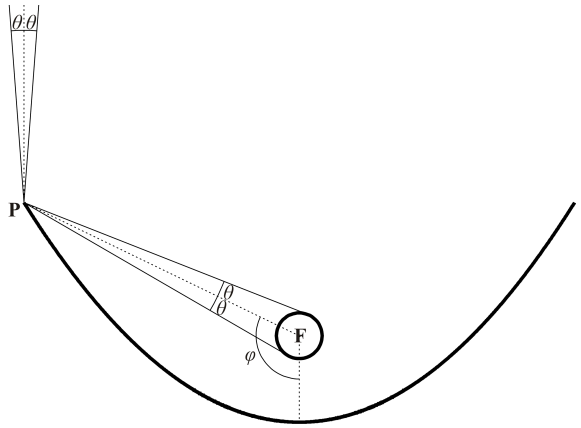

Fig. 7.2: PT of Fig. 1.1 designed to have the center of mass at point **F**; the rim angle φ will have to be about 116°, penalizing the overall achievable concentration.

Smaller entrance aperture troughs are not desirable for large fields [7, 8]. In fact the opposite tendency – larger entrance aperture troughs – is just being proposed (for instance the Ultimate Trough [8, 9]) for cost reduction. The idea is that larger entrance aperture troughs reduce the number of rows per field, and reduce accordingly a series of other losses, like thermal losses, parasitic pumping and power tracking losses, fluid volume, etc., and direct investment cost reduction from the reduction of the number of receiver, pipe length, number of connections, O&M costs, etc.

Of course the use of a larger evacuated inner receiver tubes (for instance with 90mm as it is being proposed by tube manufacturers (for instance, SCHOTT [5]) would, by itself, allow for a larger entrance aperture through as in Fig. 7.2. However, this increased size results simply from scaling up the whole system and concentration ratio remains the same.

Another possibility – and the object of this paper – is to keep on considering the use of the present evacuated "standard" receiver tube of 70 mm and take advantage of the fact that parabolic trough optics is very far from the concentration limit, designing a new optic with a second stage concentrator, which can be conceived

to yield a higher concentration for the same acceptance-angle or design for a wider acceptance angle (relaxing manufacturing accuracy and/or other aspects influencing the average intercept factor) while preserving concentration.

In this case, for a proof of concept and in view of the fact that the idea is to keep on using the same evacuated tubular receiver with 70mm diameter, θ will be chosen to be the same as in a conventional trough (a value between 2 and 3 times the half-angular width of the sun), but with a higher value concentration, yielding a larger aperture.

It is clear that if a manufacturer cares to adopt this idea, many aspects should be adjusted for a final optimization and that is far beyond the scope of this paper.

This paper will, in fact, present two different solutions: (i) an infinitesimal etendue concentrator and (2) an ideal NonImaging Optics (NIO) solution designed with the Simultaneous Multiple Surface (SMS) method for two reflective (X) surfaces (XX SMS) [7, 10]. For comparison purposes, the acceptance angle of interest of the SMS optic, defined as the incidence angle at which the concentrator collects 90% of the on axis-power [11], is the same as that of a conventional PT (the trough used in this work was the "Flagsol SKAL-ET 120" [2]) (see section 7.4).

The analysis will also take into account the reduction of Fresnel losses through the glass envelope of the vacuum tube for the radiation coming from the secondary stage of the concentrator optics. [7]

An indication is given for the procedure to calculate the center of mass of the optic again with no concern for the presentation of a final solution, since it will depend on manufacturing details not handled in this paper.

The paper will end with a performance comparison between a conventional PT and the new designs, both in terms of their optic characteristics and also in terms of the energy delivered to the receiver, taking into account DNI data from a specific location (Faro, Portugal).

The new optic solutions presented in this paper can be developed for receivers of any diameter. The concern with what is readily available on the market and used in most CSP troughs today, was just to provide a context for performance comparison and a motivation for the effort around the development of second stage concentration solutions for fixed receiver troughs.

As a final comment it should also be noted that several proposals have already been made to increase the concentration of conventional PT concentrator, using many different types of second-stage NIO concentrators, such as CPC (Compound Parabolic Concentrator) and CEC (Compound Elliptical Concentrator) type concentrators, TERC (Tailored Edge-Ray Concentrator), Trumpet, etc. [10, 12, 13]. However, these proposals were not intended for fixed receiver solutions.

7.2 Primary/secondary concentrator combinations for fixed receivers

7.2.1 Presentation of two different possible solutions

In search for a solution approaching the limits of concentration, and in view of the large gap between the inner receiver tube and the outer glass envelope of evacuated tubular receivers, a first idea could be to use the SMS method ([7, 10]), since this will yield a NIO solution approaching the limits of possible concentration, for any given half-acceptance angle θ.

However, for high solar energy concentration, as is the case here, the acceptance angle of concentrating optics is small. Therefore, it is possible to start the design process by performing a simpler exercise: to find a first solution on a limiting case, the infinitesimal etendue approximation, and then improve that solution with a full NIO, SMS, ideal optics approach for a given acceptance angle 2θ.

The infinitesimal etendue limit can be considered as the limit case of an SMS optic, when the acceptance angle of the optic goes to zero and, therefore, the size of the receiver would be infinitesimal [14]. The infinitesimal etendue limit will not yield a concentrator as close to the limit as the one from the SMS method, but it is considerably easier to design. It has been shown that up to $\theta = 20$mrad that type of solution is only very little worse than a full-fledged, ideal, NIO [15] and can yield a very high concentration when the acceptance angle is small.

7.2.2 XX Infinitesimal etendue optic design

Fig. 7.3(a) shows an optic O with small half-acceptance angle θ and circular receiver (a tube in 3D) of diameter D immersed in a medium of refractive index n. Light enters the optic through an infinitesimal aperture dx and will eventually reach the receiver with an angular aperture $d\alpha$. Conservation of etendue U in this case is given by:

$$U = 2dx \sin\theta = 2nD \sin(\frac{d\alpha}{2}) \tag{7.2}$$

When $d\alpha \longrightarrow 0$, one may make $\sin(d\alpha) \approx d\alpha$ resulting in:

$$\frac{dx}{d\alpha} = \frac{nD}{2\sin\theta} \tag{7.3}$$

Which is a differential equation for $x(\alpha)$, and one gets:

$$x = \frac{nD}{2\sin\theta}\alpha + K \tag{7.4}$$

Where K is a constant of integration, which may be determined by an initial condition $x(\alpha_1) = x_1$ resulting in:

$$x = x_1 + \frac{nD}{2\sin\theta}(\alpha - \alpha_1) \tag{7.5}$$

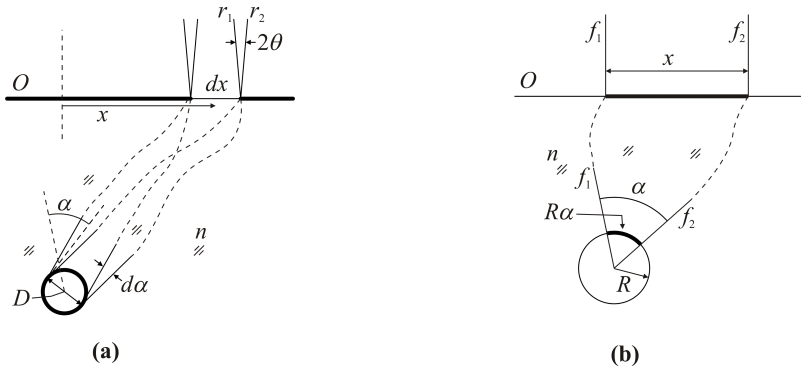

Fig. 7.3: Concentrating optics with an aperture O. (a) A pencil of light entering optic O within small aperture dx reaches the small receiver of diameter D with angular aperture $d\alpha$.(b) The etendue between flow lines f_1 and f_2 is conserved as light travels from the entrance aperture of the optic O to its receiver.

When applied to a solar concentrator, this equation will only guarantee that the incoming edge rays are redirected in directions tangent to the tubular receiver when the acceptance angle goes to zero (in the limit of infinitesimal acceptance). This means that these concentrators will only reach the thermodynamic limit of concentration in this extreme case. This is what is also referred to as the aplanatic approximation [15, 16], when the receiver is a straight segment. However, this equation can still be used with finite (but small) values of θ to obtain concentrators which are not ideal, but still have practical interest, because they approach the thermodynamic limit of concentration.

When the receiver is in air (or vacuum), n=1 and in the particular case in which $\alpha_1 = x_1 = 0$, one gets:

$$x = \frac{D}{2\sin\theta}\alpha \tag{7.6}$$

Which may also be written as $2x\sin\theta = 2R\alpha$ where $R = D/2$ is the radius of the circular receiver and Rα is the receiver arc length between two flow lines f_1 and f_2. This expresses the conservation of etendue between flow lines f_1 and f_2, as shown in Fig. 7.3(b).

For an infinitesimal acceptance angle θ, rays r_1 and r_2 collapse onto one merged ray, which coincides with the flow line bisecting them. The path of this merged ray inside the optic must satisfy Eq.,7.5. Fig. 7.4 shows a possible application of

this procedure to a concentrator with primary mirror m_1, secondary mirror m_2 and (point) receiver C.

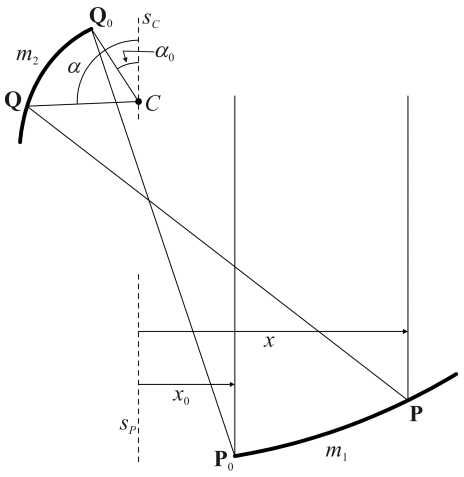

Fig. 7.4: Primary-secondary concentrator for a small circular receiver C.

Primary mirror m_1 starts at point $\mathbf{P}_0$ at a horizontal distance m_0 from a reference line s_P. The corresponding secondary mirror m_2 starts at position $\mathbf{Q}_0$, making an angle α_0 to reference line s_C. Two other points $\mathbf{P}$ and $\mathbf{Q}$ on the primary and secondary mirrors are related by Eq. 7.5. A possible way to construct these mirrors is to start at $\mathbf{P}_0$ and $\mathbf{Q}_0$ and advance in very small steps intersecting each new ray with the tangent planes defined by the previous ray. This is the same method used to design infinitesimal etendue (aplanatic) concentrators for flat receivers [14].

This approach can be applied to the design of a concentrator whose primary mirror is divided into three sections, as shown in Fig. 7.5 and Fig. 7.6. The first section p_1 from $\mathbf{P}_0$ to $\mathbf{P}_1$ is a parabola with focus $\mathbf{F}$. The second section of primary p_2 from $\mathbf{P}_1$ to $\mathbf{P}_3$ reflects light to section $\mathbf{S}_1$ to $\mathbf{S}_3$ of the secondary (portion s_2), which redirects it to focus $\mathbf{F}$. The third section of primary p_3 from $\mathbf{P}_4$ to $\mathbf{P}_5$ reflects light to section $\mathbf{S}_4$ to $\mathbf{S}_5$ of the secondary (portion s_3), which again redirects it to focus $\mathbf{F}$.

The design process starts by defining a (small) acceptance angle θ for the optic and a receiver of radius R centered at point $\mathbf{F}$, as shown in Fig. 7.5.

The distance from the focus $\mathbf{F}$ to the vertex $\mathbf{C}$ of the parabola may be obtained by $[\mathbf{F},\mathbf{C}]=R/\tan\theta$ (where $[\mathbf{F},\mathbf{C}]$ is the Euclidean distance between points $\mathbf{F}$ and $\mathbf{C}$). This ensures that incoming edge rays r_{C1} and r_{C2} incident at $\mathbf{C}$ are reflected in directions tangent to the circular receiver. Points $\mathbf{P}_0$ and $\mathrm{P}\mathbf{P}_1$ where the central parabola starts and ends, i.e., its lower and upper rim angle (φ_{p0} and φ_{p1}, respectively) are variables to be optimized during the design process, as will be seen later.

The second portion of the primary starts at point $\mathbf{P}_1$ and its corresponding

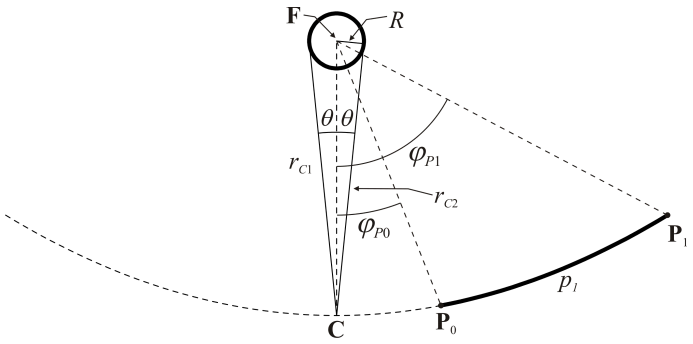

Fig. 7.5: Central arc of parabola of the solar concentrator.

secondary at point $\mathbf{S}_1$ whose position must also be optimized in the design process. It should be noted that at point $\mathbf{P}_1$ the primary mirror has a "kink" (discontinuous derivative) as this point belongs both to p_1 and p_2 and, therefore, ray r_1 incident at this point is split in two, r_{1F} reflected to $\mathbf{F}$ and r_{1S} reflected to $\mathbf{S}_1$, as shown in Fig. 7.6. Vertical ray r_1 is reflected by portion p_2 of the primary at point $\mathbf{P}_1$ towards $\mathbf{S}_1$ and from there to $\mathbf{F}$. Ray r_1 enters the concentrator at x=x_1 (the horizontal coordinate of point $\mathbf{P}_1$) and reaches the absorber at an angle to the vertical α_1=0. Replacing these initial conditions into Eq. 7.5, the result is:

$$x = x_1 + \frac{nD}{2\sin\theta}\alpha \tag{7.7}$$

The path of incoming vertical ray r_1 through points $\mathbf{P}_1$, $\mathbf{S}_1$ and $\mathbf{F}$ allows us to calculate the normals $\mathbf{n}_1$ at point $\mathbf{P}_1$ of mirror p_2 and $\mathbf{m}_1$ at point $\mathbf{S}_1$ as shown in Fig. 7.6(a). Now consider another vertical ray r_2, at a horizontal distance x_2 from the optical axis, and displaced by a small amount $\Delta\, x$ relative to x_1. Eq. 7.7 for this ray becomes:

$$x_2 = x_1 + \frac{nD}{2\sin\theta}\alpha_2 \tag{7.8}$$

yielding the corresponding value of α_2. Now the incoming vertical ray r_2 intersects the plane defined by $\mathbf{P}_1$ and normal $\mathbf{n}_1$, determining the position of a new point $\mathbf{P}_2$ on the primary mirror. Also, a ray launched from $\mathbf{F}$ at an angle α_2 to the vertical intersects the plane defined by point $\mathbf{S}_1$ and its normal $\mathbf{m}_1$, thus defining a new point $\mathbf{S}_2$ on the secondary mirror. Connecting $\mathbf{P}_2$ with $\mathbf{S}_2$ completes the path of the ray and determines the normals $\mathbf{n}_2$ at $\mathbf{P}_2$ and $\mathbf{m}_2$ at $\mathbf{S}_2$. The process can then be repeated with another ray further to the right of r_2, determining new points on the primary and secondary mirrors. Proceeding in very small steps, this method provides the calculation of the complete shape of both the primary and secondary mirrors.

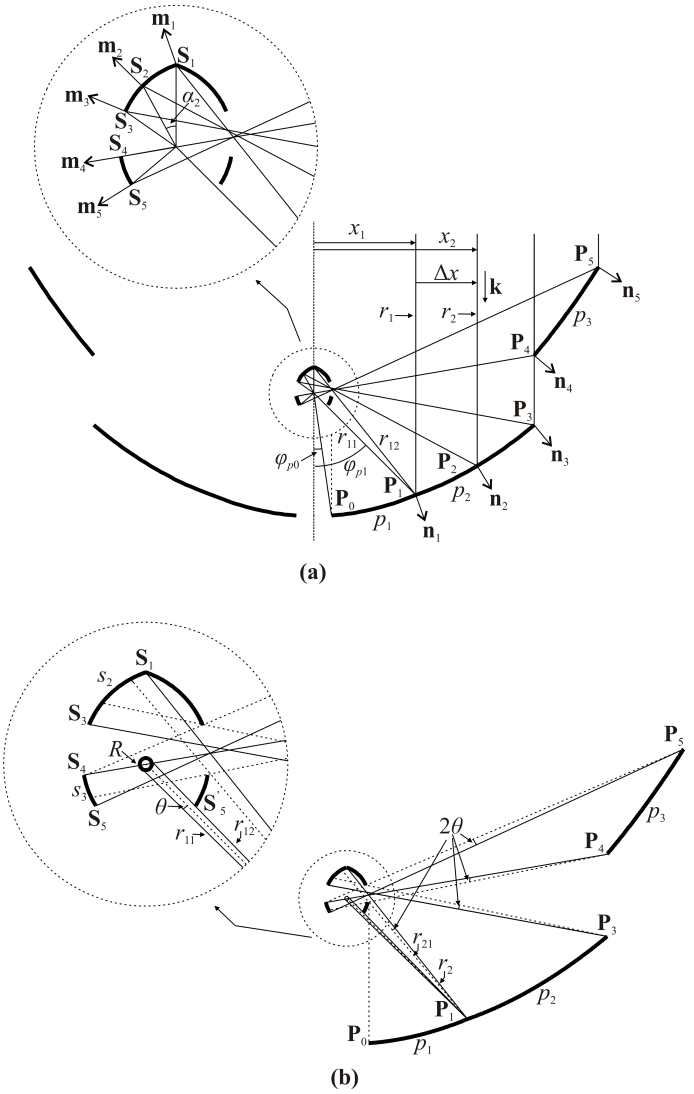

Fig. 7.6: The XX infinitesimal etendue optic. (a) The XX infinitesimal etendue design method; (b) Optimization of the position of each section in the optic.

Next, a point $\mathbf{P}_4$ is chosen on the vertical of point $\mathbf{P}_3$ as the first point of the third portion of the primary, p_3, leaving a vertical gap between $\mathbf{P}_3$ and $\mathbf{P}_4$. This gap is needed to also induce a gap on the secondary (between $\mathbf{S}_3$ and $\mathbf{S}_4$), as shown in Fig. 7.6(a), since otherwise the latter would block the great majority of the light reflected by the primary. In other words, the gap on the secondary will be the "focal point" of the portions p_2 and p_3, through which the light enters. Along with $\mathbf{P}_4$, a corresponding point on the secondary $\mathbf{S}_4$ is chosen (first point of the new portion of secondary) and using the method described above, new sections of primary and secondary mirrors are calculated, ending at point $\mathbf{P}_5$ and $\mathbf{S}_5$ respectively. The other half of the optic is symmetric with respect to the vertical axis through $\mathbf{F}$.

After completing the design of the optic, the position of each section of primary

and secondary, should be optimized as mentioned before. This optimization can be done by using the angular aperture 2θ for the incoming light to optimize the position of the initial points of the primary and secondary and, in particular, define the size of the gap between both sections of the secondary. The infinitesimal etendue optic is used as a first step for the SMS optic since it conserves etendue between flow lines (which in this case of an infinitesimal acceptance θ coincide with the paths of the rays). Also, it is simpler to design and gives a good approximation of what the shape of the SMS optic will be, as will be seen later. The use of an angular aperture 2θ is important to optimize the position of each part of the concentrator, as the SMS optic uses a finite size receiver.

The optimization is schematically shown in Fig. 7.6(b). From point $\mathbf{P}_1$, seen as belonging to the mirror section p_1, two edge rays r_{11} and r_{12} are launched towards the edges of R, i.e., the tangent points "seen" from $\mathbf{P}_1$. Ray r_{12} is used to optimize the position of $\mathbf{S}_5$, since the secondary should surround the receiver as much as possible (to maximize concentration), but without shading the light from the primary. Note that the angle between r_{11} and r_{12} is $\alpha < 2\theta$ because of the way parabola p_1 was defined in Fig. 7.5. It is also possible to define parabola p_1 in such a way that $\alpha = 2\theta$, in which case no light will be lost at point $\mathbf{P}_1$ for incoming light with angular aperture θ.

Now, again from point $\mathbf{P}_1$ seen as belonging to the mirror section p_2, we launch a ray r_{1R} (dashed line) rotated 2θ clockwise relatively to vertical ray r_{1S}. In this construction the incoming edge rays making angles -θ and +θ to the vertical are not reflected at $\mathbf{P}_1$, but instead those between 0 and 2θ clockwise. The reason for this is that light (ray r_{1S}) that makes an angle of 0º with the vertical and hits the edge $\mathbf{P}_1$ of the primary section p_2 is reflected towards the edge $\mathbf{S}_1$ of the corresponding section s_2 of the secondary. If two edge rays were used, the light between 0 and θ counterclockwise would miss the secondary. The reason for this construction is to ensure that light with angular aperture 2θ will be able to pass through the aperture in the secondary.

Now, from point $\mathbf{P}_3$ we launch a ray r_{3L} (dashed line) rotated 2θ counterclockwise relatively to vertical ray r_{34}. In this construction, again the incoming edge rays making angles -θ and +θ to the vertical are not reflected at $\mathbf{P}_3$, but instead those between 0 and 2θ counterclockwise. The reason for this is that light (ray r_{34}) that makes an angle of 0º with the vertical and hits the edge $\mathbf{P}_3$ of the primary is reflected towards the edge $\mathbf{S}_3$ of the corresponding section s_2 of the secondary. If two edge rays were used, the light between 0 and θ clockwise would miss the secondary. The reason for this construction is again to ensure that light with angular aperture 2θ will be able to pass through the aperture in the secondary. A similar procedure is used at points $\mathbf{P}_4$ and $\mathbf{P}_5$ using rays r_{4R} and r_{5L}. The positions of end points $\mathbf{S}_3$,

$\mathbf{S}_4$ and $\mathbf{S}_5$ of the secondary must be optimized in such a way that the secondary mirrors clear all these rays (r_{12}, r_{1S}, r_{1R}, r_3, r_{3L}, r_4, r_{4R}, r_5, r_{5L}) and yet enclose as much as possible of receiver R to maximize concentration.

The position of $\mathbf{P}_0$ is also optimized in order to guarantee that the secondary does not produce any shading over the primary.

The reason for using these rays (r_{12}, r_{1S}, r_{1R}, r_3, r_{3L}, r_4, r_{4R}, r_5, r_{5L}) in the optimization process is that the resulting infinitesimal etendue design will be used as a basis for the SMS design presented below. In the case of the SMS, the angular aperture of the rays coming from the edges of the primary mirrors is 2θ and these edge rays must be able to go through the hole in the secondary, whose size should be minimized to maximize concentration.

7.2.3 XX SMS optic design

As mentioned in the previous section, the infinitesimal etendue optic can be used as a starting point for the SMS optic design. The edges of each mirror section of the SMS optic are taken as either the same, or very close to the ones obtained for the infinitesimal etendue optic.

Ray assignation can then be made for the first section p_{11} and, with it, design the SMS chains of the primary and secondary mirrors, as shown in Fig. 7.7(a). The design starts with the definition of wavefronts w_1 and w_2, making an angle 2θ to each other. Incoming rays r_1 and r_2, perpendicular to w_1 and w_2 respectively, are launched from points $\mathbf{W}_{11}$ and $\mathbf{W}_{12}$ and reflected at edge $\mathbf{P}_1$ (same location as for the infinitesimal etendue optic) of the primary and then by portion s_{11} of the secondary in directions tangent to the "right" of the circular receiver, that is, perpendicular to wave front w_3 according to the edge-ray principle [10, 12]. This process defines mirror s_{11}, a macrofocal ellipse [12], between its end points $\mathbf{S}_1$ and $\mathbf{N}_1$. It has focus $\mathbf{P}_1$, macrofocus centered at $\mathbf{F}$ with radius r (radius of the circular receiver) and goes through $\mathbf{S}_1$.

By reflecting rays between r_1 and r_3 coming from the circular receiver (both tangent to it) at point $\mathbf{S}_1$, a new portion p_{11} of the primary may also be defined, by reflecting these rays in directions parallel to r_1 and r_3. This portion of primary is therefore a parabola with focus on $\mathbf{S}_1$ passing through $\mathbf{P}_1$ and whose axis is tilted counterclockwise by an angle θ relatively to the vertical direction.

Now, we may reflect on p_{11} a set of rays parallel to r_2 and calculate a new portion of secondary s_{12} to the left of s_{11} that redirects these rays in directions perpendicular to wavefront w_3. Also, we may reflect on s_{11} a set of rays perpendicular to wave front w_4 and calculate a new portion of primary mirror p_{12} to the right of p_{11} that redirects these rays in the direction of rays r_1 and r_3.

This process is repeated several times in order to get other portions of the primary

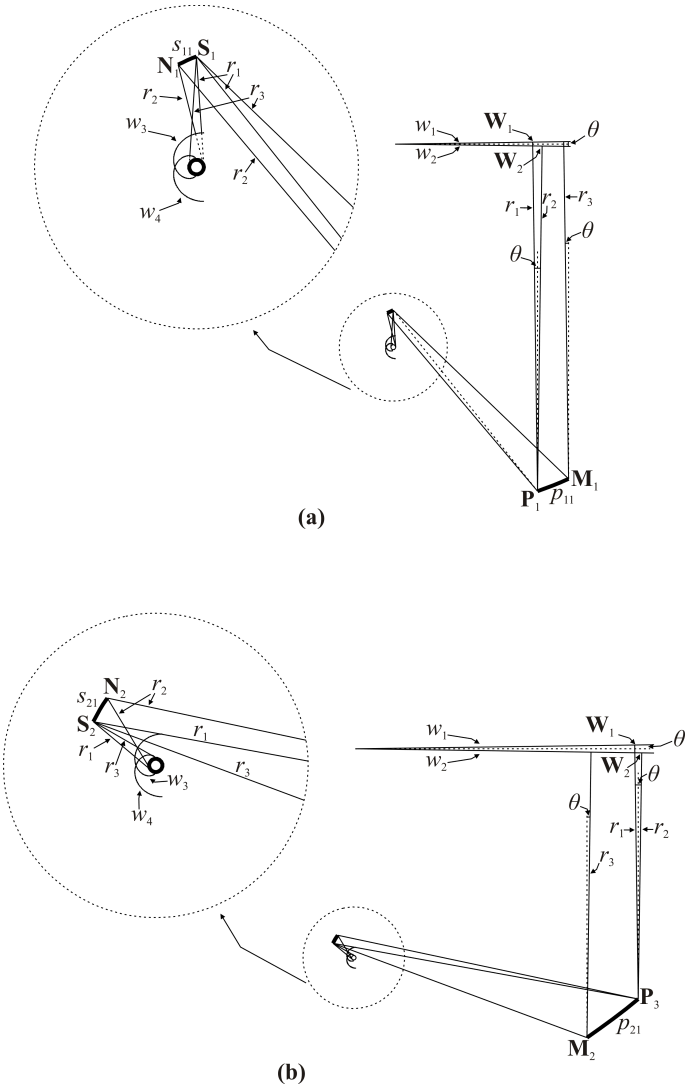

Fig. 7.7: The XX SMS optic design method. (a) The lower portion starting from the point $\mathbf{P}_1$. (b) The lower portion starting from $\mathbf{P}_3$.

and secondary (SMS chains). The process stops when the rightmost edge of the primary extends beyond $\mathbf{P}_3$ (see Fig. 7.6(a). Therefore, a primary mirror results which starts at $\mathbf{P}_1$ but ends at some point above $\mathbf{P}_3$ (not shown in the figure).

This process is next done in the opposite direction, as shown in Fig. 7.7(b). This time portion p_{21} starts at point $\mathbf{P}_3$ (same location as for the infinitesimal etendue optic) but the complete SMS mirror ends at some point below $\mathbf{P}_1$. The design process is similar to the one used for the SMS mirrors starting at $\mathbf{P}_1$ and $\mathbf{S}_1$ but in this case the ray assignation is different.

The set of rays between r_1 and r_2 incident at point $\mathbf{P}_3$ is now reflected by s_{21} towards the "left" of the receiver, i.e., perpendicular to wave front w_4. Cartesian oval s_{21} is then a macrofocal ellipse with focus $\mathbf{P}_3$ and macrofocus at the circular

receiver. Rays between r_2 and r_3 (tangent to the tubular receiver) and incident on $\mathbf{S}_2$ are now reflected by p_{21} in directions the direction of r_2 and r_3 perpendicular to flat wavefront w_2, that is, tilted by an angle θ clockwise relative to the vertical. Cartesian oval p_{21} is then a parabola with focus $\mathbf{S}_2$ and axis perpendicular to flat wavefront w_2.

Now, we may reflect on p_{21} a set of rays parallel to r_1 and calculate a new portion of secondary s_{22} to the right of s_{21} that redirects these rays in directions perpendicular to wavefront w_4. Also, we may reflect on s_{21} a set of rays perpendicular to wave front w_3 and calculate a new portion of primary mirror p_{22} to the left of p_{21} that redirects these rays in the direction of rays r_2 and r_3.

Calculating more SMS sections will eventually extend the primary mirror below point $\mathbf{P}_1$ (extended mirror not shown).

At the end of the design process, there will be two SMS sections, one of them starting at $\mathbf{P}_1$ and "moving up" and the other starting at $\mathbf{P}_3$ and "moving down". The method for joining these two sections is similar to what is done, for instance, for the RR SMS lens [10, 12] but in this case the optic is asymmetric and, therefore, there will be a gap between the two sections, as shown in Fig. 7.8. A line v_2 is chosen to separate the two SMS secondary mirror sections, and another line v_1 to separate the two SMS primary mirror sections. In practice, these gaps can be eliminated by simply joining the two respective sections with a straight line, originating, as a consequence, a "kink". If this would be a practical problem, it is possible to iterate on the positions of $\mathbf{P}_1$ or $\mathbf{P}_3$ where p_{11} or p_{21} start to reduce or eliminate the size of this gap.

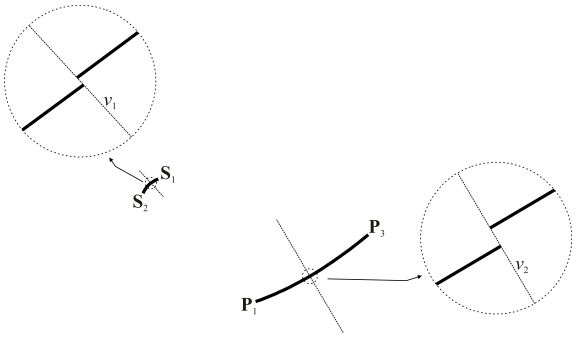

Fig. 7.8: The complete lower mirror portion of the primary and upper mirror portion of the secondary.

Repeating the process for the upper mirror portion of the primary (lower mirror portion of the secondary) the optic is completed, as shown in Fig. 7.9.

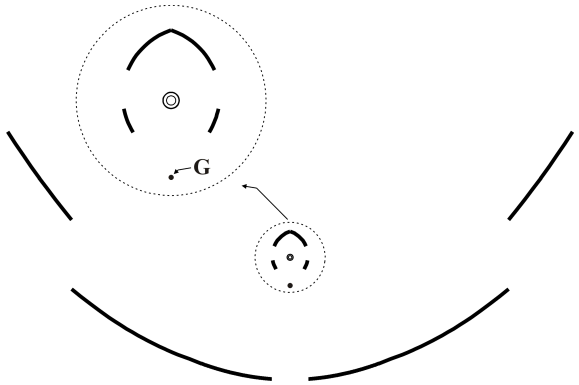

Fig. 7.9: The complete XX SMS optic with a center of gravity at point **G**.

7.3 Center of mass and analytical calculation

A curve **c** is defined between points **A** and **B**, as shown in Fig. 7.10.

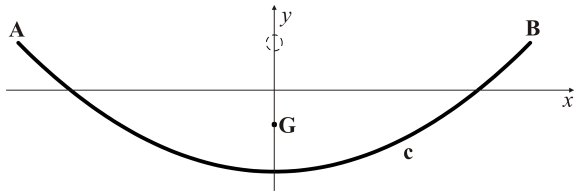

Fig. 7.10: Analytical calculation of the center of gravity of a curve **c**.

In order to calculate the center of mass of the curve **c** an analytical calculation can be made. $\mathbf{c}(\sigma)=(c_x(\sigma),c_y(\sigma))$ is taken as a parametric equation for the curve where σ is the parameter defined, for example, for σ_1 ¡ σ ¡ σ_2 (the curve may be defined, for example, as a spline function [12]). If $\mathbf{c}'(\sigma)$ is the derivative of **c**, the length w of curve **c** is given by:

$$w = \int_{\sigma}^{\sigma_2} \|\mathbf{c}'(\sigma)\| d\sigma \tag{7.9}$$

If the curve is assumed to have a constant density (weight per unit length), w is also proportional to the "weight" of the curve. The curve's center of mass is defined by:

$$\mathbf{G} = \frac{1}{w} \int_{\sigma}^{\sigma_2} \mathbf{c}(\sigma) \|\mathbf{c}'(\sigma)\| d\sigma \tag{7.10}$$

If the curve is symmetrical relative to the y axis, G_x=0 and the y component of **G** is given by:

$$G_y = \frac{1}{w}\int_{\sigma}{}_{1}^{\sigma}{}_{2}c_y(\sigma)\|\mathbf{c}'(\sigma)\|d\sigma \tag{7.11}$$

7.4 Results and comparison

The XX infinitesimal etendue optic and the XX SMS optic obtained, are compared with the PT solar concentrator (Table 7.1 and 7.2, below) with the same vacuum receiver tube. The comparison is done with the following assumptions:

- The half-acceptance angle, θ, is the same (same overall tolerances for both optics). Again, in this analysis the effective acceptance angle of the optic is defined as the incidence angle for which the concentrator collects 90% of the on-axis power [11].
- The size (diameter) of the receiver is the same.
- Same evacuated tubular receiver [5].
- Same mirror materials.
- Same intercept factor [8] (equal to 1).

All optics are assumed to have the same overall tolerances to errors, such as optical quality, sun tracking accuracy and effects from wind, dust and others. Optics with the same tolerances can be made and assembled using similar methods. Since the diameter of the vacuum tube considered is the same in all cases, the entrance aperture of the concentrators will change to accommodate the different optical architectures, i.e., concentrators to be compared have the same acceptance angle and same exit aperture (tube perimeter), but different entrance aperture widths. It should be noted that a fixed exit aperture is only a scale factor of the concentrators. In the Concentrated Photovoltaics (CPV) field, an equivalent comparison would be to impose the same acceptance angle and the same entrance aperture, but different exit apertures, since solar cells can then be cut in different sizes to accommodate the different Concentration Acceptance Produce (CAP) values ([7, 11]), given by $CAP{=}C\sin\theta$.

The new optics developed in this paper were compared for η_{opt0} (optical efficiency at normal incidence), C (geometric concentration) and CAP. The details of the PT considered in this comparison are shown in Table 7.1 and in Table 7.2 This choice represents what can be characteristically found on the market without attempting to be specific about one brand or another, using the values and descriptions common to different studies, as for instance those in [2].

Materials properties considered for both optics are shown in Table 7.2.

Table 7.1: Details of the conventional PT concentrator.

Optic	Aperture size (m)	Receiver radius (m)	Focal length (m)	φ (deg)	C_g	θ
PT	5.77	0.035	1.71	80.3	26.26	0.694

Table 7.2: Materials properties.

Optical element	Reflectivity	Absorptivity	Transmissivity
Primary mirror	92% [17]	-	-
Secondary mirror	92% [17]	-	-
Receiver tube	-	95% [5]	-
Glass cover	-	-	96% AR-coated glass tube [5]

Two different models for both the infinitesimal etendue and the SMS optics were designed, with a slightly higher and a slightly lower acceptance angle than that of the PT. That was done to show how CAP varies with the acceptance angle for each new optic analyzed and to add useful information (interpolation) for the comparison with the PT, if they had the same acceptance angle (see Fig. 7.11(a)).

In Fig. 7.11(b) a more precise comparison of the optical efficiency at normal incidence (with a sunlight angular aperture of $\approx 0.27^{\text{o}}$) η_{opt0}, can be made by considering the values on the interpolation line for $\theta = 0.694^{\text{o}}$ (the PT half acceptance angle value).

The values of CAP and η_{opt0} for the XX SMS and XX infinitesimal etendue optic, as well as other technical details are summarized in Table 7.3.

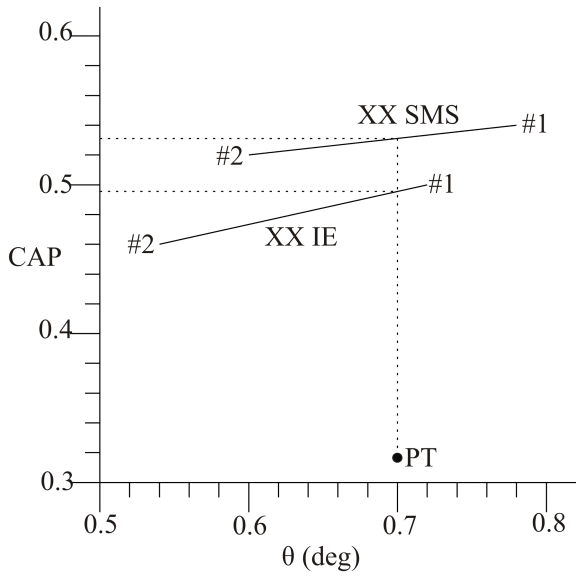

(a)

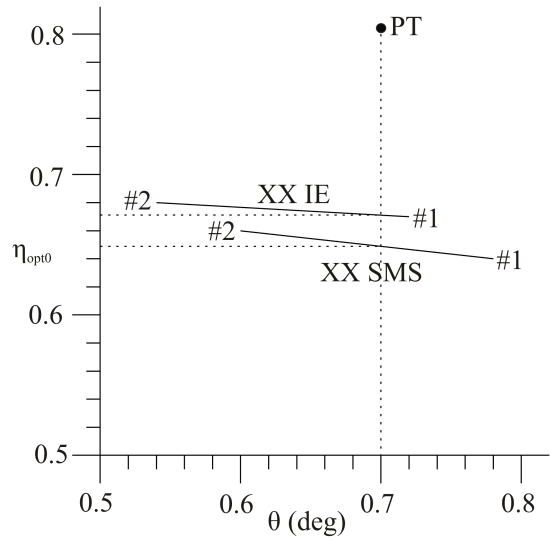

(b)

Fig. 7.11: Comparison between the XX SMS, XX infinitesimal etendue (XX IE) and PT concentrators. (a) *CAP* comparison. It can been seen that, for the same acceptance angles, the XX SMS has a higher *CAP* and, therefore, reaches higher concentrations; (b) η_{opt0} comparison. The PT has a higher optical efficiency due to the lower number of reflections of the light.

Table 7.3: Comparison between the PT, XX SMS and XX infinitesimal etendue concentrators.

Configuration	Aperture width (m)	Mirror length (m)	Receiver radius (m)	**G** (G_x,G_y)	h_R	φ (°)	C (×)	θ (°)	CAP	η_{opt0}	η^*_{opt0}
PT	5.77	6.40	0.035	$(0, -1.27)$	1.06	80.30	26.24	0.69	0.32	0.80	0.81
XX SMS #1	8.63	10.87	0.035	$(0, -0.41)$	0.10	112.92	39.24	0.78	0.54	0.64	0.65
XX SMS #2	10.84	13.63	0.035	$(0, -0.58)$	0.11	113.15	49.29	0.60	0.52	0.66	0.67
XX Infitesimal etendue #1	8.62	10.86	0.035	$(0, -0.41)$	0.10	112.91	39.20	0.72	0.49	0.67	0.69
XX Infitesimal etendue #2	10.84	13.60	0.035	$(0, -0.58)$	0.11	113.15	49.29	0.54	0.47	0.68	0.69

The values of η_{opt0} and CAP were calculated through ray tracing. η^*_{opt0} is the optical efficiency with shading losses deducted, i.e., it is the optical efficiency defined as the fraction of the (direct) sunlight captured by the primary mirror aperture that is absorbed by the receiver. This value is important to calculate the total amount of collected energy because, for that calculation, it makes more sense to use the mirror aperture area and not the total aperture area (which may include a gap between the two heliostats, as shown, for instance, in Fig. 7.5). The ray tracing includes material properties and the solar angular profile (non-parallel rays).

h_R is an adimensional factor (see Fig. 7.12.) and it relates the position of the center of mass (point **G**) of each optic with its geometric dimensions. It is given by:

$$h_R = \frac{a}{b} \tag{7.12}$$

where a is the vertical distance between the center of the tubular receiver and point **G** and b the vertical distance between the edges of the two mirror sections, as shown in Fig. 7.12.

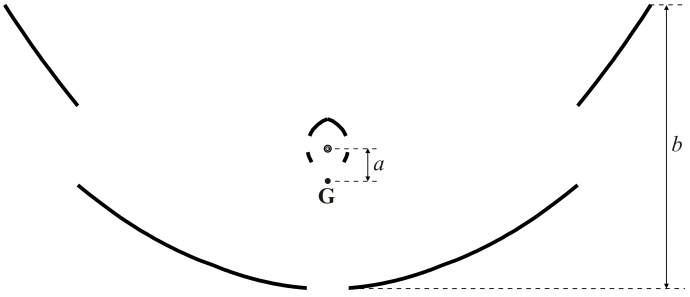

Fig. 7.12: Definition of h_R.

No effort was made to find a design where a would be equal to zero, in truth the final objective of the whole exercise. However a final result would now depend crucially on many manufacturing details not dealt with in this paper[1]. Thus it was judged sufficient to show that the infinitesimal etendue and SMS optics have hR values much lower than a conventional PT due to their wide rim angles. It should be noted that in the case of the XX SMS and XX infinitesimal etendue optics the calculation of the center of mass also takes into account the presence of the secondary

[1]Although the new optics have rim angles larger than 90°, they do not necessarily fulfill the goal of having the center of mass **G** at the center of the receiver, which is considered here to be at the origin of the coordinate axes, i.e., **F** = (0,0). It is clear that, in practical terms, this issue must be dealt with an appropriated physical structure supporting primary and secondary, with its weight properly chosen in order to redirect point **G** towards point **F**. These and other manufacturing considerations render useless the complex exercise of carrying this calculation further at this stage; it should be, however, done by any manufacturer who decides to implement this solution.

mirrors.

The results in Table 7.3 show that both XX SMS and XX infinitesimal etendue concentrators have a higher CAP than the PT concentrator, demonstrating the potential advantage of using this type of two-stage concentrators.

The value of η_{opt0} for the XX SMS and XX infinitesimal etendue optics is lower when compared to the PT optic, and this results from the fact that in these optics (almost) all the light reflected by the primary mirror is also reflected by the secondary mirror and, therefore, there is, at least, on average, one more reflection than in the PT optic. On the other hand, the difference between the XX SMS and XX infinitesimal etendue optics can be explained by the design method chosen for the XX SMS optic. In fact, each mirror obtained by the SMS design method is a result of a combination between two different portions, starting at opposing ends of the mirror and meeting at its "center" (see Fig. 7.8). These portions should contain several SMS chains (Cartesian ovals), but because of the high acceptance, these Cartesian ovals are large and only a few fit inside the mirror dimension. Therefore, this ends up penalizing the optical efficiency which, in turn, explains the results presented in Table 7.3.

In order to determine the amount of energy delivered to the receiver in real world operating conditions, a more detailed calculation is needed. Such an analysis was done using commercial ray tracing software, as well a numerical method developed in a previous work [19]. This method evaluates the optical efficiency for different θ_Z (zenith angle) and φ_S (solar azimuth angle) [3] (ray tracing for all relevant pairs of θ_Z and φ_S), calculating function $\eta_{opt}(\theta_Z,\varphi_S)$.

This function is then multiplied by the corresponding DNI (Direct Normal Irradiance) and a factor (¡1) which contains the relevant "cosine of incidence angle effect" correction to finally obtain the amount of energy collected by the receiver.

Often this calculation is alternatively performed with the help of incidence angle modifier (IAM) functions [3]. These curves are obtained from the function $\eta_{opt}(\theta_Z,\varphi_S)$ for the longitudinal plane ($\varphi_S = 0^o$) and transversal plane ($\varphi_S = 90^o$). For the sake of completeness, in Appendix A of this Chapter the IAMs for the PT, XX infinitesimal etendue #1 and XX SMS #1 optics presented in this paper are also shown.

For this simulation and performance comparison, Faro, Portugal (37º02'N, 07º55'W), was selected, with an annual average DNI of 2234 kWh/m^2 [18] (see Appendix B of this Chapter). As mentioned before in this simulation thermal losses were not included, that is, only optical losses were considered. The results are shown in Table 7.4.

The results show that using these types of second-stage concentrators corresponds to a higher energy collection performance. In fact, a slight sacrifice of optical efficiency is compensated by the large gain of aperture width, while maintaining the

Table 7.4: Comparison of collected energy in Faro, Portugal. The calculations were done for a receiver of 70 mm of diameter and 1 m of length.

Configuration	DNI (kWh/m^2)	Collected Energy same vacuum tube (kWh)
PT	2234	7527
XX SMS #1	2234	8954
XX SMS #2	2234	11650
XX infitesimal etendue #1	2234	9353
XX infitesimal etendue #2	2234	11927

same acceptance angle of the conventional PT concentrator used in the comparison.

When a complete collector field for a given power delivery is considered, this energy performance per row corresponds to a reduction of the total number of rows. Besides the potential cost reduction associated with the elimination of flexible hosing and/or rotating joints, larger troughs may imply a substantial reduction of thermal and other parasitic losses. Plus, potentially lower operating costs (less parasitic pumping losses, less heat transfer fluid, etc.) and installation costs (less pipes, less insulation and less components).These, in fact, constitute strong arguments in favor of a solution with larger aperture width. A full optimization of this sort (i.e. considering these aspects) is, again, well past the scope of this paper, since the authors currently do not have the necessary manufacturing information and field costs information to do it.

In fact, as mentioned in the Introduction, larger aperture troughs are being proposed on the market [8, 9], as a means to address the issue of cost reduction, just as referred above. A case in point is the so called Ultimate Trough [9], with its stepped mirror solution and its aperture width of $\approx 7.57\ m$, features that are also characteristic of the optics discussed in this paper.

7.5 Conclusions

Two new optical solutions were presented to solve the problem of producing parabolic troughs for fixed receivers. These solutions were designed to use the same evacuated tubular receivers which are the present market "standard". The solutions achieve the required goal by showing how to place the centre of mass of the tracking optic at the centre of the evacuated tubular receiver, thereby avoiding the need to move the tubular receiver together with the trough mirror. The final result in both cases

yields a trough with a larger aperture (a larger overall concentration) and that, in turns, adds another interesting feature to the solution: the fact that there is at present a tendency to propose larger troughs (larger apertures than the $\approx 6\ m$ of conventional PT technology) simply because this reduces the number of rows in a large collector field, with impact on piping length and all losses (thermal and other parasitic losses) associated with that and, thus, with a potential for cost reduction.

Two solutions, infinitesimal etendue and SMS, are presented and developed in the paper. They have an aspect ratio comparable to that of a conventional PT, and thus show a potential for practical manufacture and to rival favourably with other larger trough solutions coming on the market today [8].

An energy delivery performance comparison of the new solutions with that of a conventional PT was presented, to help establish their potential practical interest. It shows that the conventional PT delivers more energy on a sqm of aperture area basis (kWh/m^2) because they have a higher efficiency, but that the solutions presented deliver more energy (kWh) on a row by row basis in a collector field, since their aperture area is larger for the same acceptance angle. What really matters, however, is the final production cost of energy and when the energy delivered by a whole field is considered, production costs might very well be lower in the case of the new solutions presented in this paper. This would result from a number of effects: the fixed receiver solution proposed here, associated as they would be today with larger aperture troughs, corresponds to a smaller number of rows for the same field power, a potentially cheaper trough (on a sqm basis) and smaller pipe length, reducing pumping power, thermal losses, heat transfer fluid volume and potentially causing also lower Capex and O&M costs associated with the elimination of flexible hosings and/or rotating joints.

Appendix A

Fig. 7.13 shows the IAM curves for the PT, XX Infinitesimal Etendue #1 and XX SMS #1 optics.

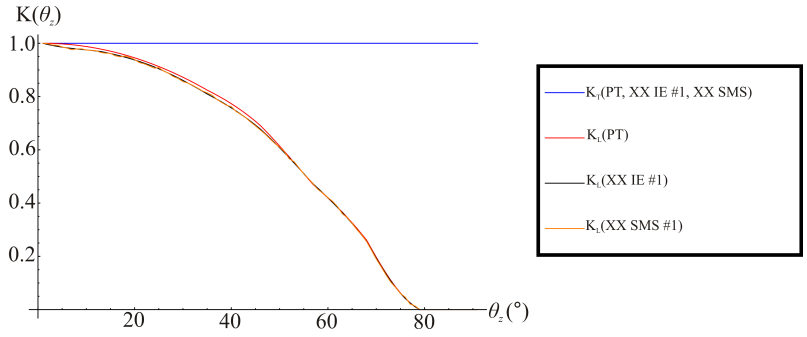

Fig. 7.13: IAM curves for the PT, XX infinitesimal etendue (XX IE) #1 and XX SMS #1 optics (longitudinal (K_L) and transversal (K_T) planes.

Appendix b

Table. 7.5 shows the DNI values used in this work.

Table 7.5: DNI value for Faro (Portugal) [18].

Month	DNI (kWh/m^2)
JAN	137
FEB	114
MAR	195
APR	168
MAY	229
JUN	244
JUL	277
AGO	254
SEP	213
OCT	181
NOV	109
DEC	113
TOTAL	2234

References

[1] Crespo, L., *The European solar thermal electric market*, Intersolar European Conference, Munich, June, 2011.

[2] Kearney, D.W., *Parabolic Trough Collector Overview*, Parabolic Trough Workshop, 2007.

[3] Rabl, A., (1985), *Active solar collectors and their applications*, Oxford University Press, New York, Oxford.

[4] Bendt, P., *Optical analysis and optimization of line focus solar collectors*, Colorado, September, 1979.

[5] SCHOTT PTR 70 Receiver brochure.

[6] Siemens Solar, *http://www.energy.siemens.com/hq/en/power-generation/renewables/solar-power/*.

[7] Canavarro, D., Chaves, J., Collares-Pereira, M., *New second-stage concentrators (XX SMS) for parabolic primaries; Comparison with conventional parabolic troughs concentrators*, Solar Energy, 92 (2013) 98–105.

[8] Riffelmann, K.J., Lüpfert, E., Richert, T. and Nava, P., *Performance of the Ultimate Trough Collector with Molten Salts as Heat Transfer Fluid*, Proceeding 18th International SolarPACES Symposium, September 11-14, Marrakech, Morocco (2012).

[9] Large Trough Dimensions Huge Cost Savings, Ultimate Trough Solar Collectors for Concentrated Solar Power (CSP) (*http://www.flabeg.com/*).

[10] Winston, R., Miñano, J.C., Benítez, P., (contributions by Shatz, N., Bortz, J.,C.), *Nonimaging Optics*, Elsevier Academic Press, Amsterdam, 2005.

[11] Benítez, P., et al., High performance Fresnel-based photovoltaic concentrator, Optical Society of America, 26 April 2010, Vol. 18, No. S1, OPTICS EXPRESS.

[12] Chaves, J., 2008, *Introduction to Nonimaging Optics*, CRC Press, Taylor and Francis Group.

[13] Collares-Pereira, M., Gordon, J.M., Rabl, A., Winston, R., *High concentration two-stage optics for parabolic trough solar collectors with tubular absorber and large rim angle*, Solar Energy 47 (6), pp. 457-466, 1991.

[14] R. John Koshel, Illumination Engineering: Design with Nonimaging Optics, Wiley, 2013.

[15] Gordon, J., *Aplanatic optics for solar concentration*, Optical Society of America, 26 April 2010, Vol. 18, No. S1, OPTICS EXPRESS.

[16] R. Winston, and J. M. Gordon, *Planar concentrators near the étendue limit* Opt. Lett. 30(19), 2617–2619 (2005).

[17] *http://www.saint-gobain-solar-power.com/mirrors-solar-glass-7* (SGG MIRALITE SOLAR 4 mm).

[18] Meteonorm hourly DNI data.

[19] Canavarro, D., *Modeling linear solar collectors of the Fresnel-type; application to an innovative CLFR collector "Etendue Matched"*, MSc thesis, Instituto Superior Técnico/UniversidadeTécnica de Lisboa, Lisbon, 2010.

Nomenclature

C	geometric concentration ($\times$)
$\mathbf{c}$	parametric curve
CSP	Concentrated Solar Power
D	diameter of a tubular receiver (m)
DNI	Direct Normal Irradiance (kWh/m^2)
$\mathbf{G}$	center of mass (m)
h_R	adimensional factor
HTF	Heat Transfer Fluid
IAM	Incident Angle Modifier
K	constant of integration
n	refractive index
NIO	Non imaging Optics
O	a generic optic
OM	Operation and Maintenance
SMS	Simultaneous Multiple Surface
U	etendue
w	length of a curve $\mathbf{c}$

Greek symbols

η_{opt0}	optical efficiency at normal incidence
η^*_{opt0}	optical efficiency at normal incidence without shading losses
θ	half-acceptance angle (grad)
σ	parameter of a curve $\mathbf{c}$
φ	rim angle (grad)

Chapter 8

Simultaneous Multiple Surface method for Linear Fresnel concentrators with tubular receiver[†]

Abstract

In order to increase the performance of conventional Linear Fresnel Reflector (LFR) concentrators it is necessary to increase their optical performance as these concentrators are still far from the theoretical limits of concentration. This paper presents a new Fresnel concentrator designed with the Simultaneous Multiple Surface (SMS) method for two reflective (X) surfaces (Fresnel XX SMS) and with a tubular receiver. This design also promotes a good light uniformity on the receiver. A comparison is made between this new Fresnel XX SMS and two present day available concentrators (a Fresnel with CPC (Compound Parabolic Concentrator) and a PT (Parabolic Trough) concentrator), as well as a calculation of the total amount of collected energy (kWh), before thermal losses, for a particular location, Faro (Portugal). Furthermore, a new definition of CAP (Concentration Acceptance Product) is proposed, as the standard definition does not fully take into account the optical nature of LFR concentrators.The paper ends with a discussion of the results obtained, their impact and possible applications in the future.

Keywords: Linear Fresnel; SMS Method; Concentrated Solar Power; Evacuated Tubular Receiver

---

[†]Diogo Canavarro[(1)], Julio Chaves[(2)], Manuel Collares-Pereira[(1)], Simultaneous Multiple Surface method for Linear Fresnel concentrators with tubular receiver, Accepted for publication in *Solar Energy*.

[(1)] BES Renewable Energies Chair, University of Évora (Portugal).

[(2)] Light Prescriptions Innovators, UPM, Madrid (Spain).

8.1 Introduction

Recent progress in the design of new linear concentrators [1, 2] led the authors to propose new solutions (based on the Simultaneous Multiple Surface (SMS) design method [3, 4]) for combinations of parabolic trough like primaries with second stage concentrators; the intention was either to increase aperture width, for the same acceptance angle and evacuated tubular receiver or to allow for fixed receiver solutions again designed for the same evacuated tubular receiver presently used in all solar concentrators [5].

These new designs were meant to have as little optical losses as possible, while approaching as much as possible the limit of $CAP = C\ \sin(\theta) = 1$, where CAP is the Concentration Acceptance-Product [6], θ is the half-acceptance angle of the concentrator [7, 8] and the receiver is in vacuum or air (n=1). These designs use just one reflection for every ray reaching the second stage mirror and a configuration achieving zero losses through the gap between the receiver and its outer glass envelope (i.e. no incoming radiation reflected escapes through the gap).

These features are complemented with an extra one: by design, radiation goes only once through the glass envelope of the evacuated tubular receiver, which helps keeping the optical efficiency as high as possible, by reducing Fresnel (transmission) losses on the glass envelope.

Conventional Linear Fresnel concentrators (LFR) have CAP(s) much smaller than 1 (i.e. there is room for substantial improvement) and are now being proposed [9] to be combined with the same evacuated tubular technology.

A higher CAP with the same design acceptance angle really means a larger aperture area for the same receiver (higher concentration). If non evacuated receivers were to be used this could also mean a smaller diameter tube for the same aperture area. This would also be an interesting configuration with smaller thermal losses (thermal losses depend on the receiver area), thereby enhancing the energy delivered by the concentrator by a significant amount.

Even with evacuated tubular technology and when the goal is to achieve operating temperatures around or even above 560°C (for instance to operate with molten salts) the higher concentration easily achieved with the new design proposed in this paper, also means lower thermal losses. In turn that means that the new LFR concept can produce electricity with an overall efficiency which is really above that achieved by conventional LFR, bringing LFR technology yearly conversion efficiency much closer to that of PT technology. This paper does not address the gains achievable through these thermodynamic considerations, but they constitute an important part of the background motivation for this development.

Given that all linear concentrators for CSP, of whatever type, are designed for

the same 70mm diameter receiver tube within a glass envelope (a sort of practical market imposed standard)[5], for the sake of comparison, the choice in this paper is to develop a new LFR concentrator for the same evacuated tube with the same acceptance angle as in [3, 4] and compare the performance of the new concentrator with that of an LFR with second stage concentrator of the CPC type (CPC for short) as well as that of a generic Parabolic Trough (PT) representative of present day PT technology [10, 11]. This comparison gives a good measure of the improvement achieved. It is made in terms of several different parameters including optical performance and energy delivered on yearly terms, with real solar radiation data and ray tracing, taking into account end effects, cosine of incidence angle effects, and incidence angle modifiers effects for the incident rays, which are not limited to transversal and at normal incidence (the design condition).

As will be shown the new design offers further advantages for a complete collector field: (i) higher concentration for a fixed receiver, results in a larger aperture and thus a substantial reduction of the number of necessary rows to achieve a given installed power, (ii) there is also a higher degree of compactness (occupied ground per peak watt). The first one will certainly impact on kWh production cost, and the second one whenever land or roof top occupation is at premium.

The paper is organized as follows: in section 8.2 the design method of the Fresnel XX concentrator is presented as well as the technique used to increase system compactness. Section 8.3 shows the results of the comparison between the Fresnel XX SMS and present day Fresnel and PT concentrators. Finally, in section 8.4 some conclusions and perspectives for the future are also discussed.

8.2 XX SMS Fresnel optic design

In conventional Linear Fresnel concentrators with primary mirrors possessing coplanar tracking axis the etendue is not conserved [1, 7], even if the primary is composed of an infinite number of infinite heliostats forming a continuum, as shown diagrammatically in Fig. 8.1. In fact, if an infinitesimal length dx of Fresnel mirror and a circular receiver R are considered, the infinitesimal incoming etendue dU_I which illuminates dx is given by:

$$dU_I = 2dx\sin(\theta) \tag{8.1}$$

On the other hand, the infinitesimal outgoing etendue dU_O emitted by dx within a cone 2θ whose bisector is a vector $\mathbf{k}$ tilted by an angle β relative to the perpendicular to dx and points towards the center of R is given by:

$$dU_O = 2dx\sin\theta\cos\beta \tag{8.2}$$

where the $\cos\beta$ factor is the projection of dx in the direction of $\mathbf{k}$ and it is given by:

$$\beta(x) = \arctan(x/h) \tag{8.3}$$

Thus, the etendue of the incoming light dU_I is higher than the etendue of the outgoing light dU_O emitted by dx and, therefore, the etendue is not conserved. The incoming light that cannot be sent towards the receiver is lost through shading between the heliostats or passes through the heliostats without being captured, or both.

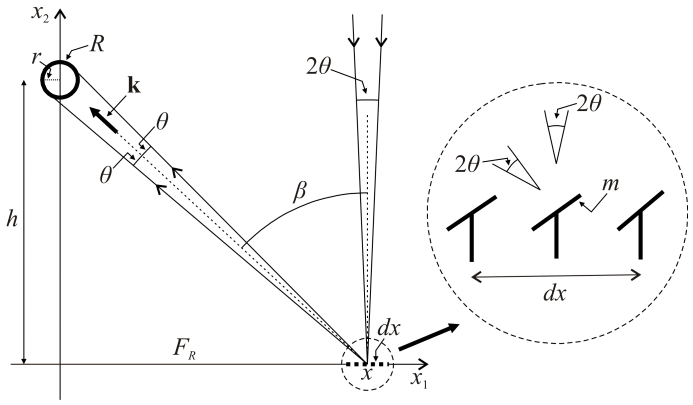

Fig. 8.1: Etendue of an infinitesimal length dx of Fresnel reflector F_R (on axis x_1). The normal to a heliostat m in the Fresnel reflector at position x is tilted by an angle $\beta/2$ relatively to the vertical and reflects a cone 2θ towards a circular receiver R of radius r.

Nevertheless, one can match the outgoing etendue dU_O with the etendue captured by the receiver.

As shown in Fig. 8.2a, in the configuration proposed here, the primary Fresnel reflector sends light towards the secondary reflector which redirects it towards the receiver, as shown by ray r. The secondary mirror surrounds the receiver R, but it has an aperture $\mathbf{S}_1\mathbf{T}_1$ for light to get in. End points $\mathbf{S}_1$ and $\mathbf{T}_1$ of the secondary mirror are located on receiver flow lines f_S and f_T, making an angle α to each other, as shown in Fig. 8.2b. Since the receiver is circular, these flow lines are straight lines diverging from its center. The etendue the secondary can send towards the receiver is given by [3]:

$$U_R = 2(2\pi - \alpha)r \tag{8.4}$$

where $(2\pi\text{-}\alpha)r$ is the top arc length of the receiver contained between flow lines f_S and f_T. On the other hand, the etendue the Fresnel reflector can send towards the secondary is given by:

$$U_O = 2\sin\theta \int_{x_i}^{x_f} \cos\beta(x)\, dx \tag{8.5}$$

Ideally, these two values of etendue should match, resulting in U_O=U_R.

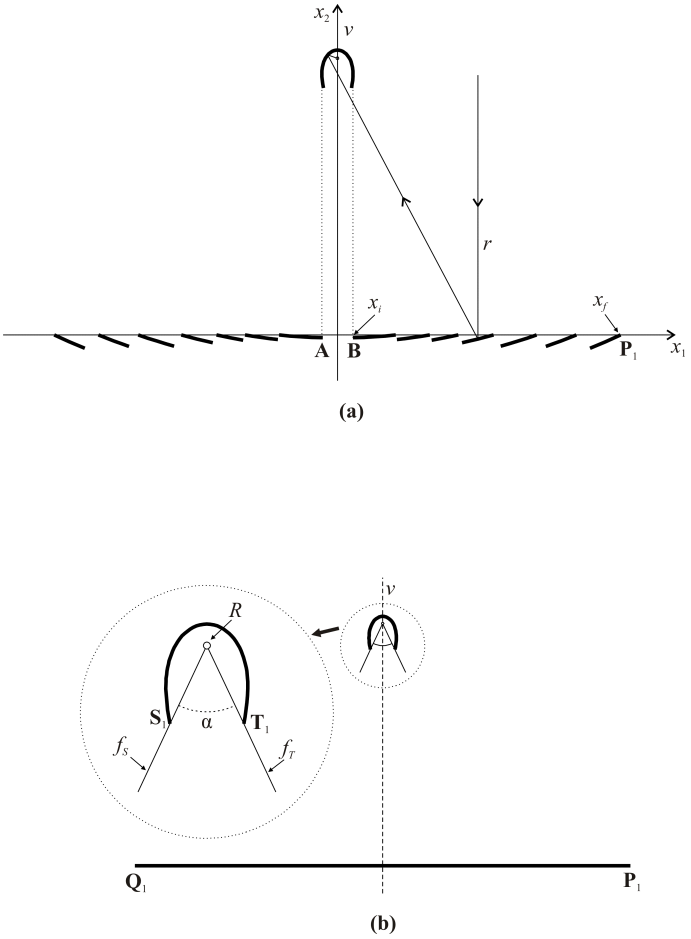

Fig. 8.2: The XX SMS Fresnel concentrator. (a) The complete Fresnel XX SMS concentrator. (b) The secondary mirror does not surrounds completely the receiver and, therefore, a recalculation of the size of the Fresnel primary is necessary in order to coupling the etendues.

The design of the Fresnel reflector starts at $\mathbf{P}_1$=(x_f,0) and progresses towards the symmetry axis v (as will be described below). Simultaneously, the secondary starts at point $\mathbf{S}_1$ and progresses upwards. During the design process, the value of x_f defining the position of $\mathbf{P}_1$=(x_f,0) must be optimized in such a way that the Fresnel reflector ends at position $\mathbf{B}$ with x_1=x_i below the rightmost point of the secondary mirror when the secondary mirror reaches the symmetry axis v (see Fig. 8.2a). When this happens, we approach condition U_O=U_R. This position of point $\mathbf{B}$ prevents the secondary from shading the primary when sunlight is in the vertical direction.

Now one must define the ray assignation as well as the optical path lengths

[7, 8] which will be used to obtain the mirrors. The design of the mirrors starts with surfaces p_1 and s_1 defined, respectively, as a parabola p_1 tilted by and angle $\pi/2$-θ relative to the x_1 axis and focus at $\mathbf{S}_1$ and an unwinding macrofocal ellipse s_1 [1] defined by its macrofocus R, point focus $\mathbf{P}_1$ and point $\mathbf{S}_1$, as shown in Fig. 8.3. According to the Edge-Ray Principle [7, 8] in order to achieve the maximum possible concentration the edge rays coming from the edges of the source (which is considered to be at an infinite distance) represented by the flat wave fronts w_1 and w_2 (tilted by angles $\pm\theta$ to the horizontal) must be redirected towards the edges of the receiver (tangent points to R) represented by the wave fronts w_3 and w_4 (involute curves). This ray assignation also allows light (its flow lines) to enter perpendicular to the receiver and, therefore, to reduce the Fresnel losses around the glass cover when vacuum tubes are used, an approach which has been successively used in previous works [3, 4].

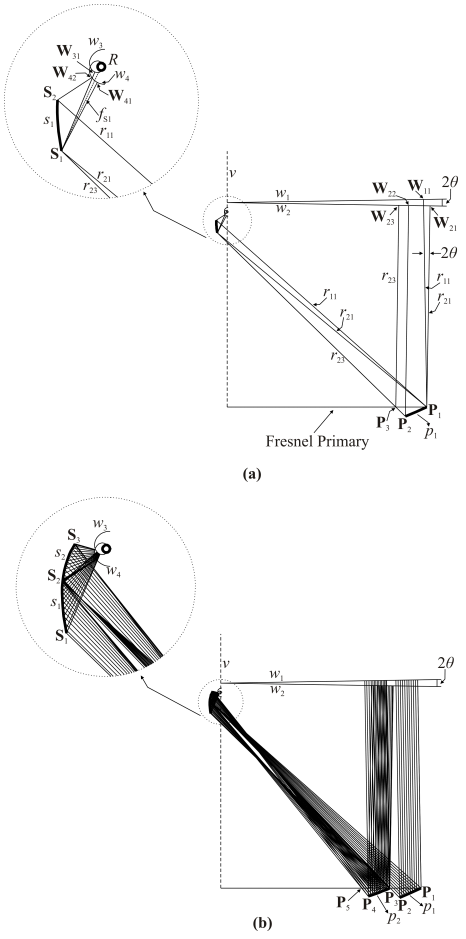

Fig. 8.3: The XX SMS Fresnel concentrator. (a) The portions p_1 and s_1 are, respectively, a parabola tilted by an angle of $\pi/2$ - θ with focus at $\mathbf{S}_1$ and an unwinding macrofocal ellipse with a macro focus R, with a point focus at $\mathbf{P}_1$ and that pass through $\mathbf{S}_1$. (b) The portions p_2 and s_2 are designed through a SMS chain.

Edge ray r_{24}, coming from point $\mathbf{W}_{21}$, is reflected at $\mathbf{P}_1$ towards point $\mathbf{S}_1$ and then reflected to the "bottom" of the receiver, that is, perpendicularly to w_4 ending at point $\mathbf{W}_{41}$. Edge ray r_{14} is launched from point $\mathbf{W}_{11}$ (wave front w_1) and it is reflected on portion p_1 at point $\mathbf{P}_1$ towards point $\mathbf{S}_2$ of surface s_1. From $\mathbf{S}_2$ the ray is reflected to the "bottom" of the receiver, perpendicularly to w_4, ending at point $\mathbf{W}_{42}$. Edge ray r_{23} coming from the "top" of the receiver, perpendicularly to w_3, (point $\mathbf{W}_{31}$) is reflected at $\mathbf{S}_1$ towards point $\mathbf{P}_2$ and finally redirected towards $\mathbf{W}_{22}$ (perpendicularly to wave front w_2). The optical path lengths in this case are given by:

$$S_{14A} = [\mathbf{W}_{11}, \mathbf{P}_1] + [\mathbf{P}_1, \mathbf{S}_2] + [\mathbf{S}_2, \mathbf{W}_{42}] \tag{8.6}$$

for ray r_{14} between wavefronts w_1 and w_4

$$S_{23A} = [\mathbf{W}_{22}, \mathbf{P}_2] + [\mathbf{P}_2, \mathbf{S}_1] + [\mathbf{S}_1, \mathbf{W}_{31}] \tag{8.7}$$

for ray r_{23} between wavefronts w_2 and w_3 and where [**A**,**B**] is the Euclidean distance between two points **A** and **B**. With portions p_1 and s_1 completely defined (including a list of points and normals for both of them), one can calculate the next optical portions of the primary and secondary mirrors.

Emitting rays from wavefront w_1 and reflecting them on p_1 (r_{14} is one of those rays), a new portion of secondary may be calculated above $\mathbf{S}_2$, by redirecting those rays to wavefront w_4. Points above $\mathbf{S}_2$ are defined by optical path length S_{14A} between w_1 and w_4. This process generates new, continuous secondary mirror above $\mathbf{S}_2$.

Emitting rays from wavefront w_3 and reflecting them on s_1 (r_{23} is one of those rays), a new portion of primary may be calculated to the left of $\mathbf{P}_2$, by redirecting those rays to wavefront w_2. Points to the left of $\mathbf{P}_2$ are defined by optical path length S_{23A} between w_2 and w_3. A constant value of S_{23A} results in a continuous primary mirror extending to the left of $\mathbf{P}_2$. However, the Fresnel primary is discontinuous and, therefore, the optical path length S_{23A} will not be constant throughout the design process. The first task is to determine where the first point of the next heliostat ($\mathbf{P}_3$) will be placed. The location of $\mathbf{P}_3$ should be as close as possible to p_1 in order to guarantee a high compactness of the system (small gaps between the heliostats) and decrease the land-use requirements for large scale applications. However, in Fresnel concentrators there are shading and blocking effects which reduce the overall efficiency of the system and these effects tend to increase as the gaps between the heliostats are smaller. Therefore, a balance between these two conditions is necessary to calculate the location of $\mathbf{P}_3$. As shown in Fig. 8.3a, one possible solution is to use one of the edge-rays to calculate point $\mathbf{P}_3$. Intersecting, for example, ray r_{23} with the horizontal line (axis x_1) the location of $\mathbf{P}_3$ is now completely defined. Ray r_{23}

would now follow path r_{23B}. When the primary mirror "jumps" to another heliostat (for example from $\mathbf{P}_2$ to $\mathbf{P}_3$), the optical path length S_{23A} must change accordingly. Therefore, the new optical path length S_{23B} for the new ray r_{23B} through point $\mathbf{P}_3$ is given by:

$$S_{23B} = [\mathbf{W}_{23}, \mathbf{P}_3] + [\mathbf{P}_3, \mathbf{S}_1] + [\mathbf{S}_1, \mathbf{W}_{31}] \tag{8.8}$$

with $S_{23B} < S_{23A}$

Note that the calculation of S_{23B} depends on the location of $\mathbf{P}_3$ which, on the other hand, depends on the size of p_1. The initial conditions θ and the height of the receiver, along with the ray assignation used, determines the width of p_1, a value which is used as a reference for the other heliostats, as shall be seen next. Although this simplifies the calculation it is not a necessary restriction that p_1 must coincide with the first heliostat, which may also be designed with a different width if needed. If a wider first heliostat is needed, the SMS would continue with optical path lengths S_{14A} and S_{23A} until the desired width is obtained or surpassed. If a narrower heliostat is needed, only part of p_1 is used as the first heliostat and point $\mathbf{P}_3$ is calculated, not based on $\mathbf{P}_2$, but on an inner point of p_1.

Using the lists of points and normals to portions p_1 and s_1 and following the ray assignation method mentioned above, the SMS chains can be generated, as shown in Fig. 8.3b. Reflecting a set of rays from wavefront w_3 tangent to the "top" of the circular receiver (r_{23} is an example of one of these rays) on s_1 a new portion p_2 of the primary is calculated using S_{23B} as the optical path length, that is, all rays from w_3 to w_2 have the same optical path length equal to S_{23B}; next, reflecting a set of rays from wavefront w_1 (r_{14} is an example of one of these rays coming from the sun) on p_1 a new portion s_2 of the secondary is calculated using S_{14A} as the optical path length, that is, all the rays from w_1 to w_4 have the same optical path length equal to S_{14A}. However, when these rays r_{14} reach point $\mathbf{P}_2$ at the edge of p_1, they also "jump" to $\mathbf{P}_3$ and the optical path length S_{14A} must change accordingly to a new value S_{14B} which needs to guarantee that the new points on the secondary are on a continuous mirror.

From a practical point of view, it is important that [$\mathbf{P}_1$,$\mathbf{P}_2$] = [$\mathbf{P}_3$,$\mathbf{P}_4$], i.e., all the Fresnel mirrors should have the same length (2D optic). Since the SMS method follows a step-by-step approach (for each point on s_1 a ray from w_3 generates a new point on the heliostat), one can verify for each new point calculated if the length of the heliostat calculated so far (2D optic) equals that of the previous heliostat. The calculation may then be stopped when we reach the desired heliostat length, and the optical path lengths recalculated before continuing the calculation. Nevertheless, this might imply an incomplete use of the list of points and normals of the previous portions (for example an incomplete use of portion s_1). In that case, the remaining

points should be saved and used for the next portion (which will use a different optical path length, as discussed above) or otherwise a gap will appear between the consecutive portions.

This process continues by choosing the location of the first point of the third portion of the primary ($\mathbf{P}_5$) in a similar way to $\mathbf{P}_3$. Repeating this process, a complete XX SMS Fresnel concentrator is designed, as shown in Fig. 8.2a. The design process stops when the secondary mirror touches the vertical axis v and, at the same, the size of the gap [$\mathbf{A}$,$\mathbf{B}$] ensures that the primary is not shaded by the secondary mirror. The other half of the primary is symmetric with respect to the vertical axis v which passes through R.

Fig. 8.4 shows a diagrammatic representation $\mathbf{P}_1\mathbf{Q}_1$ of the Fresnel primary with edge rays r_1 and r_2 (tilted by the half-acceptance angle θ to the vertical). Also shown are vertical rays r_3. When rays r_1 reach the receiver R, they will be tangent to it (edge ray principle) and will spread all around R, promoting a uniform illumination on the receiver R. The same is true for edge rays r_2. Vertical rays r_3 will reach receiver R in directions approximately perpendicular to R, again spreading all around it and promoting a uniform illumination of the receiver. Therefore, for all directions of sunlight inside the acceptance angle θ, this design promotes a uniform irradiation on the receiver. This avoids hotspots on the tube and facilitates the energy transfer to the fluid inside.

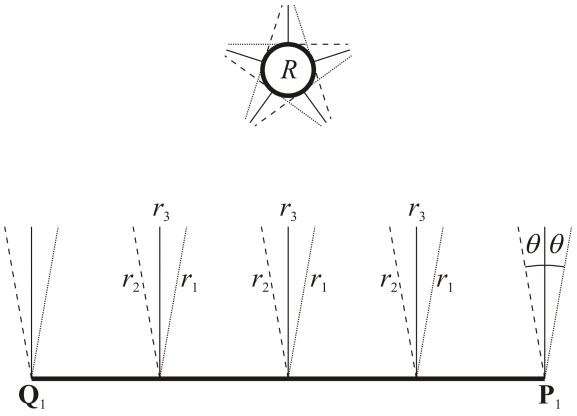

Fig. 8.4: Incoming radiation inside the acceptance angle 2θ will spread around the receiver, promoting a uniform irradiation on it.

The horseshoe shape of the secondary (Fig. 8.2) with its aperture $\mathbf{S}_1\mathbf{T}_1$ pointing down generates a cavity around the receiver reducing thermal convection losses (especially important when using non-evacuated receivers). Further reductions in convection losses may be obtained by placing an external glass cover from $\mathbf{S}_1$ to $\mathbf{T}_1$ which is perpendicular to flow-lines of the incoming radiation. Placing thin mirrors (mirrored on both sides) inside the secondary along the flow lines help further reduce

convection losses [1]. These mirrors will not disturb the light flow [7], but they will reduce convection. Another option is to use thin, transparent, (glass) barriers along the flow lines. In this case, most light will just go through the transparent barriers undisturbed. However, some light will also be reflected by Fresnel reflection. But since these barriers follow the flow lines, this reflected light will not disturb the light flow.

8.3 Results and Comparison

In order to test the merits of the Fresnel XX SMS concentrator two comparisons are presented. The first one is made between the Fresnel XX SMS and a commercial Fresnel with a CPC-type (Compound Parabolic Concentrator for short) as a second-stage concentrator (secondary mirror) (see Fig. 8.5a); the second one will be between the Fresnel XX SMS and a commercial Parabolic Trough (PT) concentrator (see Fig. 8.5b). The comparison with these "commercial" solutions is important from a practical point of view, since the results will allow the familiar reader, to have an immediate idea of what can be achieved/gained in potential performance (cost-effectiveness) with the Fresnel XX SMS in real world conditions.

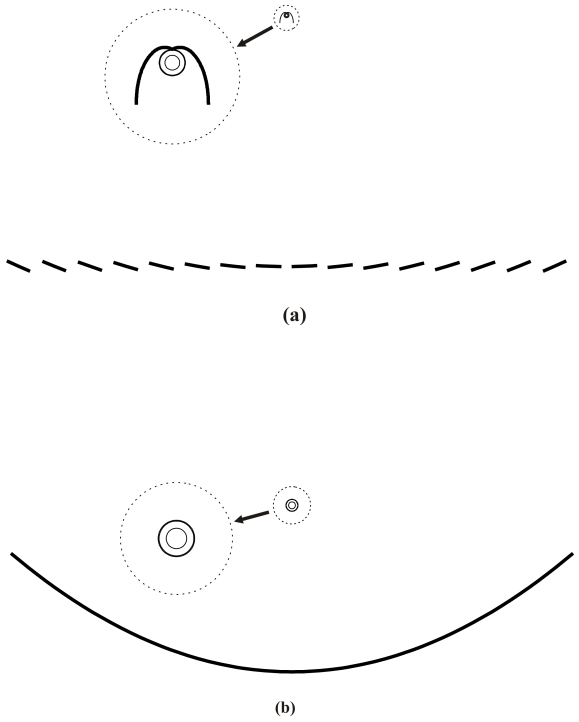

Fig. 8.5: (a) The Fresnel CPC concentrator. (b) The PT concentrator.

As explained in the introduction, the choice was to consider that the same receiver is used in all collectors compared. It might have been another choice that of a

fixed entrance aperture size, for instance, but then the new design, with its higher concentration, would not have an evacuated tubular technology to be associated with.

It should be noted that a fixed exit aperture is only a scale factor of the concentrators. This approach has also been successfully used for other SMS optics with vacuum tubes [3, 4].

In the field of Concentrated Photovoltaics (CPV), other choices are made. For instance an equivalent comparison would impose the same acceptance angle and the same entrance aperture, but different exit apertures, since solar cells can then be cut in different sizes to accommodate the different Concentration Acceptance Produce (CAP) values, given by $CAP{=}C\sin(\theta)$ [12].

Thus the comparison in this paper is done with the following assumptions:

- The half-acceptance angle, θ, calculated for the perpendicular (vertical) incidence direction, is the same (same overall tolerances for all optics). In this analysis the effective acceptance angle of the optic is defined as the incidence angle for which the concentrator collects 90% of the on-axis power [6] with fixed heliostats (no rotation of heliostats).
- The size (diameter) of the receiver is the same.
- Same evacuated tubular receiver [5].
- Same mirror materials.
- Same intercept factor [13] (equal to 1).

All optics are assumed to have the same acceptance angle for the perpendicular (vertical) incidence direction and, therefore, same overall tolerances to errors, such as optical quality of the components, sun tracking accuracy and effects from wind, dust and others. Optics with the same tolerances can be made and assembled using similar methods (similar costs).

In Fresnel concentrators, the acceptance-angle does not remain constant for different incidence angles θ_Z of the sunlight (see Fig. 8.6). As the sun moves in the sky, heliostats rotate to a different orientation to track it. For each orientation of the heliostats, one may calculate the acceptance angle of the optic. Again this is done by keeping the heliostats fixed (no further rotation) and determining the incidence angles of sunlight for which the concentrator collects 90% of the maximum power collection for that orientation of heliostats.

It should however be noted that, when comparing different Fresnel optics, matching the same acceptance-angle for the perpendicular direction does not guarantee, *per se*, the same overall tolerances for every concentrator. A possible metric would

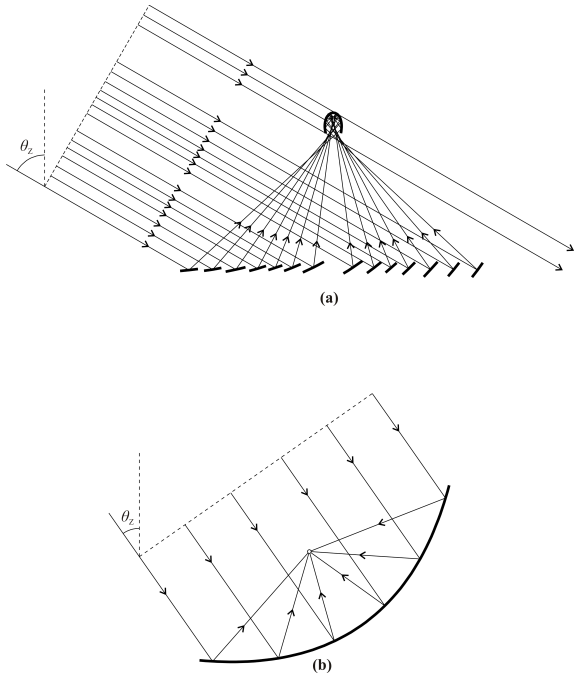

Fig. 8.6: The effect of θ_Z: (a) In Fresnel concentrators, for large values of θ_Z, the secondary mirror might not produce shading over the primary field; (b) In PT concentrators the concentration C does not change for different values of θ_Z.

be to match a weighted mean value of the acceptance-angle, something which can be very difficult from a practical point of view, as it would be necessary to design an optic, calculate the acceptance-angle for different incidence angles and, finally, match this weighted mean value. Thus, in this paper it was considered enough to match the acceptance-angle for the perpendicular incidence direction.

For practical reasons, the geometric concentration C is defined as the ratio between the mean Irradiance (W/m^2) on the receiver and the Irradiance of the uniform source which fully illuminates the concentrator (sunlight irradiance). From a practical point of view, C can be calculated using ray tracing software, creating an uniform source of rays with a well-defined Irradiance value and calculating the mean Irradiance on the receiver. In this specific calculation, the material properties of all the optical elements should be ideal, i.e., the optical losses of the concentrator are due only to the geometry of the concentrator and not to optical characteristics such as reflectivity or absorption. In this way, only the geometry of the system comes into play and one can calculate how many times (X) the mean Irradiance on the receiver is higher than the Irradiance of the uniform source, which is the geometric concentration C.

In Fresnel concentrators, the acceptance angle varies with angle θ_Z of direction of the incident sunlight (as referred above), and so does concentration. For that

reason, CAP is now a function of the incidence angle of sunlight. In other words, the transversal component of the IAM (Incidence Angle Modifer) [14] (2D optic) is not constant and equal to 1, as happens for Parabolic-type concentrators. In this sense, the standard definition of CAP, instead of being a number (as desired), it is now a function $CAP(\theta_Z)$ where θ_Z is the zenith angle (the angle that sunlight makes to the vertical, as shown in Fig. 8.4). However, the amount of light captured by a Fresnel concentrator varies with $K_T(\theta_Z)$ (when the sun moves in the transversal vertical plane perpendicular to the tubular receiver). For that reason, one may use $K_T(\theta_Z)$ two weigh the importance of $CAP(\theta_Z)$ for a given value of θ_Z. Therefore, it is possible to define a new metric CAP_F (CAP Fresnel) as:

$$CAP_F = \frac{\int_{\theta_i}^{\theta_f} CAP(\theta_z) K_T(\theta_Z)\, d\theta_Z}{\int_{\theta_i}^{\theta_f} K_T(\theta_Z)\, d\theta_Z} \tag{8.9}$$

where the integrals are calculated in the range $\theta_i \leq \theta_Z \leq \theta_f$ and θ_i and θ_f define the range of incidence angles used by the concentrator (typically θ_i = -$\pi/2$ and θ_f = $\pi/2$), where $CAP(\theta_Z)$ is the CAP of the Fresnel concentrator as a function of the zenith angle θ_Z [14] (transversal plane) and where $K_T(\theta_Z)$ is the transversal component of the IAM. The CAP_F can be seen as a weighted mean value which takes into account the loss of concentration of the Fresnel concentrator due to its specific geometry and tracking-system. It should be noted that for Parabolic-type concentrators $CAP_F = CAP$, since for those types of concentrators C, θ and $K_T(\theta_Z)$ remain constant for different incidence angles, a consequence of the tracking system which keeps the light entering perpendicularly to the entrance of the concentrator (the mean Irradiance on the receiver remains constant if the Irradiance of the uniform source also remains constant), as shown in Fig. 8.6b. The IAM is defined in a similar way to what is done for the acceptance-angle. Using a raytracing software and defining an uniform source with a constant Irradiance value, one can calculate the total amount of energy captured by the receiver, E_R, for different θ_Z both on the transversal plane ($K_T(\theta_Z)$) and longitudinal plane ($K_L(\theta_Z)$). Normalizing the values one can obtain the curves for each plane as shown in Fig. 8.7.

Finally, the optical efficiency η_{opt} is defined, for a certain incidence angle, as the ratio of energy captured by the receiver E_R and the energy intersected by the whole optic, composed of primary (E_P) and secondary (E_S) mirrors:

$$\eta_{opt} = \frac{E_R}{E_P + E_S} \tag{8.10}$$

One possible way to estimate E_P is to consider that all primary mirrors (optical surfaces) are perfect absorbers and calculating how much incident light (sunlight) they absorb. This gives us the maximum amount of light that the primary could

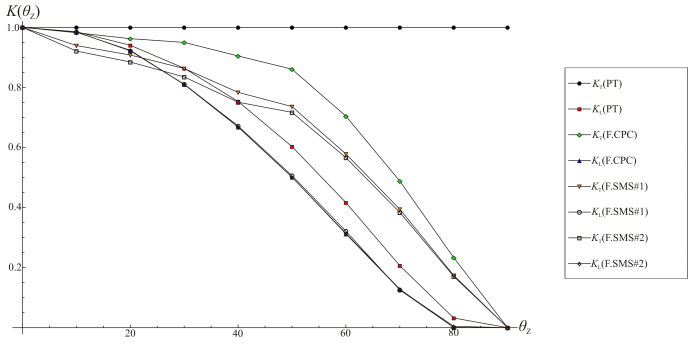

Fig. 8.7: The IAM curves (transversal plane (K_T) and the longitudinal plane (K_L)) for the Parabolic Trough (PT), Fresnel CPC (F.CPC), Fresnel XX SMS #1 (F.SMS#1) and Fresnel XX SMS #2 (F.SMS#2).

ideally send towards the receiver. E_S can also be estimated considering the secondary mirror as a (zero thickness) perfect absorber and calculating how much sunlight it absorbs (see Fig. 8.6). Then, in a second phase, the mirrors (both primary and secondary) are given their actual optical properties and the amount of sunlight E_R reaching the receiver may be estimated. These calculations may be done using a raytracing software. The definition of opt takes into account the shading losses of the secondary, which is generally correct for small incidence angles θ_Z. However, for large incidence angles the definition η_{opt} might not be fully correct since for such angles the shade produced by the secondary might not be located over the primary field, that is, the heliostats are not shaded by the secondary, as shown in Fig. 8.6a.

Therefore, it is appropriated to define an optical efficiency η^*_{opt} as an optical efficiency without the shading losses produced by the secondary:

$$\eta^*_{opt} = \frac{E_R}{E_P} \tag{8.11}$$

The Fresnel XX SMS concentrator was compared for η_{opt} and η^*_{opt} (optical efficiency at perpendicular direction), C and CAP_F. These calculations were performed with commercial raytracing software which includes the material properties and also the sunlight semi-angular aperture (≈ 0.27). The details of Fresnel CPC-type concentrator ("Fresnel NOVA-1" [10]) and PT concentrator ("SKAL-ET 120" [11]) considered in this comparison are shown, respectively, in Table. 8.1 and Table. 8.2. This choice represents what can be typically found on the market without attempting to be specific about one brand or another.

Table 8.1: Details of the Fresnel CPC concentrator. "P." stands for Primary and "R." stands for Receiver.

Optic	P. width (m)	P. length (m)	R. radius (m)	R. height (m)	Number of mirrors	Mirror width (m)	φ (°)	C (×)	θ (°)
Fresnel CPC	16.56	44.8	0.035	7.4	16	0.75	48.21	50.13	0.44

Table 8.2: Details of the conventional PT concentrator.

Optic	Aperture size (m)	Receiver radius (m)	Focal length (m)	φ (deg)	C_g (×)	θ (°)
PT	5.77	0.035	1.71	80.3	26.26	0.694

Materials properties considered for all optics are shown in Table. 8.3.

Table 8.3: Materials properties.

Optical element	Reflectivity	Absorptivity	Transmissivity
Primary mirror	92% [15]	-	-
Secondary mirror	92% [15]	-	-
Receiver tube	-	95% [5]	-
Glass cover	-	-	96% AR-coated glass tube [5]

The first comparison was done between Fresnel CPC and Fresnel XX SMS. In order to distinguish between the two Fresnel XX SMS concentrators used in this work, one defines:

- Fresnel XX SMS #1: A Fresnel XX SMS with the same acceptance-angle (vertical sunlight) and the same tubular receiver of the Fresnel CPC-type concentrator.
- Fresnel XX SMS #2: A Fresnel XX SMS with the same acceptance-angle (vertical sunlight) and the same tubular receiver of the PT concentrator.

Following the assumptions presented above, the acceptance-angle of the Fresnel CPC-type for a tubular evacuated receiver was calculated and, then, a Fresnel XX SMS with the same acceptance-angle and the same tubular vacuum receiver was

designed. The angular transmission curves are shown in Fig. 8.8. Curves [c_0, c_{20},..., c_{80}] are calculated, respectively, for θ_Z =[0, 20,...,80]. It should be noted that the transmission curve c_0 of the Fresnel XX SMS is much more step-shaped than the Fresnel CPC-type, a common characteristic for NIO (NonImaging Optics) devices (ideally it should be a perfect step-shaped function as in an ideal CPC concentrator [7, 8]). Therefore, although both optics have the same acceptance-angle this is a clear indication that the Fresnel XX SMS has a better optical (CAP) performance, as can be seen in Table. 8.3.

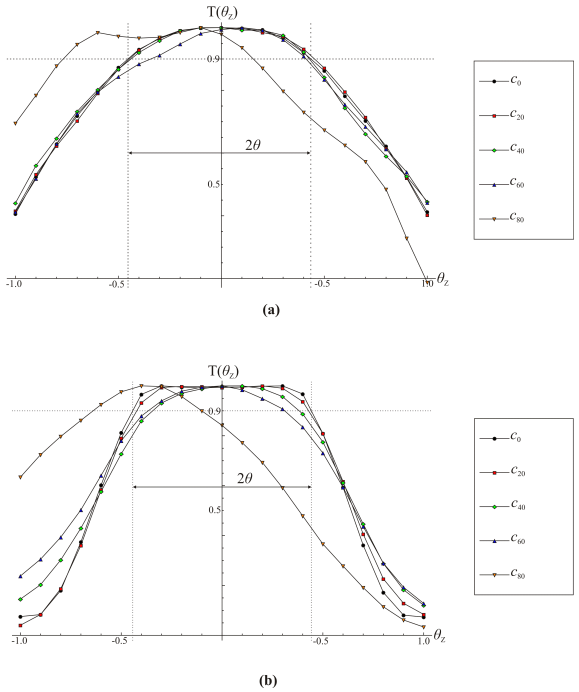

Fig. 8.8: The angular transmission curves c for different solar zenith angles θ_Z (deg). (a) Fresnel CPC concentrator (b) Fresnel XX SMS #1 concentrator.

Table 8.4: Comparison between Fresnel CPC-type and Fresnel XX SMS. The mirror length value of Fresnel XX SMS #1 is the mean value, i.e., not all the heliostats have the same width due to the optimization process.

Optic	Primary width (m)	Total mirror aperture length (m)	Receiver height (m)	Number of mirrors	Mirror length (m)	φ (°)	C (×)	θ (°)	CAP_0	CAP_F	η_{opt0}	η^*_{opt0}
Fresnel CPC	16.56	12	7.4	16	0.75	48.21	50.13	0.44	0.38	0.33	0.68	0.70
Fresnel XX SMS #1	20.11	17.1	9.8	16	1.06	45.79	73.71	0.44	0.57	0.40	0.69	0.72

Where CAP_0 is the CAP for the perpendicular direction θ_Z=0 and is the CAP peak value.

As can be seen, the Fresnel XX SMS #1 has a better optical performance in terms of CAP_0 and CAP_F (larger aperture width, higher concentration, for the same acceptance-angle) and also, remarkably, in terms of η_{opt0} and η^*_{opt0}. About the later, there are two main explanations for the result:

The design of the CPC for a Fresnel Primary implies that for the perpendicular direction, the light is focused at the center of the entrance aperture of the CPC [7]. Therefore, after crossing the CPC's entrance, the light describes a very similar path to Fresnel XX SMS one (Primary – Secondary – Tube).

In the case of Fresnel XX SMS, the optic is designed in such a way that light enters perpendicularly to the tube to reduce the Fresnel losses. Nevertheless, this is not the case of Fresnel CPC-type which contains more Fresnel losses (multiple transmission losses through the glass).

In practical terms a row of the Fresnel XX SMS will be larger than that of the comparable Fresnel CPC one with its higher concentration associated with less thermal losses, achieving higher conversion efficiency to electricity, at whatever temperature and choice of same operating fluid. The reader familiar with the performance of any specific own design can at once use this information and that in Table. 8.6, below, for a comparison.

The second comparison was done between the Fresnel XX SMS and PT concentrator. Following the same approach used before, the acceptance-angle of the PT was calculated and, then, a Fresnel XX SMS with the same acceptance-angle (and same tubular vacuum receiver) was designed. Fig. 8.9 and Table. 8.5 shows, respectively, the angular transmission curves and the comparison data of both optics.

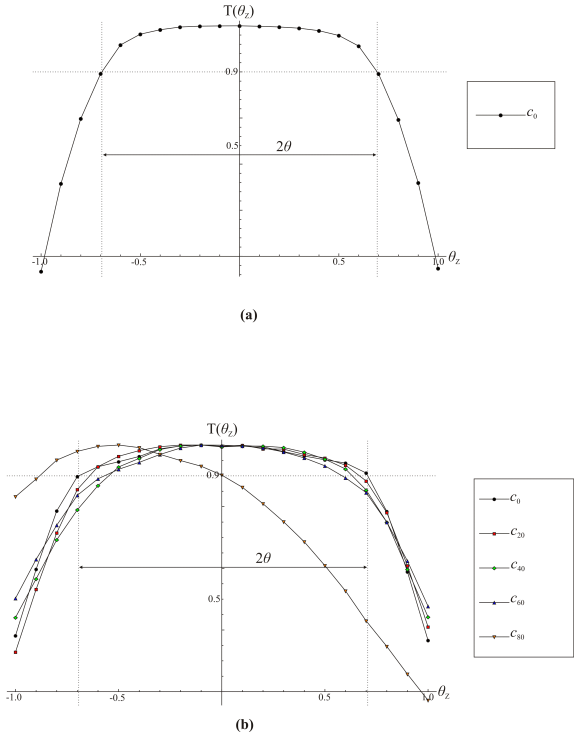

Fig. 8.9: The angular transmission curves c for different solar zenith angles θ_Z (deg). (a) PT concentrator (b) Fresnel XX SMS #2 concentrator.

As can be seen, Fresnel XX SMS #2 has a better performance in terms of CAP_0 and CAP_F (higher concentration factors) and a worse performance in terms of η_{opt0} and η^*_{opt0} (due to the reflections on the secondary mirror). Nevertheless, the gain of concentration is more relevant for a high energy collection, as shall be seen next.

In order to determine the amount of energy delivered to the receiver in real world operating conditions, a more detailed calculation is needed. This analysis was done, again, using commercial raytracing software, as well a numerical method developed in a previous paper [16]. However, in this paper a slightly different approach was used due to the characteristics of the Fresnel concentrator. Here, the total amount of energy captured by the receiver, E_R, is evaluated for an uniform source which fully covers the primary, varying the source irradiance according to the solar irradiance value for each sun direction $I(\theta_Z, \varphi_S)$, and calculating a function $E_R(\theta_Z, \varphi_S)$.

Table 8.5: Comparison between Fresnel CPC and Fresnel XX SMS. The mirror length value of Fresnel XX SMS #1 is the mean value, i.e., not all the heliostats have the same width due to the optimization process.

Optic	Primary width (m)	Total mirror aperture length (m)	Receiver height (m)	Number of mirrors	Mirror length (m)	φ (°)	C (×)	θ (°)	CAP_0	CAP_F	η_{opt0}	η^*_{opt0}
PT	5.77	5.77	1.41	-	-	80.3	26.24	0.69	0.39	-	0.81	-
Fresnel XX SMS #2	15.04	12.71	9.8	14	0.88	45.65	52.95	0.69	0.64	0.45	0.66	0.70

For practical purposes this Fresnel XX SMS #2 can be seen as a much larger PT trough, reducing by a factor of ≈ two (12.71/5.77) the number of rows in a standard PT trough field, with a clear impact on pipe length and receiver length, and the corresponding associated losses reduction.

Again the much higher concentration of the Fresnel solution, will determine less thermal losses and, thus, higher thermodynamic conversion into electricity, bringing the overall performance of the Fresnel design, closer to that of the standard PT solution, at the same temperature. The reader familiar with the performance of any specific own design can at once use this information and that in Table. 8.6 below, for a comparison.

As said, in this paper, the thermal aspects are not considered, just the optical performance. For this simulation and performance comparison, Faro, Portugal (37°02'N, 07°55'W), was selected, with an annual average DNI of 2234 kWh/m^2 [17] (see Appendix A of this Chapter). This calculation includes all optical losses which are present when, as in practice, and every day, incident light is not in the design perpendicular direction.

The results are shown in Table. 8.6.

Table 8.6: Comparison of collected energy in Faro, Portugal. The calculations were done for a receiver of 70 mm of diameter and 1 m of length.

Optic	DNI (kWh/m^2)	Collected energy same vacuum tube (kWh)
Fresnel CPC	2234	11361
Fresnel XX SMS #1	2234	15122
PT	2234	7527
Fresnel XX SMS #2	2234	10622

From the results presented in Table. 8.6 one can conclude that Fresnel XX SMS 1 collects more energy than the Fresnel CPC and that Fresnel XX SMS #2 collects more energy than the PT, a result of having a much larger aperture width (higher CAP_F) while keeping the same overall optical tolerances (same peak acceptance-angle).

8.4 Conclusions

A Fresnel XX SMS concentrator has been presented. The results shows that Fresnel XX SMS has a high potential for a better cost-effectiveness (euro/kWh) since it collects more energy in comparison with Fresnel CPC-type and PT concentrators

while maintaining the same type of geometry as that of a Fresnel CPC-type. The thermodynamic calculation was not done, but it was noted that a substantially higher concentration will result into smaller thermal losses, thus providing higher conversion efficiency at whatever operating temperature.

The proposed Fresnel XX SMS concentrator has similar overall optical tolerances (as indicated by the same acceptance-angle for the perpendicular incidence direction) and, therefore, it can be manufactured with the same techniques and materials commonly used in this type of applications. The economic viability of this kind of solutions was not studied in this paper, but this should not constitute a major handicap, since there is nothing particularly special or different in the new solutions, in comparison with the more conventional ones.

A generalization of the concept of CAP was also presented, since, as shown, the standard definition is not readily applicable for Fresnel concentrators. This definition of CAP_F combines CAP with IAM. Moreover, the definitions of optical efficiency, geometric concentration, IAM, CAP are now re-defined in a simple, practical and effective way. By using a raytracing software to calculate these parameters, one avoids the common analytical approach, which can be sometimes quite difficult to use (and validate) in practice due the geometry of the concentrator. More importantly, the definitions presented are completely general and one can apply them to any concentrator, as opposed to the analytical approach since with the later, a set of equations which defines completely, for example, a PT concentrator might not be correct for a Fresnel concentrator.

Appendix A

Table. 8.7 shows the DNI values used in this work.

Table 8.7: DNI value for Faro (Portugal) [17].

Month	DNI (kWh/m^2)
JAN	137
FEB	114
MAR	195
APR	168
MAY	229
JUN	244
JUL	277
AGO	254
SEP	213
OCT	181
NOV	109
DEC	113
TOTAL	2234

References

[1] Chaves, J., Collares-Pereira, M., *Etendue-matched two stage concentrators with multiple receivers*, Solar Energy 84 (2009), pp. 196-207.

[2] Canavarro, D., Chaves, J., Collares-Pereira, M., *New Optical Designs For Large Parabolic Troughs*, Proceeding 19th International SolarPACES Symposium, September 17-20, Las Vegas, USA (2013).

[3] Canavarro, D., Chaves, J., Collares-Pereira, M., *New second-stage concentrators (XX SMS) for parabolic primaries; Comparison with conventional parabolic troughs concentrators*, Solar Energy, 92 (2013) 98–105.

[4] Canavarro, D., Chaves, J., Collares-Pereira, M., *Infinitesimal etendue and Simultaneous Multiple Surface(SMS) concentrators for fixed receiver troughs*, Solar Energy, 97 (2013) 493—504.

[5] SCHOTT PTR 70 Receiver brochure

[6] Benítez, P., *Advanced concepts of non-imaging optics: design and manufacture*, PhD Thesis, Presented in Madrid, January 16, 1998

[7] Chaves, J., 2008, *Introduction to Nonimaging Optics*, CRC Press, Taylor and Francis Group

[8] Winston, R., Miñano, J.C., Benítez, P., (contributions by Shatz, N., Bortz, J.,C.), *Nonimaging Optics*, Elsevier Academic Press, Amsterdam, 2005.

[9] Heimsath, A., et al., *Linear Fresnel collector receiver: heat losses and temperatures*, Proceeding 19th International SolarPACES Symposium, September 17-20, Las Vegas, USA (2013).

[10] Novatec Solar, NOVA-1Turnkey solar boiler, mass produced in industrial precision – with performance guarantee, NOVA-1 brochure.

[11] Kearney, D.W., *Parabolic Trough Collector Overview*, Parabolic Trough Workshop, 2007.

[12] Benítez, P., et al., High performance Fresnel-based photovoltaic concentrator, Optical Society of America, 26 April 2010, Vol. 18, No. S1, OPTICS EXPRESS.

[13] Riffelmann, K.J., Lüpfert, E., Richert, T. and Nava, P., *Performance of the Ultimate Trough Collector with Molten Salts as Heat Transfer Fluid*, Proceeding 18th International SolarPACES Symposium, September 11-14, Marrakech, Morocco (2012).

[14] Rabl, A., *Active Solar Collectors and their applications*, Oxford University, Oxford, 1985

[15] *http://www.saint-gobain-solar-power.com/mirrors-solar-glass-7* (SGG MIRALITE SOLAR 4 mm).

[16] Canavarro, D., Modeling linear solar collectors of the Fresnel-type; application to an innovative CLFR collector "Etendue Matched", MSc thesis, Instituto Superior Técnico/UniversidadeTécnica de Lisboa, Lisbon, 2010.

[17] Meteonorm hourly DNI data

Nomenclature

$[\mathbf{A}, \mathbf{B}]$	euclidean distance between points **A** and **B**
C	geometric concentration ($\times$)
CAP	Concentration Acceptance-Product
CAP_F	Concentration Acceptance-Product Fresnel
CPC	Compound Parabolic Concentrator
CPV	Concentrated PhotoVoltaics
CSP	Concentrated Solar Power
dx	infinitesimal length
dU	infinitesimal etendue
DNI	Direct Normal Irradiance
E_R	energy captured by the receiver
E_P	energy captured by the primary
E_S	energy captured by the secondary
IAM	Incidence Angle Modifier
K	constant of integration
n	refractive index
NIO	NonImaging Optics

OM	Operation and Maintenance
PT	Parabolic Trough
R	circular receiver
S	optical path length
SMS	Simultaneous Multiple Surface
U	etendue
w	flat wave front

Greek symbols

η_{opt0}	optical efficiency at normal incidence
η^*_{opt0}	optical efficiency at normal incidence without shading losses
θ	half-acceptance angle (grad)
θ_Z	half-acceptance angle (grad)
φ	rim angle (grad)
φ_S	solar azimuth angle (grad)
β	tilt angle (grad)

Chapter 9

Future perspectives and lines of investigation

9.1 Future perspectives and lines of investigation

The results obtained throughout this work give a clear indication that there is still a large room for further developments. Important advancements and improvements have been presented for thermal solar concentrators and, therefore, this gives a solid foundation for future developments. Furthermore, with the growing relevance of this type of systems, especially the rising of the Concentrated Solar Power (CSP) as a promising alternative to Concentrated PhotoVoltaics (CPV), this line of work and investigation is very pertinent and it can lead to important academic, technological and economical developments in the future. In fact, a proposal for a demonstration project of a Fresnel XX SMS with a tubular vacuum receiver has been presented under the European Program Horizon 2020 and was admitted to second stage consideration. More details about this proposal can be found in Annex A in the end of this thesis.

Regarding new lines of investigation there are several improvements which can be achieved in a near future. Considering the promising results obtained through the use of the SMS method it is natural to continue using it and develop new ideas for improving current solutions. On the other hand, the importance and relevance of the concept "Etendue-Matched" might open new ways for future developments. Among others, possible line of investigation in a near future can be as follows:

1. Development of an Asymmetric Fresnel XX SMS concentrator.
2. Development of a XX SMS Compact Linear Fresnel Reflector "Etendue-Matched" (CLFR-EM).
3. Study and development of the extension of the concept "Etendue-Matched" to

3-dimensional systems.

4. Study and development of the extension of the XX SMS concept to 3-dimensional systems.

The first task is simply a natural continuation of the present Fresnel XX SMS. In fact, the Fresnel XX SMS presented in this work is symmetric with respect to the vertical line which passes through the receiver. This can designed differently, i.e., with the primary field placed over to the right or left of the receiver. This approach can lead to interesting practical solutions. If two such systems are placed side by side, this can increase the compactness of the system. On the other hand, the use of two receiver tubes can be also interesting from a operational point of view. For example, in one of the tubes a normal Heat Transfer Fluid can be used while in the second tube Molten Salts can be used. This increases the flexibility of the system and the management of the storage systems, which are crucial for the viability of CSP systems. Moreover, this asymmetric approach can be seen as a first test of the XX SMS for a CLFR-EM concentrator, since it would be difficult, at least from a practical point of view, to apply this concept directly to such a concentrator, without going through some intermediate steps.

The second task can represent an important breakthrough. The potential of the CLFR-EM concentrator has already been proved but, as mentioned before, it contains some drawbacks, especially the optical gap losses between the vacuum tubular receiver and the secondary TERC mirror. By applying the XX SMS concept on a CLFR-EM concentrator, there is the potential to eliminate gap losses as well as decreasing the Fresnel losses around the glass cover of the vacuum tubular receiver. This might increase the overall performance of the concentrator and, therefore, its potential for practical solutions.

The third and fourth tasks can be seen as an extension of the analysis and the ideas presented in this thesis for 3-dimensional systems. In fact, this thesis dealt with 2-dimensional systems only but many progresses can be made in 3-dimensional systems as well. Moreover, the most common 3-dimensional systems used in CSP field (Central Tower Receivers and Parabolic Dishes) also fall short from the theoretical limits of concentration which penalizes their overall efficiency.

Chapter 10

Conclusions

10.1 Conclusions

The purpose of this chapter is to conduct a general review of the entire work. It is important to note that due to the structure of this PhD thesis (organized through a set of scientific publications with peer review), the (re)inclusion of the conclusions drawn in each of these works would become redundant. Therefore, we chose to make a global and qualitative analysis of the work, its relevance and immediate and future impacts for the development of this area of knowledge.

In this PhD thesis, several advancements and developments were presented in the design of solar concentrators for thermal applications - with emphasis on CSP (Concentrated Solar Power). These advances represented, by themselves, an important contribution for the development of this area, since advances in optics has been scarce in recent years and these advances represent an essential condition for the increase of overall efficiency of conversion from solar to electricity through a thermodynamic cycle.In fact, despite adjustments that the initial PhD program had to undergo - due to events unrelated to the author and their advisors (see Chapter 1) - it always had a clear objective: to improve the overall performance of the optical and global performance of solar concentrator systems for CSP applications, in particular Fresnel concentrators, through the use of NonImaging Optics (NIO) for a significant approximation to the theoretical limits of concentration. This idea and this objective provided strong identity to this PhD thesis which was essential to its success.

This success was expressed in many different results. From an academic point of view, 7 scientific publications with peer review were produced (See List of Papers) confirming their quality and pertinence. Important steps were made in the consolidation of the concept Compact Linear Fresnel Reflector "Etendue-Matched" (CLFR-EM) through an in-depth analysis of the optical, thermal and costs characteristics of this concentrator as well as through the presentation of possible improve-

ments. For example: 1) the use of a curved glass cover to reduce the optical losses; 2) the use of anti-convection baffles to reduce the thermal losses without penalizing the optical efficiency and 3) the introduction of thermal storage to increase this dispatchability of the electricity produced (Chapter 3, 4 and 5). On the other hand, the results obtained were not just related with the optimization of an existing systems, but as well to the introduction of theoretical/practical novelties. In fact, the SMS XX concentrator presented for continuum and Fresnel primaries is a very interesting and important solution due to the possibility of its application for vacuum tubular receivers, something not done before. This is an important contribute both for NIO theory as well as for practical cases, making an important connection between the academic and industrial fields (Chapters 6, 7 and 8).

Another important result was the author's participation in the 1^{st} NIO Design Silent Online Contest organized by the American association OSA (Optical Society of America) [1]. The author was the winner of the "Viewer's Choice Award" (public voting) and the contest consisted in a "silent" presentation (no audio) about a topic related with the NIO field chosen by the author. The topic chosen was the development obtained for continuum primaries and fixed receivers using the SMS method (Chapters 6 and 7). Beyond recognition in this international event, this award has enhanced the quality of the work developed in this PhD thesis.

From a practical point of view, this PhD thesis obtained also a very positive result. In fact, the recent developments obtained with the Fresnel SMS XX (Chapter 8) triggered a strong interest in major European companies and other R&D institutions (including one from South Africa, site of strong market development for these technologies) who came together to submit a proposal to the Program H2020, H2020-LCE-2014-1, on the topic "Developing the next generation of technologies Renewable Electricity and Heating and Cooling, Specific Challenge: Making CSP Plants more cost competitive" under the leadership of the University of Évora [2]. In this project several important companies are included such as Schott Solar (manufacturer of vacuum tubes - Germany) [3], Solar Euromed (manufacturer of Fresnel concentrators - France) [4] and Generg (promoter of renewable electricity systems - Portugal) [5] and research institutions such as DLR (Germany) [6], ETH Zürich (Switzerland) [7] and Stellenbosch University (South Africa) [8]. The project entitled InnovLFR, as a final value of 6MEuro and intends to develop and install in Évora a first Fresnel XX SMS concentrator system with $\approx 2500\ m^2$ to operate at 565ºC directly circulating molten salts of sodium and potassium, and also considering the energy storage through its direct storage.

This project has successfully passes the first approval of the program (Stage 1. Note: Due to confidentiality reasons it is not possible to reproduce the respective document in this thesis) and at the present time a second proposal is being pre-

pared for the second stage (Stage 2). If implemented, this will be an unique project worldwide and, of course, in Portugal, with an experimental test of a new technology and its integration with new engineering solutions for the collection, conversion and storage of solar energy. This project will be essential to demonstrate the potential of Fresnel technology and its ability to be truly competitive with other electricity generation technologies in their way to reduce costs to below 10c.Euro/kWh. It will also contribute significantly to assert Portugals role in the global context of high solar concentration.

In short, one can say that this thesis has fulfilled its objectives and opens new ways for future developments in this field.

References

[1] Optical Society of America, *http://www.osa.org/en-us/*

[2] Horizon 2020 Project, *http://ec.europa.eu/programmes/horizon2020/en*

[3] Schott Solar, *http://www.schott.com/csp/english/index.html*

[4] Solar Euromed, *http://www.solareuromed.com/*

[5] Generg Portugal, *http://www.generg.pt/*

[6] DLR, *http://www.dlr.de/*

[7] ETH Zurich, *https://www.ethz.ch*

[8] Stellenbosch University, *http://www.sun.ac.za/english*

Contactos:
Universidade de Évora
Instituto de Investigação e Formação Avançada - IIFA
Palácio do Vimioso | Largo Marquês de Marialva, Apart. 94
7002-554 Évora | Portugal
Tel: (+351) 266 706 581
Fax: (+351) 266 744 677
email: iifa@uevora.pt